Study on the interaction of cesium with clay minerals aiming electrokinetic remediation of contaminated soil

（汚染土壌の動電的修復を指向した
セシウムと粘土鉱物との相互作用に関する研究）

Yasuhiro AKEMOTO

Graduate School of Environmental Science
Hokkaido University

Contents

Chapter 1

General introduction

1.1. Environmental pollution in soil

Soil is a basis for many kinds of lives which live there. Soil is also an essential resource for the ecosystem and human living because soil can provide minerals, organics, moisture, and so on that they need. These roles of soil come from the diverse components and properties of soil. Soil is composed of clay minerals, organic substances, microorganisms, water, air, etc., and each component has various functions. For example, clay minerals have the ability which can adsorb many kinds of metal ions including alkali metals, heavy metals, and radionuclides, moreover, organic substances in the soil also interact with metal ions and sometimes organic compounds. Unfortunately, much soil pollution has happened in the world by human daily activities and sometimes accidents. There are a variety of organic pollutants such as pesticides, herbicides, surfactants, oils, and volatile organic compounds (VOCs), and inorganic pollutants such as heavy metals, excess salts, anionic substances, and so on. In particular, contamination by radioactive species has a serious influence on the environment. In 2011, numerous radionuclides were released into the environment from Fukushima Daiichi Nuclear Power Plant (FDNPP) in Japan. The amounts of ^{131}I and ^{137}Cs released into the environment were estimated to be approximately 1.5×10^{17} and 1.3×10^{16} Bq, respectively [1]. Even after 30 years, that is the half-life of ^{137}Cs, the volume of contaminated soil above 8,000 Bq/kg will be 105,000 m^3, of which 98,000 m^3 is clayey soil [2]. Therefore, ^{137}Cs in the soil will continue to affect the ecosystem and human living for a long time, and the establishment of effective remediation methods is required. However, the development of effective soil remediation technologies for Cs is difficult due to the high stability of cesium on clay minerals in the environment.

1.2. Behavior of Cs in the soil environment

Various radionuclides have been released into the environment due to the atmospheric nuclear test conducted in the mid-1900s, the accident at the Chernobyl Nuclear Power Plant in 1986, and the FDNPP in 2011. After these accidents, various studies on the dynamics of radionuclides in the environment and their effects on the ecosystem have been conducted. Through those studies, it is known that radioactive Cs settled on the ground surface and remain in a relatively shallow layer of soil (around 0–15 cm) [3,4]. This phenomenon is due to the strong interaction between Cs and clay minerals in the soil. The interaction between Cs and clay minerals is very specific and strong, and then the adsorbed Cs with clay minerals cannot be desorbed easily. The structure of clay minerals is indicated in **Fig. 1-1**. Tetrahedrons and octahedrons form sheets horizontally, which stack to form clay minerals. These numbers of each sheet, interlayer materials, basal spacing, and electric charges are used to classify clay minerals. The inner diameter of the six-membered rings on the tetrahedral sheet is similar to the diameter of Cs, the adsorbed Cs is considered to be fixed in the interlayer of 2:1 type clay mineral. Since the amount and sort of clay minerals in soil differ in each area, the adsorption and retention behaviors of Cs in soil are changed. RIP (Radiocesium Interception Potential) is known as an indicator of the adsorption ability of radioactive Cs in soil and is used for the evaluation of the adsorption capacity of the soil [5–7]. The RIP correlates with the vermiculite content in the soil, and the larger this value is, the more difficult the desorption of Cs from the soil is [8]. Fukushima prefecture in Japan is known as a production area for biotite and vermiculite derived from Abukuma granite [9,10], and these contents in Fukushima soil are estimated to be high. Biotite and vermiculite have a slight difference in the chemical component and structure depending on the production

environment, however, there are few reports which are focusing on this difference. The investigation of the interaction between Cs and biotite and vermiculite is essential for the consideration of the behavior of Cs in soil.

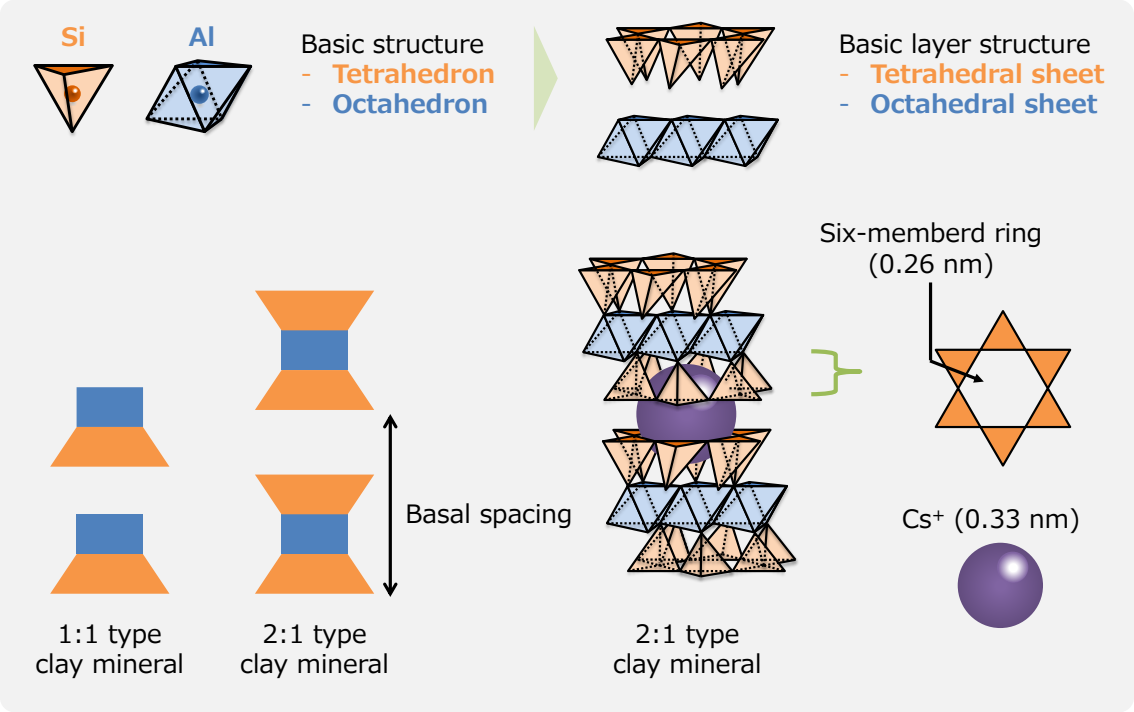

Fig. 1-1. Basic structure of clay minerals and the relationship between six-membered ring on tetrahedral sheet and Cs.

1.3. Remediation of soil environment

Various soil remediation technologies have been investigated. These technologies were classified into three types [11]. The first is containment such as a slurry wall, solidification, and stabilization, which can prevent pollutants from spreading in the surrounding environment. In containment technologies, pollutants remain in the contaminated area and there are some concerns about secondary contamination in the future. The second is degradation such as incineration, bioremediation, and oxidation, which can degrade pollutants to a harmless substance, but this method can be applied to

only organic pollutants. The third is separation such as washing, solvent extraction, phytoremediation, and electrokinetic process, in which pollutants are removed from the contaminated site. Since all technologies have both advantages and disadvantages, the most suitable method should be chosen for pollutants and contaminated sites. In the case of radioactive species, separation is thought to be the most expected method, however, effective remediation technology has not yet been established.

1.4. Electrokinetic process

The electrokinetic (EK) process is one of the environmental remediation methods, in which the electromigration and electroosmotic flow (EOF) in the electric field are used as the driving force for the removal of pollutants from the contaminated area [12–14]**.** This process can be applied to even low permeable soils because a water flow of the EOF is induced in soil under the electric field. The electromigrative velocity ($u_{e,m}$) is expressed by **Eq. 1-1** [15].

$$u_{e,m} = v_i\, z_i\, n\, \tau\, F\, \nabla E \qquad \textbf{(1-1)}$$

Here, v_i is the ionic mobility (m/V s), z_i is the ionic valance (dimensionless), n is the soil porosity, τ is the tortuosity of the soil, F is the Faraday constant (C/mol), and E is the potential gradient (V/m). Notably, z_i, n, and τ are dimensionless and depend on the soil properties; typically, the range of n is 0.1–0.7 and that of τ is 0.01–0.84 [12].

The electroosmotic velocity (J_{eo}) is expressed as **Eq. 1-2**.

$$u_{e,o} = \frac{\varepsilon\zeta}{\mu}\nabla E \qquad \textbf{(1-2)}$$

Here, ε is the permittivity of the fluid (C/V m), ζ the zeta potential (V), and μ the viscosity of the liquid (Pa s) [14].

Electrolysis significantly affects the soil pH (**Eqs. 3 and 4**).

$2H_2O \rightarrow O_2 \uparrow + 4H^+ + 4e^-$ (anode) **(1-3)**

$2H_2O + 2e^- \rightarrow H_2 \uparrow + 2OH^-$ (cathode) **(1-4)**

Hydrogen ions (H^+) are generated at the anode and introduced into the soil by electromigration, which creates an acidic region near the anode. Likewise, hydroxide ions (OH^-) also form a basic region near the cathode. This acidification promotes the solubilization of heavy metals in the soil, enhancing their removal efficiency by EK remediation. Conversely, low pH conditions make it difficult to reuse the soil for agricultural use, for which soil neutralization is often required after remediation. The EOF velocity is also dependent on the zeta potential of the soil particles (**Eq. 1-2**); however, in most cases, the zeta potential is neutralized in the acidic region, and then the EOF velocity decreases. For the effective use of EOF for pollutant removal, it is required to maintain the soil pH around neutral.

The schematic diagram of the EK process is shown in **Fig. 1-2**. Cationic substances are migrated to the cathode side and anionic substances are migrated to the anode side by the electromigration. Typically, the soil particles have a negative charge, positively charged substances are concentrated to satisfy the electrical neutrality, and an electric double layer is formed. The locally excess positive ions migrate toward the cathode side by electromigration, and the water molecules that surrounded them also move with these positive ions. Additionally, these water molecules move with surrounding other water molecules due to their viscosity and then produce EOF. Therefore, the nonpolar substance also can be moved to the cathode side by the EOF if the substance dissolves in water [15].

Many types of the EK process have been studied, by using various pollutants (pesticides, surfactants, heavy metals, and anionic substances) [16–23], various mediums (soils, sediments, groundwater, ash, and concrete) [24–31] and sorts of places (factory

site, agricultural field, and greenhouse) [32–37]. Many kinds of substances, reagents, and other remediation technologies have been combined with the EK process to improve the removal efficiency of pollutants from soil [38–42].

The first field application of the EK process as a soil remediation method was conducted to remove Pb^{2+} and Cu^{2+} from a former paint factory in Groningen in the northern part of the Netherlands in 1987 [43]. The removal of Zn^{2+} from a galvanizing plant (Delft, the Netherlands) [44] and the removal of various heavy metals from paddy soil (Chungnam, South Korea) was also conducted [45], and many field scale experiments can be found in the world.

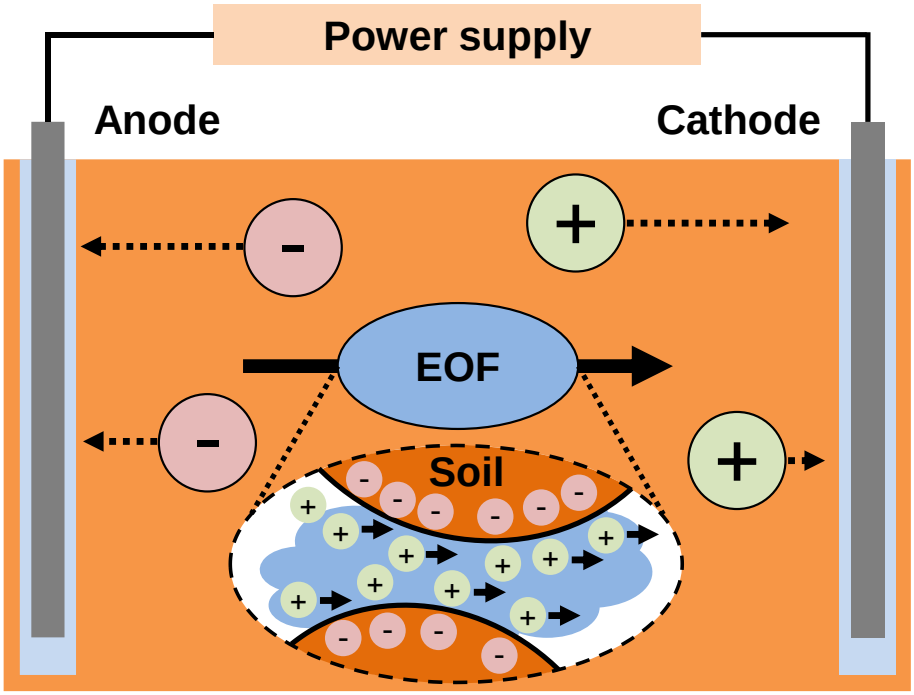

Fig. 1-2. Schematic diagrams of the EK process.

1.5. Remediation of Cs contaminated soil

Many decontamination methods have been investigated using specific reactions and functions for the removal of radioactive Cs from the soil which was generated by the accident of FDNPP. The ion exchange with a high concentration of Mg was investigated, and the intercalated Cs in vermiculite was fully removed by the replacement with Mg^{2+} within 2 h, the re-adsorption can be prevented with Cs^{+}-capturing ligand (tetrakis(4-fluorophenyl)borate sodium salt) [46]. The vacuum heat treatment under low-pressure conditions was applied to remove Cs from the soil, approximately 40% of Cs was desorbed at 800 °C for 3 min and the heating at 650 °C for 30 min was also effective to desorb Cs^{+} from vermiculite by the combination with NaCl and $CaCl_2$ salts [47]. Moreover, other decontamination methods have been studied using such as magnetic separation [48], organic acid and ionic liquid [49], and hydrothermal treatment [50]. However, these methods still have some problems in the points of aging effect, cost, equipment, and efficiency.

The EK process has also been investigated for the removal of Cs from the contaminated soil (described in Chapter 6), and this technology is expected to be able to restore the radioactively contaminated soil generated by the accident of FDNPP [51]. Although some previous studies have reported that Cs in the soil can be removed by the EK process, the properties of soil, especially the types of clay minerals, and the associated chemical forms of Cs have not been mentioned in detail. In order to remediate contaminated soil with Cs, it is necessary to remove not only the ion exchangeable form of Cs but also the forms of Cs that are specifically adsorbed on clay minerals. However, whether the EK process is effective for Cs adsorbed on clay minerals has not yet been discussed. Therefore, the possibility and limit of the EK process should be discussed from

the point of interaction with clay minerals, and it is necessary to investigate how to improve the removal efficiency of Cs from the soil by the EK process.

1.6. Objectives of this study

The investigation of the dynamics of pollutants in the soil is important for the consideration of environmental protection and remediation. In particular, radioactive Cs will affect the ecosystem and human living for a long time and then the prediction of the dynamics of Cs in soil and the establishment of remediation methods are required for the stable management of radioactive pollutants.

In this thesis, using stable isotope Cs as a target substance, the adsorption and desorption mechanism of Cs on 2:1 type clay mineral, which have different chemical compositions and structures, was evaluated through the adsorption kinetic study, adsorption isotherm model, and desorption experiment. Moreover, the separation of Cs from the soil by the EK process was investigated, and then the possibility of the EK process as soil remediation technology to remove Cs was discussed as well as the limitation.

This thesis consists of the following seven chapters.

In Chapter 1, the background of this study and previous studies on this topic were described.

In Chapter 2, the adsorption behavior of Cs on 2:1 type clay minerals such as biotite and vermiculite was evaluated by batch adsorption experiments and structural evaluation of these clay minerals.

In Chapter 3, the desorption behavior of Cs from biotite, which is considered to be the main clay mineral that adsorbs Cs in Fukushima Prefecture, Japan, was investigated

by using inorganic and organic acids.

In Chapter 4, the effect of sodium citrate treatment was investigated to enhance the adsorption capacity of vermiculite. Moreover, the collectable adsorbent, in which vermiculite was encapsulated into an alginate gel bead, was developed to remove Cs from the aquatic environment.

In Chapter 5, the dynamics of Cs in the soil were attempted to be evaluated by the EK process. Since the electroosmotic flow (EOF) generated in the EK process occurs regardless of the soil properties, it can flow water through the low permeable soil. This phenomenon was applied to evaluate the stability of Cs in clayey soil.

In Chapter 6, the EK remediation was applied to artificially contaminated soil with Cs. The potential of oxalic acid leaching as a desorption method of Cs from biotite was indicated in Chapter 3. Therefore, in this chapter, the EK process combined with oxalic acid leaching was attempted as a remediation method for Cs contaminated soil.

In Chapter 7, the findings obtained from each chapter were summarized and the possibility and limitation of the EK process as a remediation method of Cs in soil were discussed on the basis of the results of this thesis.

1.7. References

[1] M. Chino, H. Nakayama, H. Nagai, H. Terada, G. Katata, H. Yamazawa, Preliminary estimation of release amounts of ^{131}I and ^{137}Cs accidentally discharged from the Fukushima Daiichi Nuclear Power Plant into the atmosphere, J. Nucl. Sci. Technol. 48 (2011) 1129–1134. doi:10.1080/18811248.2011.9711799.

[2] Japan Ministry of the Environment, Volume reduction and recycling technology development strategy, (2018) (in Japanese). http://josen.env.go.jp/chukanchozou/facility/effort/investigative_commission/pdf/proceedings_181217_04.pdf (accessed September 13, 2021).

[3] P. Bossew, M. Gastberger, H. Gohla, P. Hofer, A. Hubmer, Vertical distribution of radionuclides in soil of a grassland site in Chernobyl exclusion zone, J. Environ. Radioact. 73 (2004) 87–99. doi:10.1016/j.jenvrad.2003.08.004.

[4] B.L. Rosenberg, J.E. Ball, K. Shozugawa, G. Korschinek, M. Hori, K. Nanba, T.E. Johnson, A. Brandl, G. Steinhauser, Radionuclide pollution inside the Fukushima Daiichi exclusion zone, part 1: Depth profiles of radiocesium and strontium-90 in soil, Appl. Geochemistry. 85 (2017) 201–208. doi:10.1016/j.apgeochem.2017.06.003.

[5] A. Cremers, A. Elsen, P. De Preter, A. Maes, Quantitative analysis of radiocaesium retention in soils, Nature. 335 (1988) 247–249. doi:10.1038/335247a0.

[6] S. Ogasawara, A. Nakao, J. Yanai, Radiocesium interception potential (RIP) of smectite and kaolin reference minerals containing illite (micaceous mineral) as impurity, Soil Sci. Plant Nutr. 59 (2013) 852–857. doi:10.1080/00380768.2013.862158.

[7] A. Nakao, S. Ogasawara, O. Sano, T. Ito, J. Yanai, Radiocesium sorption in relation to clay mineralogy of paddy soils in Fukushima, Japan, Sci. Total Environ. 468–469 (2014) 523–529. doi:10.1016/j.scitotenv.2013.08.062.

[8] B. Delvaux, N. Kruyts, A. Cremers, Rhizospheric mobilization of radiocesium in soils, Environ. Sci. Technol. 34 (2000) 1489–1493. doi:10.1021/es990658g.

[9] K. Omori, Mode of occurrence and chemical composition of Mg-vermiculite from Odaka and Uzumine, Fukushima Prefecture, J. Mineral. Soc. Japan. 3 (1958) 478–485 (in Japanese).

[10] K. Nagasawa, H. Morishima, Weathered biotite from Ono-Niimachi, Fukushima prefecture, Nendo Kagaku. 30 (1990) 101–108 (in Japanese).

[11] Graduate School of Environmental Science Hokkaido University, Science and

Technology of Environmental Remediation, Hokkaido University Press, Sapporo, (2007) (in Japanese).

[12] Y.B. Acar, A.N. Alshawabkeh, Principles of electrokinetic remediation, Environ. Sci. Technol. 27 (1993) 2638–2647. doi:10.1021/es00049a002.

[13] R.F. Probstein, R.E. Hicks, Removal of contaminants from soils by electric fields, Science. 260 (1993) 498–503. doi:10.1126/science.260.5107.498.

[14] A.P. Shapiro, R.F. Probstein, Removal of contaminants from saturated clay by electroosmosis, Environ. Sci. Technol. 27 (1993) 283–291. doi:10.1021/es00039a007.

[15] K.R. Reddy, C. Cameselle, Electrochemical remediation technologies for polluted soils, sediments and groudwater, John Wiley & Sons, Inc., Hoboken, (2009).

[16] G.C.C. Yang, S.-L. Lin, Removal of lead from a silt loam soil by electrokinetic remediation, J. Hazard. Mater. 58 (1998) 285–299. doi:10.1016/S0304-3894(97)00139-8.

[17] G.C.C. Yang, Y.-W. Long, Removal and degradation of phenol in a saturated flow by in-situ electrokinetic remediation and Fenton-like process, J. Hazard. Mater. B69 (1999) 259–271. doi:10.1016/S0304-3894(99)00059-X.

[18] N. Eid, W. Elshorbagy, D. Larson, D. Slack, Electro-migration of nitrate in sandy soil, J. Hazard. Mater. B79 (2000) 133–149. doi:10.1016/S0304-3894(00)00238-7.

[19] A. Giannis, E. Gidarakos, A. Skouta, Application of sodium dodecyl sulfate and humic acid as surfactants on electrokinetic remediation of cadmium-contaminated soil, Desalination. 211 (2007) 249–260. doi:10.1016/j.desal.2006.02.097.

[20] T. Kimura, K. Takase, N. Terui, S. Tanaka, Ferritization treatment of copper in soil by electrokinetic remediation, J. Hazard. Mater. 143 (2007) 662–667. doi:10.1016/j.jhazmat.2007.01.010.

[21] Y.-J. Lee, J.-H. Choi, H.-G. Lee, T.-H. Ha, J.-H. Bae, Pilot-scale study on in situ electrokinetic removal of nitrate from greenhouse soil, Sep. Purif. Technol. 79 (2011) 254–263. doi:10.1016/j.seppur.2011.02.011.

[22] T. Suzuki, M. Moribe, Y. Okabe, M. Niinae, A mechanistic study of arsenate removal from artificially contaminated clay soils by electrokinetic remediation, J. Hazard. Mater. 254–255 (2013) 310–317. doi:10.1016/j.jhazmat.2013.04.013.

[23] F.L. Souza, C. Saéz, J. Llanos, M.R.V. Lanza, P. Cañizares, M.A. Rodrigo, Solar-powered electrokinetic remediation for the treatment of soil polluted with

the herbicide 2,4-D, Electrochim. Acta. 190 (2016) 371–377. doi:10.1016/j.electacta.2015.12.134.

[24] Y.B. Acar, A.N. Alshawabkeh, R.J. Gale, Fundamental aspects of electrokinetic remediation of soils, Waste Manag. 13 (1993) 513. doi:10.1016/0956-053X(93)90081-7.

[25] Y.B. Acar, R.J. Gale, A.N. Alshawabkeh, R.E. Marks, S. Puppala, M. Bricka, R. Parker, Electrokinetic remediation: Basics and technology status, J. Hazard. Mater. 40 (1995) 117–137. doi:10.1016/0304-3894(94)00066-P.

[26] S.K. Puppala, A.N. Alshawabkeh, Y.B. Acar, R.J. Gale, M. Bricka, Enhanced electrokinetic remediation of high sorption capacity soil, J. Hazard. Mater. 55 (1997) 203–220. doi:10.1016/S0304-3894(97)00011-3.

[27] K.R. Reddy, M. Donahue, R.E. Saichek, R. Sasaoka, Preliminary assessment of electrokinetic remediation of soil and sludge contaminated with mixed waste, J. Air Waste Manage. Assoc. 49 (1999) 823–830. doi:10.1080/10473289.1999.10463849.

[28] L. Cang, D.-M. Zhou, A.N. Alshawabkeh, H.-F. Chen, Effects of sodium hypochlorite and high pH buffer solution in electrokinetic soil treatment on soil chromium removal and the functional diversity of soil microbial community, J. Hazard. Mater. 142 (2007) 111–117. doi:10.1016/j.jhazmat.2006.07.067.

[29] A. Colacicco, G. De Gioannis, A. Muntoni, E. Pettinao, A. Polettini, R. Pomi, Enhanced electrokinetic treatment of marine sediments contaminated by heavy metals and PAHs, Chemosphere. 81 (2010) 46–56. doi:10.1016/j.chemosphere.2010.07.004.

[30] G.-N. Kim, W.-K. Choi, K.-W. Lee, Decontamination of radioactive concrete using electrokinetic technology, J. Appl. Electrochem. 40 (2010) 1209–1216. doi:10.1007/s10800-010-0088-8.

[31] H.B. Jung, J.-S. Yang, W. Um, Bench-scale electrokinetic remediation for cesium-contaminated sediment at the Hanford Site, USA, J. Radioanal. Nucl. Chem. 304 (2015) 615–625. doi:10.1007/s10967-014-3852-0.

[32] K.R. Reddy, P.R. Ala, S. Sharma, S.N. Kumar, Enhanced electrokinetic remediation of contaminated manufactured gas plant soil, Eng. Geol. 85 (2006) 132–146. doi:10.1016/j.enggeo.2005.09.043.

[33] J.-H. Choi, S. Maruthamuthu, H.-G. Lee, T.-H. Ha, J.-H. Bae, A.N. Alshawabkeh, Removal of phosphate from agricultural soil by electrokinetic remediation with iron electrode, J. Appl. Electrochem. 40 (2010) 1101–1111. doi:10.1007/s10800-010-0073-2.

[34] D.-H. Kim, J.-M. Cho, K. Baek, Pilot-scale ex situ electrokinetic restoration of saline greenhouse soil, J. Soils Sediments. 11 (2011) 947–958. doi:10.1007/s11368-011-0394-8.

[35] J.-H. Choi, Y.-J. Lee, H.-G. Lee, T.-H. Ha, J.-H. Bae, Removal characteristics of salts of greenhouse in field test by in situ electrokinetic process, Electrochim. Acta. 86 (2012) 63–71. doi:10.1016/j.electacta.2012.02.019.

[36] A.T. Lima, P.J. Kleingeld, K. Heister, J.P.G. Loch, In situ electro-osmotic cleanup of tar contaminated soil—Removal of polycyclic aromatic hydrocarbons, Electrochim. Acta. 86 (2012) 142–147. doi:10.1016/j.electacta.2011.12.060.

[37] E.-K. Jeon, J.-M. Jung, W.-S. Kim, S.-H. Ko, K. Baek, In situ electrokinetic remediation of As-, Cu-, and Pb-contaminated paddy soil using hexagonal electrode configuration: a full scale study, Environ. Sci. Pollut. Res. 22 (2015) 711–720. doi:10.1007/s11356-014-3363-0.

[38] L.M. Ottosen, T. Eriksson, H.K. Hansen, A.B. Ribeiro, Effects from different types of construction refuse in the soil on electrodialytic remediation, J. Hazard. Mater. 91 (2002) 205–219. doi:10.1016/S0304-3894(01)00388-0.

[39] A. Sawada, S. Tanaka, M. Fukushima, K. Tatsumi, Electrokinetic remediation of clayey soils containing copper(II)-oxinate using humic acid as a surfactant, J. Hazard. Mater. 96 (2003) 145–154. doi:10.1016/S0304-3894(02)00168-1.

[40] T. Kimura, K. Takase, S. Tanaka, Concentration of copper and a copper-EDTA complex at the pH junction formed in soil by an electrokinetic remediation process, J. Hazard. Mater. 143 (2007) 668–672. doi:10.1016/j.jhazmat.2007.01.011.

[41] M. Niinae, K. Nishigaki, K. Aoki, Removal of lead from contaminated soils with chelating agents, Mater. Trans. 49 (2008) 2377–2382. doi:10.2320/matertrans.M-MRA2008825.

[42] R.S. Putra, Y. Ohkawa, S. Tanaka, Application of EAPR system on the removal of lead from sandy soil and uptake by Kentucky bluegrass (Poa pratensis L.), Sep. Purif. Technol. 102 (2013) 34–42. doi:10.1016/j.seppur.2012.09.025.

[43] R. Lageman, Electroreclamation. Applications in the Netherlands, Environ. Sci. Technol. 27 (1993) 2648–2650. doi:10.1021/es00049a003.

[44] R. Lageman, R.L. Clarke, W. Pool, Electro-reclamation, a versatile soil remediation solution, Eng. Geol. 77 (2005) 191–201. doi:10.1016/j.enggeo.2004.07.010.

[45] G.-N. Kim, S. Kim, H.-M. Park, W.-S. Kim, U.-R. Park, J.-K. Moon, Cs-137 and Cs-134 removal from radioactive ash using washing–electrokinetic equipment,

Ann. Nucl. Energy. 57 (2013) 311–317. doi:10.1016/j.anucene.2013.02.016.

[46] K. Tamura, H. Sato, A. Yamagishi, Desorption of Cs^+ ions from a vermiculite by exchanging with Mg^{2+} ions: effects of Cs^+-capturing ligand, J. Radioanal. Nucl. Chem. (2015) 2205–2210. doi:10.1007/s10967-014-3744-3.

[47] I. Shimoyama, N. Hirano, Y. Baba, T. Izumi, Y. Okamoto, T. Yaita, S. Suzuki, Low-pressure sublimation method for cesium decontamination of clay minerals, Clay Sci. 18 (2014) 71–77.

[48] S. Igarashi, F. Mishima, Y. Akiyama, S. Nishijima, Fundamental study of cesium decontamination from soil by superconducting magnet, Phys. C Supercond. 494 (2013) 221–224. doi:10.1016/j.physc.2013.05.019.

[49] S. Ishiwata, A. Taga, F. Ogata, M. Kitakouji, H. Ouchi, H. Yamanishi, I. Masayo, Removal of radioactive cesium from soil by ammonium citrate solution and ionic liquid, J. Smart Process. 4 (2015) 294. doi:10.7791/jspmee.4.294.

[50] X. Yin, X. Wang, H. Wu, T. Ohnuki, K. Takeshita, Enhanced desorption of cesium from collapsed interlayer regions in vermiculite by hydrothermal treatment with divalent cations, J. Hazard. Mater. 326 (2017) 47–53. doi:10.1016/j.jhazmat.2016.12.017.

[51] M. Igawa, View for the achievement award 2016 from Japan Society of Ion Exchange, J. Ion Exch. 28 (2017) 45–50. doi:10.5182/jaie.28.45.

Chapter 2

Effects of the structure of biotite and vermiculite on adsorption behavior of cesium

2.1. Introduction

There are various 2:1 type clay minerals in nature. For example, biotite has potassium ions in the interlayer spaces, and then these potassium ions in the interlayer leach away during weathering, and biotite gradually transforms into vermiculite [1–4]. As a result, the edges of the clay mineral form a wedge shape, and the boundary between the non-expanded layer and the expanded layer can act as a frayed edge site (FES), which has strong interaction and high selectivity for Cs (**Fig. 2-1**). The weathered biotite has a higher selectivity for Cs adsorption and has been considered to be one of the main clay minerals that can adsorb radioactive Cs in the soil of Fukushima Prefecture, Japan [5]. However, some studies using imaging plates (IP) have indicated that adsorbing sites of biotite for radioactive Cs did not necessarily exist only at the outer edge of clay minerals. According to this study, the radiation intensity per mass of weathered biotite did not decrease after reducing the mass by trimming [6]. Moreover, when a small lump of weathered biotite was divided into several pieces, the radioactivity of each piece was similar to each other even though some pieces did not share equally the surface of the original lump [7]. These results indicated that radioactive Cs was not accumulated only at the specific part of the outer edge of clay minerals but was uniformly distributed over the weathered biotite. Vermiculite is a weathering product from biotite, and it is difficult to separate only vermiculite. Thus, biotite and vermiculite with various structural differences co-exist in most cases, and there is a possibility that their adsorption behavior to Cs is also different. Although the investigation of the adsorption behavior of Cs onto clay minerals is essential to develop the remediation method for the contaminated soil with Cs, it has not been discussed from a structural point of view.

In this chapter, the characteristics of six types of commercially available biotites

and vermiculites with different structures and localities were assessed. More specifically, the adsorption kinetics of Cs on these clay minerals and the differences between their Cs adsorption capacities were evaluated. From these results, the differences in the adsorption mechanism of each clay mineral were discussed in terms of its structure.

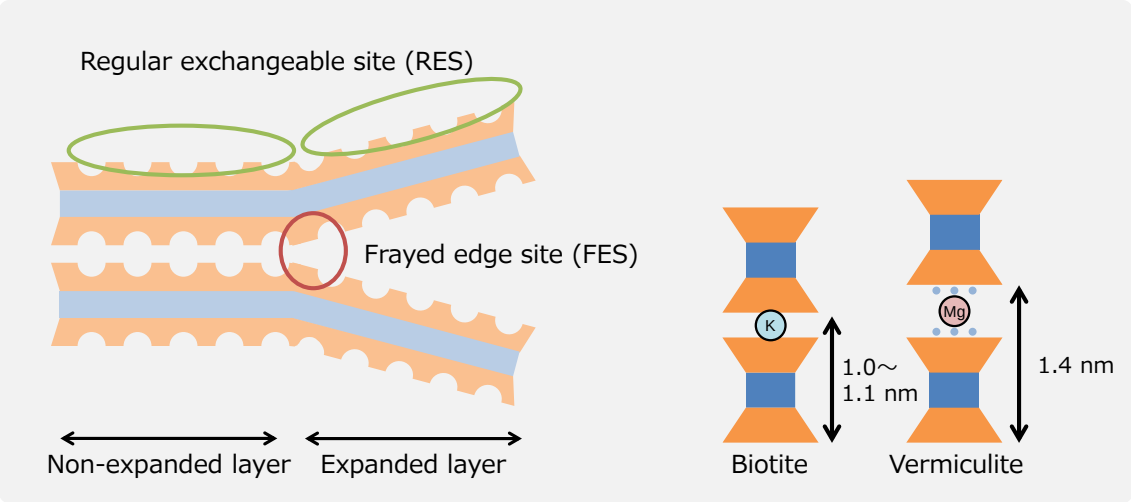

Fig. 2-1. Frayed edge site (FES) on clay minerals and structure of biotite and vermiculite.

2.2. Materials and methods

2.2.1. Materials and chemicals

The commercially available biotites and vermiculites used in this chapter were vermiculite (Verm-P) from Palabora mine (North Transvaal province, Republic of South Africa), vermiculite (Verm-L) from Libby (State of Montana, USA), vermiculite (Verm-I) from Ishikawa-Gun district (Fukushima Prefecture, Japan), biotite (Bio-T) from Tamura-Gun district (Fukushima Prefecture, Japan), biotite (Bio-C) from Shijiazhuang (Heibei province, China). These five kinds of clay minerals were purchased from Geo-Science Materials Nichika Inc., Japan. Exfoliated vermiculite for horticultural use (Verm-E) from China (the detailed location was not provided by the distributor) was

manufactured by thermal treatment and obtained from Kenis Limited, Japan.

Cesium chloride (CsCl), calcium chloride ($CaCl_2$), potassium chloride (KCl), ammonium acetate (CH_3COONH_4), sodium carbonate (Na_2CO_3), and $NaHCO_3$ (sodium hydrogen carbonate) were purchased by Fujifilm Wako Pure Chemical Corporation, Japan.

2.2.2. Characteristics of clay mineral

Fine clay mineral particles were prepared using a blender (WB-1, Osaka Chemical Co. Ltd., Japan) and sieved through a mesh to obtain particles smaller than 53 μm. The chemical composition of clay minerals was measured using an energy dispersive X-ray fluorescence spectrometer (XRF, JSX-3100RII, JEOL Ltd., Japan). The basal spacing of the clay minerals was measured using X-ray diffractometry (XRD, SmartLab, Rigaku Corporation, Japan). The diffractogram was recorded under the following conditions: Cu K*a* radiation (λ = 0.154 nm) at 40 kV and 30 mA, a scan rate of 1 °/min, and an angle step of 0.01°.

2.2.3. Adsorption experiment

A batch adsorption experiment was adopted for the adsorption kinetics. The procedure involved adding 20 mL of CsCl solution (1.0 mmol/L) to the clay minerals samples (sample weight 0.05 g) and shaking the mixture various times at 1000 rpm (Cute Mixer, CM-1000, EYELA, Tokyo Rikakikai, Co. Ltd., Japan). The shaken mixture was then filtered through a filter paper (5C, pore size 1 μm, Toyo Roshi Kaisha, Ltd., Japan) and a 0.45 μm Omnipore hydrophilic membrane filter (JHWP02500, Millipore, USA). The amount of Cs was determined using an atomic absorption spectrophotometer (AAS,

A-2000, Hitachi, Ltd., Japan) at 852.1 nm. The amount of Cs adsorbed onto clay minerals is given by **Eq. 2-1**.

$$q = \frac{(C_0 - C_e)V}{W} \quad \textbf{(2-1)}$$

Here, q indicates the adsorption capacity of clay minerals toward Cs (mg/g), and C_0 and C_e are the initial and final concentrations of Cs (mg/L), respectively. V indicates the volume of Cs solution (L), and W indicates the weight of each clay mineral (g).

Since CsCl was used as a chemical for the origin of Cs, the solution contained Cl and, the concentration of Cl was measured using an ion chromatography (IC) system with a conductivity detector (Compact IC 861, Metrohm Ltd., Switzerland) that included an anion column (IC SI-90 4E, 4.0 mm i.d. × 250 mm length, Shodex, Japan). The mobile phase was 0.18 mmol/L Na_2CO_3 and 0.17 mmol/L $NaHCO_3$, and the flow rate was 1.0 mL/min.

2.2.4. Adsorption kinetics model

The pseudo-first (**Eq. 2-2**) and pseudo-second (**Eq. 2-3**) order models were used for the estimation of the adsorption kinetics in this study.

$$\ln(q_e - q_t) = \ln q_e - \left(k_{p1}\, t\right) \quad \textbf{(2-2)}$$

$$\frac{t}{q_t} = \left(\frac{1}{k_{p2}\, q_e^2}\right) + \frac{t}{q_e} \quad \textbf{(2-3)}$$

where q_e and q_t are the adsorption capacities of clay minerals for Cs at the equilibrium time and time t, respectively, and k_{p1} (min^{-1}) and k_{p2} (g/mg/min) are the pseudo-first and pseudo-second order rate constants, respectively.

2.2.5. Adsorption isotherm model

The Langmuir and Freundlich adsorption isotherm models were used for the evaluation of the adsorption mechanism. The Langmuir adsorption isotherm model was expressed by **Eq. 2-4**:

$$K_L = \frac{q}{(q_m - q)C_e} \quad \textbf{(2-4)}$$

where K_L is the adsorption constant (L/mg), q_m is the maximum adsorption capacity (mg/g), C_e is the equilibrium concentration of Cs (mg/L).

The Freundlich adsorption isotherm model is expressed by **Eq. 2-5**:

$$q = K_F {C_e}^n \quad \textbf{(2-5)}$$

where K_F is the Freundlich constant, and n is a dimensionless parameter. The evaluation of the model equation of the adsorption isotherm was also performed by chi-square analysis (**Eq. 2-6**).

$$X^2 = \sum \frac{(q_e - q_{e,m})^2}{q_{e,m}} \quad \textbf{(2-6)}$$

The adsorption isotherm which had a lower value of X^2 was selected as an optimal isotherm [8].

2.2.6. Evaluation of RIP

Radiocesium interception potential (RIP) is an index for the Cs adsorption affinity on clay minerals [9]. In the procedure to obtain the RIP value, by meaning the regular exchangeable sites (RES) (**Fig. 2-1**), that is the adsorption sites on clay minerals except for the FES, were masked by silver thiourea or Ca ions, the amounts of Cs adsorbed just on the FES were estimated [10]. Conventionally, radioactive Cs has been used for this RIP evaluation, but there is a report of RIP evaluation using a stable isotope of Cs [11].

In this study, the RIP of clay minerals for Cs was evaluated using the following procedure.

The solution of 0.1 mol/L $CaCl_2$ and 0.5 mmol/L KCl was added to each clay mineral (solid:liquid ratio of 1:50), and the mixture was horizontally shaken at 150 rpm for 24 h at 25 °C (BR-40LF, Taitec Corporation, Japan). After centrifugation of the mixture at 10,000 rpm for 15 min (3700, Kubota Corporation, Japan), the supernatant was removed by decantation, then the fresh solution (0.1 mol/L $CaCl_2$ and 0.5 mmol/L KCl) was added again and shaken. This procedure was repeated six times to ensure the masking of the RES with Ca ions. The final mixture was filtered using a 5C filter paper and dried for 24 h at 80 °C in an oven (DK-62, Yamato Scientific Co., Ltd., Japan). The dried clay mineral (0.1 g) was added to 200 mL of solution (0.1 mol/L $CaCl_2$, 0.5 mmol/L KCl, and 0.5 mmol/L CsCl) and the solution was shaken at 150 rpm for 24 h at 25 °C. After filtration using a 5C filter paper, the concentration of Cs in the filtrate was measured by AAS. Since the RES was masked with Ca ion, Cs was adsorbed only on the FES. The RIP, which is an indicator of the FES, is calculated by **Eq. 2-7**.

$$\mathrm{RIP} = K_d^{Cs}\ [mK] \qquad \textbf{(2-7)}$$

Here, RIP is an indicator of FES on clay minerals toward Cs (mg/g), K_d^{Cs} indicated the solid-liquid distribution coefficient of Cs (L/g), and *[mK]* is the concentration of potassium ion (K^+) in solution (mg/L).

2.2.7. Desorption experiment

The desorption experiment for the evaluation of ion exchangeable form of Cs in clay minerals was conducted by using CH_3COONH_4 [12]. The amount of Cs which can be desorbed with a large amount of ammonium ion is evaluated as an ion exchangeable form. Clay minerals with saturated adsorption of Cs were prepared as follows. CsCl

solution (1.0 mmol/L) was added to 0.05 g of clay mineral samples, and the mixture was shaken for 24 h at 1,500 rpm. After filtration using a 5C filter paper, the solid on the filter was dried. The clay minerals with saturated adsorption of Cs were used for the evaluation of desorption. CH_3COONH_4 (1.0 mol/L) was added to each clay mineral (solid:liquid ratio was 1:5) and the mixture was shaken for one week at 1,500 rpm. The mixture was then centrifuged at 10,000 rpm for 15 min and the resulting supernatant liquid was filtered through a 0.45 μm Omnipore hydrophilic membrane filter. The amount of desorbed Cs was determined by AAS. The desorption efficiency was calculated using **Eq. 2-8**.

$$D_{ion} = \frac{C_{Des} \times V_{Ext}}{Q \times W_{Des}} \times 100 \quad \textbf{(2-8)}$$

Here, D_{ion} is the desorption efficiency with CH_3COONH_4, C_{Des} is the concentration of Cs extracted with CH_3COONH_4 (mg/L), and V_{Ext} is the volume of CH_3COONH_4 as an extraction solution (L). W_{Des} is the amount of contaminated clay mineral with Cs (g).

2.2.8. Preparation of Verm-P and Bio-T pretreated with K^+

Verm-P and Bio-T pretreated with K were used to understand the significance of basal spacing on the uptake of Cs. Prior research has demonstrated that the pretreatment of 2:1 type clay mineral with K reduced the basal spacing to 1.0 nm [2]. The pretreatment of Verm-P and Bio-T with K was conducted according to the previous study [13]. A volume of 50 mL of KCl solution (1.0 mol/L) was added to Verm-P and Bio-T (0.1 g) and the mixture was shaken for 24 h at 1,000 rpm. The mixture was then centrifuged at 4,000 rpm for 15 min and the resulting supernatant was discarded. A new solution of 50 mL of KCl (1.0 mol/L) was added to the mixture, followed by agitation and centrifugation. This procedure was repeated four times to ensure that the clay minerals were fully saturated with K. Then, the pretreated Verm-P and Bio-T were washed three times with distilled

water. The pretreated Verm-P and Bio-T after drying at 80 °C in an oven were subjected to XRD analysis.

2.3. Results and discussion

2.3.1. Characterization of clay mineral

The chemical components of the clay minerals used in this experiment were measured by XRF (**Table 2-1**) and compared with the literature values of clay minerals obtained from a similar production area. Verm-P and Verm-L had a similar chemical composition to "Hydrobiotite" and "Li1Ul" in previous studies [13,14]. Regarding Bio-T, the contents of Si, Al, and Mg were higher, and Fe was lower than that of "Fresh biotite" [15]. The Verm-E composition could not be compared with that obtained in the same production area but compared with that of Verm-L used in this study. Verm-E had a higher content of Al and a lower content of Mg than Verm-L.

Table 2-1. Chemical composition of oxides obtained by XRF in weight percent (wt%) for each clay mineral.

Clay	Chemical component, wt%								
mineral	SiO_2	Al_2O_3	TiO_2	Fe_2O_3	MnO	MgO	CaO	Na_2O	K_2O
Verm-P	48.7	11.3	0.9	3.9	ND	27.4	1.6	ND	6.2
Verm-L	47.9	12.7	1.0	6.1	ND	23.1	4.8	ND	4.1
Verm-I	45.2	19.1	0.2	2.8	ND	32.5	ND	ND	0.3
Verm-E	47.5	20.6	1.6	7.4	ND	15.9	1.4	ND	5.6
Bio-T	50.3	21.5	2.2	8.9	ND	9.9	1.4	ND	5.8
Bio-C	47.2	19.0	1.6	9.6	ND	15.6	1.0	ND	6.3

ND: Not detected

2.3.2. Adsorption kinetics

The amount of Cs adsorbed onto each clay mineral over the various contact times is shown in **Fig. 2-2**, and the kinetics parameters are listed in **Table 2-2**. In terms of the uptake of Cs by clay minerals, the pseudo-second order model was a suitable kinetic model for all clay minerals. Adsorption of Cs by clay minerals often follows the pseudo-second order model, indicating chemisorption [16–18]. On the other hand, the adsorption capacities calculated from the pseudo-second order model showed some differences between various types of clay minerals. According to **Fig. 2-2**, the adsorption equilibrium time was reached within 24 h in this study. The equilibrium times shorter than 48 h have also been reported in some previous studies [19–21]. In this study, the amount of Cs adsorbed by clay minerals changed rapidly up to 360 min, and the subsequent change was gradual. Therefore, 24 h was used as the equilibrium time for the adsorption isotherm evaluation in this study.

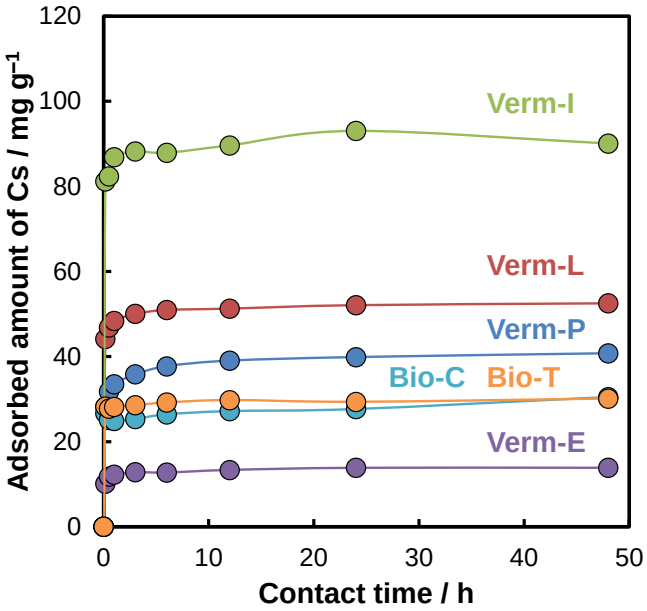

Fig. 2-2. Adsorbed amount of Cs onto each clay mineral as a function of the contact time.

Table 2-2. Parameters of adsorption kinetics of each clay mineral.

Clay	Pseudo-first order				Pseudo-second order			
mineral	q_e[a]	k_{p1}[b]	R^2	χ^2	q_e[a]	k_{p2}[c]	R^2	χ^2
Verm-P	37.2	0.131	0.951	1.695	38.5	0.006	0.983	0.639
Verm-L	50.4	0.207	0.974	0.488	51.2	0.011	0.997	0.156
Verm-I	88.3	0.250	0.991	0.726	89.4	0.009	0.995	0.361
Verm-E	12.6	0.158	0.772	0.215	13.2	0.023	0.970	0.057
Bio-T	29.0	0.368	0.994	0.149	29.2	0.068	0.996	0.111
Bio-C	26.7	0.639	0.964	0.877	27.0	0.077	0.966	0.830

[a] q_e in mg g^{-1}

[b] k_{p1} in min^{-1}

[c] k_{p2} in g mg^{-1} min^{-1}

2.3.3. Adsorption isotherm

Figure 2-3 shows the adsorption isotherms of each clay mineral for Cs, and **Table 2-3** shows the parameters obtained from the isotherm evaluations. According to the chi-square analysis, the adsorption isotherms of Verm-P, Verm-L, and Verm-I fitted better with the Langmuir adsorption isotherms. In contrast, Verm-E, Bio-T, and Bio-C fitted better with the Freundlich adsorption isotherm. The implications of these results are further discussed concerning the structure of these clay minerals in the following section.

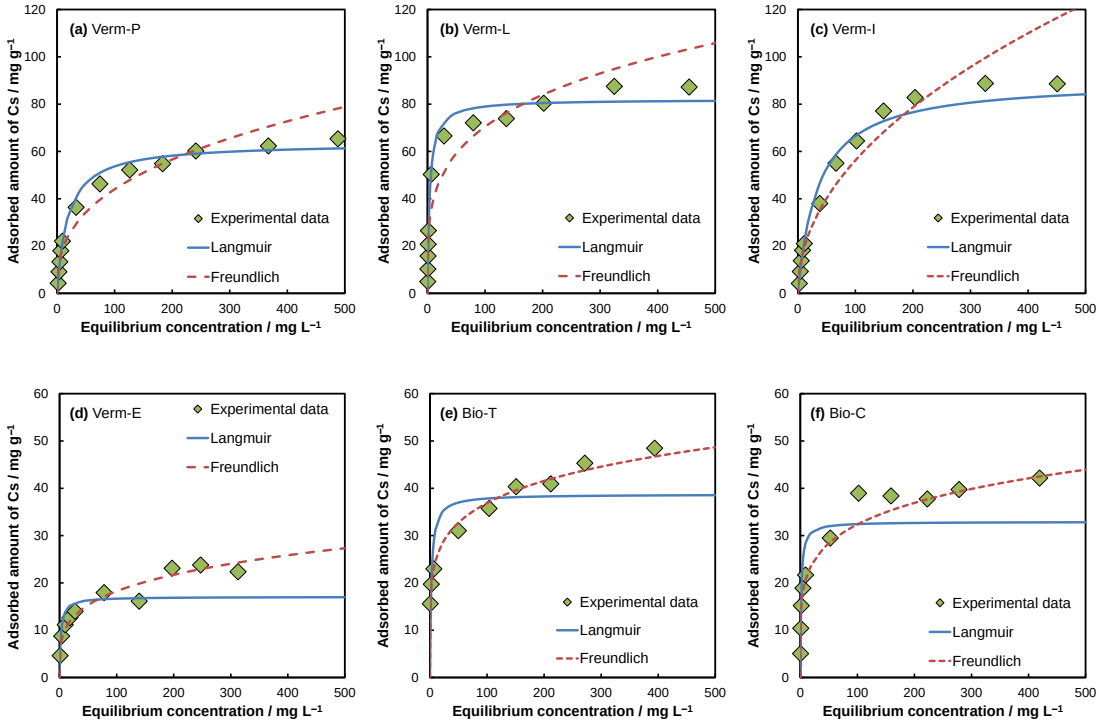

Fig. 2-3. Cs adsorption isotherm of **(a)** Verm-P, **(b)** Verm-L, **(c)** Verm-I, **(d)** Verm-K, **(e)** Bio-T, and **(f)** Bio-C. Fittings for Langmuir and Freundlich adsorption isotherm models are depicted as solid blue and dashed red lines, respectively.

Table 2-3. Parameters of the Langmuir and Freundlich isotherm models for Cs adsorption onto each clay mineral.

Clay	Langmuir				Freundlich			
mineral	q_{max}[a]	K_L[b]	R^2	χ^2	K_F[c]	$1/n$	R^2	χ^2
Verm-P	60.4	0.047	0.987	2.56	10.6	0.308	0.953	12.46
Verm-L	81.7	0.242	0.982	4.32	23.6	0.230	0.914	32.15
Verm-I	110.4	0.010	0.963	17.59	5.2	0.477	0.865	46.67
Verm-E	22.6	0.071	0.893	14.40	6.7	0.216	0.941	1.52
Bio-T	41.7	0.314	0.788	43.21	17.4	0.162	0.975	0.78
Bio-C	37.9	0.262	0.925	11.12	14.0	0.179	0.891	8.05

[a] q_{max} in mg g^{-1}

[b] K_L in L mg^{-1}

[c] K_F in (mg g^{-1}) (L mg^{-1})$^{1/n}$

2.3.4. Change in basal spacing

The basal spacing in clay minerals can be estimated by the *d*-value obtained from XRD. **Figure 2-4** shows the X-ray diffractograms of each clay mineral before and after saturated adsorption with Cs. Regarding the original Verm-P, it is possible to observe some reflections, as shown in **Fig. 2-4a**. The reflection around 1.2 nm is assigned to the interstratification in which the structures of vermiculite (1.4 nm) and biotite (1.0 nm) are alternately repeated [13]. This reflection was also observed as having a basal spacing of 1.4 and 1.0 nm. However, these reflections disappeared after saturated adsorption with Cs, and only a reflection at 1.0 nm was observed. A study has shown that the basal spacing of vermiculite becomes narrow to approximately 1.0 nm when Cs enters the interlayer by ion exchange with Mg [19]. This phenomenon was also observed in our Verm-P sample due to the penetration of Cs into the interlayer. The original Verm-L had a reflection at 1.4 and 1.3 nm of the *d*-value (**Fig. 2-4b**), and these reflections disappeared and gave place to a new reflection at approximately 1.0 nm after Cs adsorption. This change was similar to that observed in Verm-P. Verm-P and L are often written as hydrobiotite which has the interstratification structure of vermiculite (1.4 nm) and biotite (1.0 nm) [22,23]. Vermiculite and hydrobiotite are often produced from similar places [24], and it is difficult to distinguish them quantitatively, however, both clay minerals can capture Cs in their interlayer.

The basal spacing of the original Bio-T was estimated to be 1.1 nm (**Fig. 2-4e**), and this reflection became definite and the basal spacing became narrower after Cs adsorption. The clay mineral's basal spacing is expanded to more than 1.4 nm by leaching K from the interlayer during the weathering process and receiving Mg into the interlayer. However, Bio-T had no reflection in the range of angles lower than 1.4 nm ($2\theta = 6.3°$). Therefore,

Bio-T in this study was estimated to have been unaffected by weathering and was under relatively early conditions before weathering [15]. X-ray diffractograms of Verm-E are shown in **Fig. 2-4d**. It has been reported that when water molecules of hydrated ions in the interlayer space are removed, the structure of vermiculite collapses to reduce the basal spacing to approximately 1.0 nm [3]. Since Verm-E had been incinerated for horticultural use, the basal spacing of the original Verm-E could be considered to be approximately 1.0 nm. The XRD results indicated no significant change in the Verm-E basal spacing before and after Cs adsorption. This result was similar to that of Bio-T.

The thickness of the 2:1 type clay mineral sheet is approximately 1.0 nm [1,2], and the basal spacing of vermiculite is 1.4 nm. The calculated width of the interlayer space was approximately 0.4 nm in Verm-P and Verm-L, while the width of Bio and Verm-E having a basal spacing of 1.0 nm was almost 0 nm. This width suggests that Cs can penetrate the inner part of the interlayer space of Verm-P and Verm-L easily because this distance is sufficiently larger than the diameter of anhydrate Cs (0.33 nm). Verm-P had an interstratification structure, consisting of both the biotite structure with a narrow basal spacing (1.0 nm) and the vermiculite structure with a large basal spacing (1.4 nm). The reflection of 1.2 nm in Verm-P also disappeared after Cs adsorption. Because the basal spacing of the vermiculite structure of Verm-P became 1.0 nm from 1.4 nm due to Cs adsorption, and then the interstratification structure of Verm-P disappeared. On the other hand, the interlayer space of Verm-E, Bio-T, and Bio-C was almost 0 nm, and it was too narrow for Cs to enter the interlayer space. As a result, Cs was estimated to be adsorbed only on the surface ion exchangeable sites on Verm-E, Bio-T, and Bio-C. Verm-I showed different basal spacing changes with other clay minerals before and after Cs adsorption, it will be described in Chapter 4.

Consequently, the adsorption capacities of Verm-E, Bio-T, and Bio-C were smaller than those of Verm-P and Verm-L. According to a previous study, the ion exchange energy of clay minerals with a 1.1 nm basal spacing was almost 0 kJ/mol. While that of clay minerals with 1:2 nm basal spacing resulted in a negative ion exchange energy (i.e., the adsorption occurred easily) [25]. Such results agree with our study that the clay minerals with a basal spacing of 1.4 nm (Verm-P and Verm-L used in our study) could adsorb a larger amount of Cs effectively because the adsorbing sites existing in the interlayer space were used for Cs adsorption, which, in turn, resulted in large adsorption capacities (**Fig. 2-2**). On the other hand, clay minerals with a narrow basal spacing of approximately 1.0 nm (Verm-E, Bio-T, and Bio-C) could not strongly interact with Cs physically. This weak interaction is well reflected in the adsorption capacities of Verm-E, Bio-T, and Bio-C, whose capacities were smaller than those of Verm-P, Verm-L, and Verm-I (**Fig. 2-2**). The adsorption isotherms of Verm-E, Bio-T, and Bio-C did not fit well with the Langmuir adsorption isotherm model. For a more detailed consideration of the isotherm fitness, the adsorption/desorption experiments were carried out as follows.

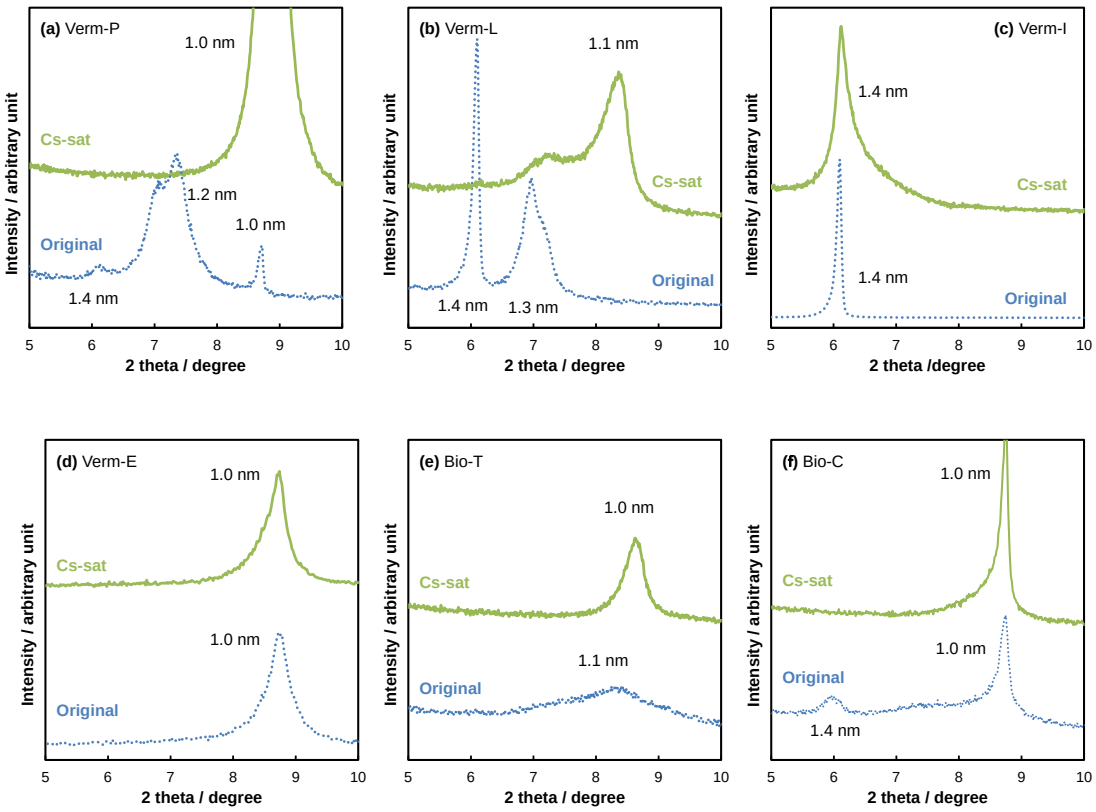

Fig. 2-4. X-ray diffractograms of **(a)** Verm-P, **(b)** Verm-L, **(c)** Verm-I, **(d)** Verm-E, **(e)** Bio-T, and **(f)** Bio-C. "Original" indicates before the adsorption of Cs, while "Cs-sat" indicates the clay mineral after the saturated adsorption of Cs. The numbers next to the peaks represent the *d*-values obtained for each clay mineral.

2.3.5. Evaluation of the adsorption site

From the investigation of the basal spacing in clay minerals in the previous section, clay minerals probably have some adsorption sites for Cs. Therefore, the amounts of each adsorption site in selected four kinds of clay minerals (Verm-P, Verm-L, Verm-E, and Bio-T) were estimated by RIP, an indicator of FES, and the ion exchangeable sites from Cs desorption with CH_3COONH_4.

The RIP of Verm-P, Verm-L, Verm-E, and Bio-T were 17.2, 37.8, 10.8, and 18.4 mg/g, respectively. **Figure 2-5** shows the X-ray diffractograms of each clay mineral after

Cs adsorption in the presence of Ca^{2+} and K^{+}. The basal spacing of clay minerals would become narrow (1.0 nm) when Cs adsorbs into the interlayer. A similar tendency was observed for the clay minerals used in this study without Ca^{2+} and K^{+} coexistence (**Fig. 2-4**). Verm-P and Verm-L could adsorb a certain amount of Cs even in the presence of Ca^{2+} and K^{+}, but the adsorption of Cs did not change the basal spacing to 1.0 nm (**Fig. 2-5**). Therefore, Cs might adsorb on the FES of these clay minerals but not on the interlayer sites in the presence of Ca^{2+} and K^{+}. This result indicated that the RIP obtained experimentally did not include the adsorption sites in the interlayer. The RIP was divided by the adsorption capacity after 24 h contact time to estimate the RIP contribution to the total capacity of each clay mineral. As mentioned in Section 2.2.7, the amount of Cs desorbed with CH_3COONH_4 indicated the ion exchangeable form of Cs in the clay mineral. The contribution of the ion exchangeable form was also calculated using the same procedure as used for the RIP contribution (**Fig. 2-6**).

RES indicates the adsorption sites in the planar and/or interlayer on the clay mineral [10], and Cs adsorbed on the RES could be desorbed easily by an ion exchange mechanism [12]. On the other hand, when Cs was adsorbed on the interlayer sites, it was difficult to desorb Cs by ion exchange because the collapse (narrowing the basal spacing) of the interlayer fixed Cs tightly in the narrowed interlayer [5,26]. Therefore, a portion of Cs that could not be desorbed by ion exchange was considered to be adsorbed in the interlayer site. Consequently, in the case of Verm-P, 15.8% of Cs was estimated to be adsorbed on the surface sites as the ion exchangeable form, 43.1% as RIP, and 41.1% was in the interlayer sites. In the case of Verm-L, 12.9% of Cs was in the ion exchangeable form, 72.6% as RIP, and 14.6% as the interlayer sites. On the other hand, the sum of ion exchangeable form and RIP in Bio-T was almost 100%, this was also true of Verm-E.

Such results suggest that the adsorption sites in the interlayer of Verm-E and Bio-T could not act as adsorption sites for Cs. As described in Section 2.3.4, the basal spacing was too narrow to receive Cs into their interlayer.

The Langmuir adsorption isotherm explained the adsorption behavior of Cs by Verm-P and Verm-L, these clay minerals had a high contribution of the interlayer and RIP to the total Cs adsorption. Both Cs adsorbed on the interlayer and Cs adsorbed on the FES formed similar inner sphere complexes [27]. Therefore, the affinity of the two adsorption sites (interlayer and FES) and Cs might be similar to each other. As a result, the difference between the interlayer and FES as the adsorption site was not distinguished in the adsorption isotherm evaluation, and then the adsorption of Verm-P and Verm-L could be explained by the Langmuir adsorption isotherm. According to **Fig. 2-6**, about 40% of Cs in Verm-E and Bio-T existed as the ion exchangeable form on the surface adsorption site, while others were indicated as RIP. The difference in the affinity between the ion exchangeable and FES was reflected in the isotherm, consequently, the Freundlich adsorption isotherm was more suitable for Verm-E and Bio-T than the Langmuir adsorption isotherm.

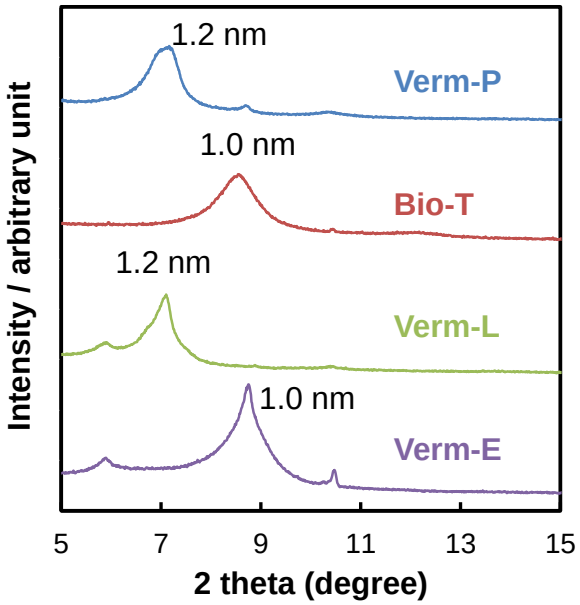

Fig. 2-5. X-ray diffractograms of each clay mineral after Cs adsorption. Solution was including 0.1 mol/L $CaCl_2$, 0.5 mmol/L KCl, and 0.5 mmol/L CsCl. The clay mineral sample was 0.1 g, the solution was 200 mL (pH 6), the contact time was 24 h, and the temperature was 25 °C.

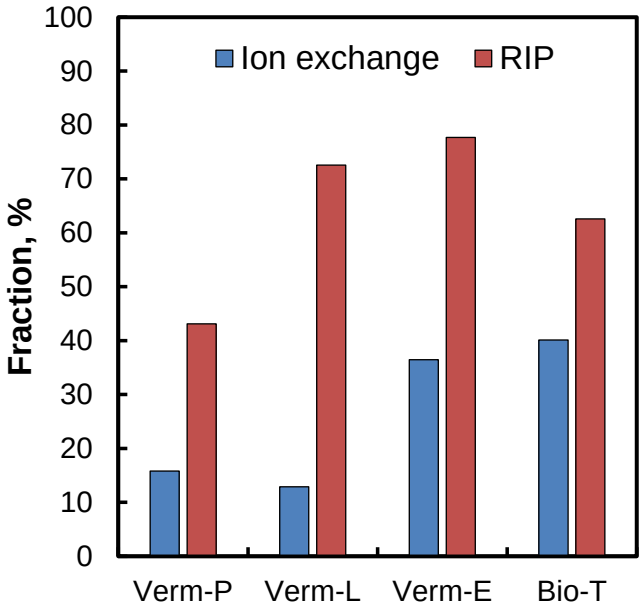

Fig. 2-6. Calculated fraction of adsorption site for Cs in each clay mineral.

2.3.6. Adsorption isotherm of pretreated Verm-P and Bio-T with K

To evaluate the effect of basal spacing on the Cs adsorption by clay minerals, the pretreated Verm-P and Bio-T with K were prepared and evaluated by XRD analysis and adsorption isotherms. Our results from the XRD analysis of pretreated Verm-P and Bio-T showed that the basal spacing of Verm-P became 1.0 nm after pretreatment. The basal spacing of Bio-T did not change significantly even though the shape of the reflection changed from broad to sharp (**Fig. 2-7**), suggesting that saturation with K did not affect the basal spacing of Bio-T.

The experimental results showed that the adsorption capacity of pretreated Verm-P was 21.5 mg/g after the contact time with K for 24 h. However, the value was almost half of the adsorption capacity of Verm-P without pretreatment with K (39.9 mg/g). On the other hand, the adsorption capacities of Bio-T did not change largely before and after pretreatment with K, just 29.4 mg/g and 24.4 mg/g, respectively.

Figure 2-8 shows the adsorption isotherms of the pretreated Verm-P and Bio-T. According to the chi-square analysis, the original Verm-P adsorption fitted well with the Langmuir adsorption isotherm (**Table 2-3**); however, it was not fitted for the pretreated Verm-P (**Table 2-4**). These findings suggest that Cs could not effectively penetrate the inner parts of the interlayer space of the pretreated Verm-P because of the reduction in the basal spacing of Verm-P due to saturation with K. On the other hand, the adsorption capacities of Bio-T before and after pretreatment with K were similar to that of the pretreated Verm-P (21.5 mg/g). Since the basal spacing of the original Bio-T was narrow from the beginning, the effect of pretreatment with K on the adsorption capacity was limited. Overall, these results show that basal spacing is a key property in controlling the adsorption capacities of Cs in 2:1 type clay mineral.

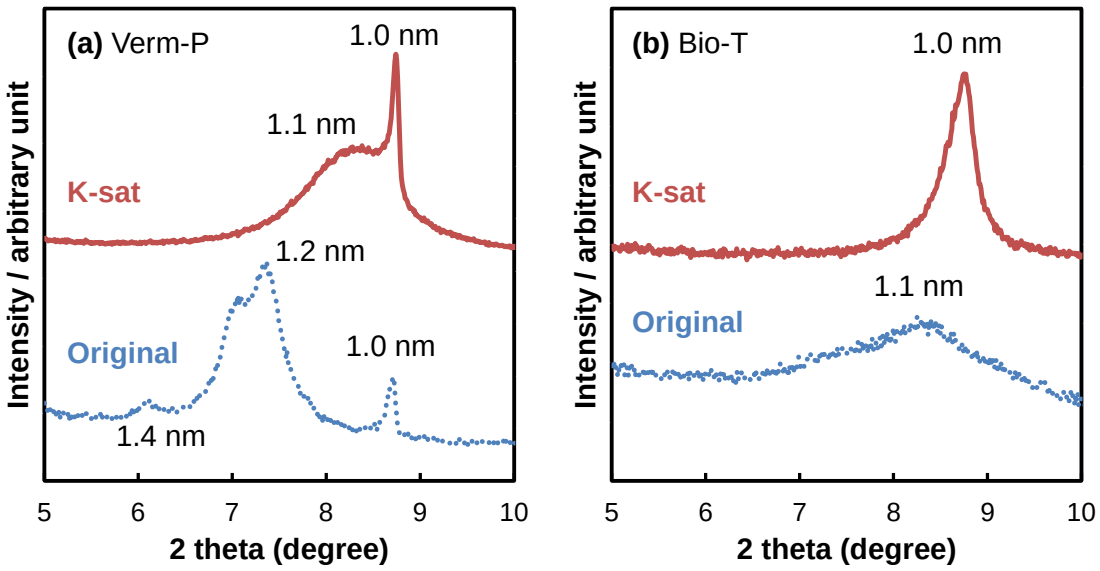

Fig. 2-7. X-ray diffractograms of **(a)** Verm-P, and **(b)** Bio-T before and after K saturation.

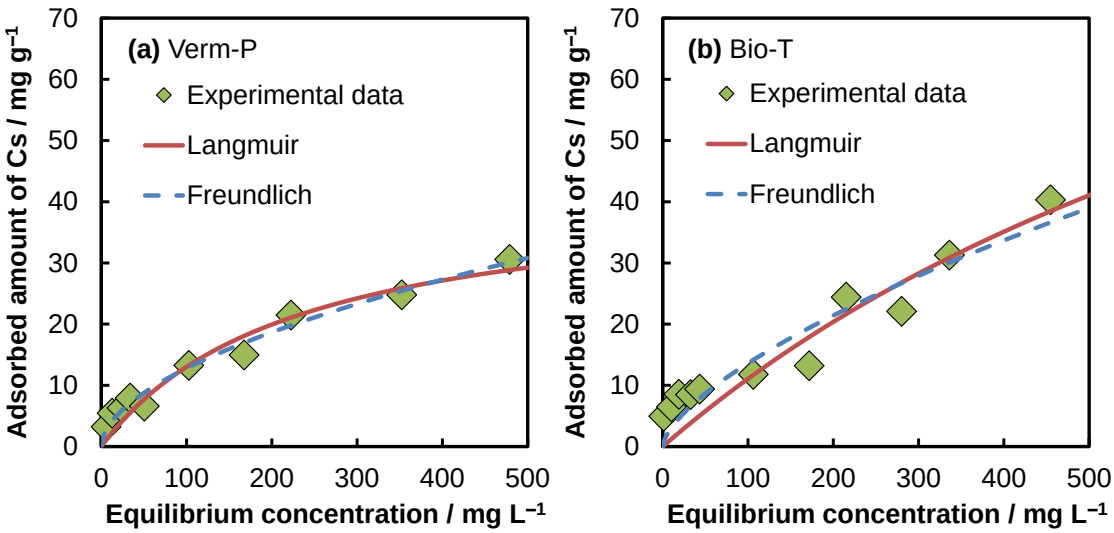

Fig. 2-8. Cs adsorption isotherms of **(a)** Verm-P and **(b)** Bio-T after K saturation. Fitting for the Langmuir and Freundlich adsorption isotherm models are shown as solid black and dashed gray lines respectively.

Table 2-4. Parameters of the Langmuir and Freundlich adsorption isotherm models for Cs adsorption onto Verm-P and Bio-T saturated with K.

Clay	Langmuir				Freundlich			
mineral	q_{max}[a]	K_L[b]	R^2	χ^2	K_F[c]	*1/n*	R^2	χ^2
Verm-P	42.4	0.004	0.971	12.77	1.03	0.546	0.967	2.61
Bio-T	127	0.001	0.923	233.0	0.67	0.654	0.913	38.17

[a] q_{max} in mg g^{-1}

[b] K_L in L mg^{-1}

[c] K_F in (mg g^{-1}) (L mg^{-1})$^{1/n}$

2.4. Summery

The adsorption kinetics, adsorption capacities, and adsorption isotherms of six commercially available 2:1 type biotite and vermiculite were discussed based on basal spacing and adsorption experiments for 24 hours and desorption experiments with CH_3COONH_4. Verm-P, Verm-L, and Verm-I had a large basal spacing enough to allow Cs to penetrate the inner part of the interlayer space. These clay minerals had a larger adsorption capacity than those of Verm-E, Bio-T, and Bio-C, which had a narrow basal spacing. The interlayer contribution to the whole Cs adsorption was high in Verm-P and Verm-L and low in Bio-T and Verm-E. The adsorption capacity of Verm-P with a narrow basal spacing by pretreatment with K was lower than that of the original Verm-P. These results indicate that the effect of the basal spacing of clay minerals is essential for the consideration of the Cs adsorption capacity and its behavior.

2.5. References

[1] J.W. Gruner, The structure of vermiculite and their collapse by dehidration, Am Mineral. 19 (1934) 557–575.

[2] H. Shirozu, Introduction to Clay Mineralogy –Fundamentals for Clay Science–, Asakura Publishing Co., Ltd., Tokyo, 1988. (in Japanese)

[3] T. Kogure, T. Murakami, Direct identification of biotite/vermiculite layers in hydrobiotite using high-resolution TEM., Mineralogical Journal. 18 (1996) 131–137. https://doi.org/10.2465/minerj.18.131.

[4] R. Motokawa, H. Endo, S. Yokoyama, H. Ogawa, T. Kobayashi, S. Suzuki, T. Yaita, Mesoscopic structures of vermiculite and weathered biotite clays in suspension with and without cesium ions, Langmuir. 30 (2014) 15127–15134. https://doi.org/10.1021/la503992p.

[5] H. Mukai, A. Hirose, S. Motai, R. Kikuchi, K. Tanoi, T.M. Nakanishi, T. Yaita, T. Kogure, Cesium adsorption/desorption behavior of clay minerals considering actual contamination conditions in Fukushima, Sci Rep. 6 (2016) 21543. https://doi.org/10.1038/srep21543.

[6] H. Mukai, T. Hatta, H. Kitazawa, H. Yamada, T. Yaita, T. Kogure, Speciation of radioactive soil particles in the Fukushima contaminated area by IP autoradiography and microanalyses, Environ Sci Technol. 48 (2014) 13053–13059. https://doi.org/10.1021/es502849e.

[7] H. Mukai, S. Motai, T. Yaita, T. Kogure, Identification of the actual cesium-adsorbing materials in the contaminated Fukushima soil, Appl Clay Sci. 121–122 (2016) 188–193. https://doi.org/10.1016/j.clay.2015.12.030.

[8] Y.-S. Ho, Selection of optimum sorption isotherm, Carbon. 42 (2004) 2115–2116. https://doi.org/10.1016/j.carbon.2004.03.019.

[9] A. Cremers, A. Elsen, P. De Preter, A. Maes, Quantitative analysis of radiocaesium retention in soils, Nature. 335 (1988) 247–249. https://doi.org/10.1038/335247a0.

[10] J. Wauters, A. Elsen, A. Cremers, A. V. Konoplev, A.A. Bulgakov, R.N.J. Comans, Prediction of solid/liquid distribution coefficients of radiocaesium in soils and sediments. Part one: A simplified procedure for the solid phase characterisation, Applied Geochemistry. 11 (1996) 589–594. https://doi.org/10.1016/0883-2927(96)00027-3.

[11] J. Lee, S.-M. Park, E.-K. Jeon, K. Baek, Selective and irreversible adsorption mechanism of cesium on illite, Applied Geochemistry. 85 (2017) 188–193. https://doi.org/10.1016/j.apgeochem.2017.05.019.

[12] L. Dzene, E. Tertre, F. Hubert, E. Ferrage, Nature of the sites involved in the process of cesium desorption from vermiculite, J Colloid Interface Sci. 455 (2015) 254–260. https://doi.org/10.1016/j.jcis.2015.05.053.

[13] R. Kikuchi, T. Kogure, Structural and compositional variances in “hydrobiotite” sample from Palabora, South Africa, Clay Science. 22 (2018) 39–52. https://doi.org/10.11362/jcssjclayscience.22.2.

[14] M.E. Gunter, Differentiation of commercial vermiculite based on statistical analysis of bulk chemical data: Fingerprinting vermiculite from Libby, Montana U.S.A., American Mineralogist. 90 (2005) 749–754. https://doi.org/10.2138/am.2005.1789.

[15] R. Kikuchi, H. Mukai, C. Kuramata, T. Kogure, Cs–sorption in weathered biotite from Fukushima granitic soil, Journal of Mineralogical and Petrological Sciences. 110 (2015) 126–134. https://doi.org/10.2465/jmps.141218.

[16] J.O. Kim, S.M. Lee, C. Jeon, Adsorption characteristics of sericite for cesium ions from an aqueous solution, Chem. Eng. Res. Design. 92 (2014) 368–374. https://doi.org/10.1016/j.cherd.2013.07.020.

[17] A.-A.M. Abdel-Karim, A.A. Zaki, W. Elwan, M.R. El-Naggar, M.M. Gouda, Experimental and modeling investigations of cesium and strontium adsorption onto clay of radioactive waste disposal, Appl Clay Sci. 132–133 (2016) 391–401. https://doi.org/10.1016/j.clay.2016.07.005.

[18] S. Khandaker, Y. Toyohara, G.C. Saha, M.R. Awual, T. Kuba, Development of synthetic zeolites from bio-slag for cesium adsorption: Kinetic, isotherm and thermodynamic studies, J. Water Process Eng. 33 (2020). https://doi.org/10.1016/j.jwpe.2019.101055.

[19] T. Kogure, K. Morimoto, K. Tamura, H. Sato, A. Yamagishi, XRD and HRTEM evidence for fixation of cesium ions in vermiculite clay, Chem Lett. 41 (2012) 380–382. https://doi.org/10.1246/cl.2012.380.

[20] N. Suzuki, S. Ozawa, K. Ochi, T. Chikuma, Y. Watanabe, Approaches for cesium uptake by vermiculite, Journal of Chemical Technology & Biotechnology. 88 (2013) 1603–1605. https://doi.org/10.1002/jctb.4145.

[21] H. Long, P. Wu, L. Yang, Z. Huang, N. Zhu, Z. Hu, Efficient removal of cesium from aqueous solution with vermiculite of enhanced adsorption property through surface modification by ethylamine, J Colloid Interface Sci. 428 (2014) 295–301. https://doi.org/10.1016/j.jcis.2014.05.001.

[22] A.L. Boettcher, Vermiculite, hydrobiotite, and biotite in the Rainy Creek igneous complex near Libby, Montana, Clay Miner. 6 (1966) 283–296.

https://doi.org/10.1180/claymin.1966.006.4.03.

[23] G.W. Brindley, P.E. Zalba, C.M. Bethke, Hydrobiotite, a regular 1:1 interstratification of biotite and vermiculite layers, Am. Mineralogist. 68 (1983) 420–425.

[24] J. Brossier, F. Altieri, M.C. de Sanctis, A. Frigeri, M. Ferrari, S. de Angelis, A. Apuzzo, N. Costa, Constraining the spectral behavior of the clay-bearing outcrops in Oxia Planum, the landing site for ExoMars "Rosalind Franklin" rover, Icarus. 386 (2022). https://doi.org/10.1016/j.icarus.2022.115114.

[25] M. Okumura, S. Kerisit, I.C. Bourg, L.N. Lammers, T. Ikeda, M. Sassi, K.M. Rosso, M. Machida, Radiocesium interaction with clay minerals: Theory and simulation advances Post–Fukushima, J Environ Radioact. 189 (2018) 135–145. https://doi.org/10.1016/j.jenvrad.2018.03.011.

[26] S.-M. Park, J.-S. Yang, D.C.W. Tsang, D.S. Alessi, K. Baek, Enhanced irreversible fixation of cesium by wetting and drying cycles in soil, Environ Geochem Health. 41 (2019) 149–157. https://doi.org/10.1007/s10653-018-0174-0.

[27] Q.H. Fan, M. Tanaka, K. Tanaka, A. Sakaguchi, Y. Takahashi, An EXAFS study on the effects of natural organic matter and the expandability of clay minerals on cesium adsorption and mobility, Geochim Cosmochim Acta. 135 (2014) 49–65. https://doi.org/10.1016/j.gca.2014.02.049.

Chapter 3

Desorption of cesium ion from biotite with organic acid

3.1. Introduction

To reduce the volume of contaminated soil with radioactive Cs, it is necessary to separate soil particles containing Cs physically from the soil or to desorb Cs from soil particles chemically. The radioactive Cs tends to be accumulated in the clay fraction of the soil which is expected to be separated based on the particle size [1]. However, this separation process is not effective in soils whose proportion of fine clay particles is high originally. Although the chemical or heating treatment is effective for such soil with fine clay particles [2], a large volume of wastewater and residual solvent after the treatment of the soil is generated newly, and thus no-pilot scale chemical treatment has currently been investigated [3].

In the previous studies on chemical treatment, inorganic acids such as hydrochloric acid, nitric acid, and hydrofluoric acid were used. The maximum removal efficiency of 71% was obtained by 6 mol/L nitric acid, however, this removal efficiency decreased increasing with fine clay particles in the soil [4]. Hydrofluoric acid has been used for the complete decomposition of soil [5], and can be used for the chemical treatment of Cs contaminated soil [6]. Hydrofluoric acid is highly corrosive, difficult to handle, and expensive among the common inorganic acids. Since these inorganic acids have a high environmental impact, the use of these acids will need additional water treatment. Therefore, organic acid which is a natural product has been attempted for the removal of Cs due to its low environmental impact. Some organic acids such as citric acid and oxalic acid have been used to remove iron as an impurity in kaolinite or quartz [7,8].

The fraction of clay minerals in the soil can be separated only by particle size, but the specific clay minerals cannot be identified quantitatively. In Fukushima Prefecture, it is known that biotite, which is a weathering product of Abukuma granite, adsorbs Cs well

[9]. Therefore, in the separation of Cs from soil aiming at reducing the volume of the contaminated soil, the desorption of Cs from this biotite is the most important. Especially, it is important to develop a method to desorb Cs bound strongly with biotite under soft and environmentally friendly conditions.

In this chapter, some organic acids were used for the desorption experiment of Cs from biotite. The effect of treatment conditions such as heating temperature and time on Cs desorption efficiency was investigated. At the same time, the changes in the chemical composition and structure of clay minerals were evaluated in various treatment conditions, and the desorption mechanism was discussed. Finally, the treatment without heating was also investigated to perform the processing with as low energy as possible.

3.2. Materials and methods

3.2.1. Materials and chemicals

In this chapter, biotite (Bio-T, Tamura-gun district, Fukushima Prefecture, Japan) was used as model soil, and the detailed properties of Bio-T were described in Chapter 2. Cesium chloride (CsCl, > 99%), acetic acid (MW = 60.05, 99%), citric acid (192.12, 98%), DL-malic acid (134.09, 99%), malonic acid (104.06, 98%), oxalic acid (90.03, 98%), and L(+)-tartaric acid (150.09, 99%) were purchased from Fujifilm Wako Pure Chemical Corporation., Japan. Hydrochloric acid (HCl, 35–37%), nitric acid (HNO_3, 60–61%), potassium hydroxide (KOH, > 86%), lithium nitrate ($LiNO_3$, > 98%), sodium oxalate (Reference materials for volumetric analysis, > 99.95%,) indole (Guaranteed reagent, > 98.0%) and sulfuric acid (Guaranteed reagent, > 96.0%) was purchased from Kanto Chemical Co., Inc., Japan. All reagents were guaranteed reagent grade and used without any pretreatment.

3.2.2. Preparation of Cs-saturated Bio-T

Bio-T pretreated by the procedure of Section 2.2.2 was used for the following procedure to prepare Cs-saturated Bio-T. The Cs solution (5,000 mg/L; pH 6.0 without any adjustment) was added to the crushed Bio-T (solid: liquid ratio of 1:10), and the mixture was horizontally shaken for 48 h at 170 rpm with a reciprocating shaker (Recipro shaker SR-2S, Taitec Corporation, Japan). The mixture was filtered using a 5C filter paper and the residues dried overnight at 80 °C. Cs adsorbed biotite on the filter paper was crushed using an agate mortar and used for subsequent experiments. The concentration of Cs in the filtrate was measured using an atomic absorption spectrophotometer (AAS, ZA-3300, Hitachi Ltd., Japan) at 852.1 nm, and then the adsorption capacity of Bio-T (q) was calculated using **Eq. 2-1**.

3.2.3. Desorption experiment

Oxalic acid is known to form complexes with heavy metals [10]. In this chapter, oxalic acid treatment at high temperatures was investigated as a desorption method for Cs from model contaminated Bio-T. The procedure was as follows: 0.05 g of model contaminated Bio-T with Cs was added to 25 mL of oxalic acid aqueous solution and heated at various temperatures and times. After heating, the mixture was filtered through a 5C filter paper. The concentration of Cs in the filtrate was measured using AAS. The desorption efficiency of Cs from Bio-T was calculated using **Eq. 3-1**.

$$\text{Desorption efficiency (\%)} = \frac{C_{Des}\, V_{Ext}}{q\, W_{Des}} \times 100 \qquad \textbf{(3-1)}$$

where C_{Des} is the concentration of Cs in the solution after each treatment (mg/L); V_{Ext} is the volume of the extraction solution (L); and q is the adsorption capacity of Bio-T; W_{Des} is the weight of model contaminated biotite with Cs used for each treatment (g).

Several organic acids (acetic, citric, malic, malonic, and tartaric acid), inorganic acids (HCl and HNO_3), and inorganic salts (KOH and $LiNO_3$) were used in the same procedure to compare their desorption efficiency with that of oxalic acid. The pH was measured using a pH meter (M-13, Horiba Ltd., Japan). The concentration of oxalic acid was measured by direct colorimetric determination with indole at 525 nm (UV-3100PC, Shimadzu Corporation, Japan) [11].

3.2.4. Effect of aging time

Cs is considered to transform into irreversible adsorption sites over time after contact with a clay mineral. Therefore, the effect of aging time should be evaluated for the desorption experiment. The Cs adsorbed biotite which was prepared according to the procedure of Section 3.2.2 was stored in a zipper plastic bag and kept for 1, 2, and 3 months at room temperature (approximately 20 °C). After that, the desorption experiment was operated according to Section 3.2.3.

3.2.5. Desorption experiment without heating

For the purpose of reducing the energy involved in desorption, the desorption efficiency was evaluated at room temperature without heating. The detailed desorption procedure was the same as that in Section 3.2.3. Bio-T which has an aging time of three months was used for the desorption experiment. The mixture of Bio-T and oxalic acid was stood for 1 h, 1 d, 3 d, 1 w, 2 w, 3 w, and 4 w at room temperature. As a comparison, 1 mol/L $LiNO_3$ as ion exchangeable form and 0.1 mol/L oxalic acid was also used as a leaching solution. The room temperature was continuously measured using a Thermo recorder (TR-71U, T&D Corporation, Japan).

3.3. Results and discussion

3.3.1. Effect of temperature and contact time

The optimal conditions for heating temperature and time were evaluated. The efficiency of Cs desorption from biotite was measured by heating Bio-T with 0.5 mol/L oxalic acid at 20, 50, 85, and 100 °C for 4 h **(Fig. 3-1a**). The desorption efficiency increased with increasing temperature. Since there was no difference between the efficiency achieved at 85 and 100 °C, 85 °C was used in the following experiments. **Figure 3-1b** shows that the maximum desorption efficiency was observed at 85 °C for 2 h. It has been previously reported that 70% of Cs was removed by heating at 200 °C with citric acid, and the desorption efficiency increased to 95% by repeating the hydrothermal treatment five times [12]. However, this study shows that a single oxalic acid treatment provides high desorption efficiency at a lower temperature (85 °C) compared to the treatment with citric acid (200 °C) [12], thus reducing the energy required for heating. According to a previous study, when oxalic acid dissolves iron, the iron surface needs to be enough protonated under low pH conditions [13]. Since the pH of the citric acid solution (approximately 1.6) is not as low as that of the oxalic acid solution (0.8), the protonation of the iron surface by citric acid is lower than that of oxalic acid. As described later, the desorption of Cs from biotite with organic acid was induced by the degradation of clay mineral structure and it was triggered by the dissolution of iron in clay mineral. Therefore, oxalic acid treatment is more effective for Cs desorption than citric acid.

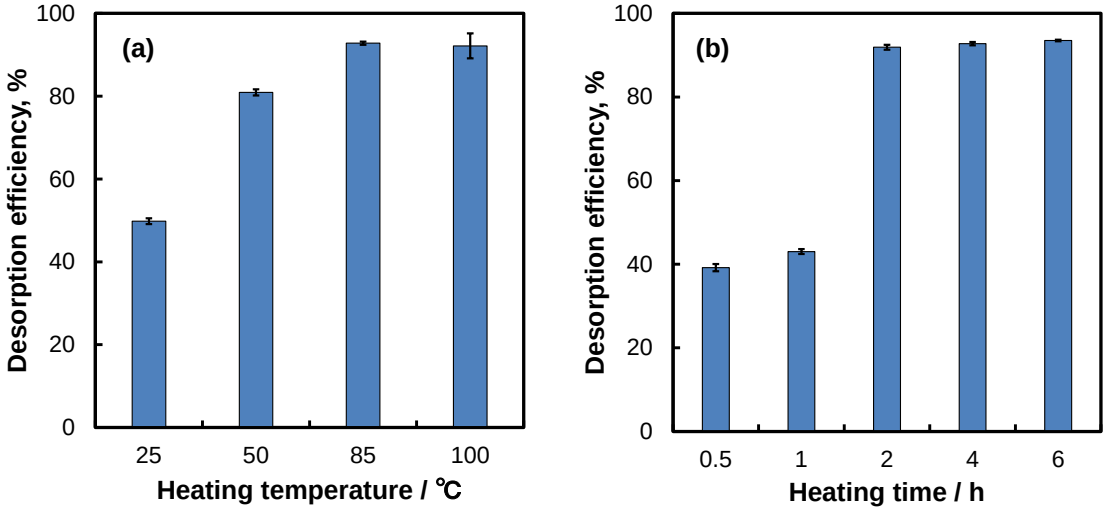

Fig. 3-1. Desorption efficiency of Cs from biotite by the oxalic acid treatment as a function of **(a)** temperature (4 h reaction time) or **(b)** heating time (85 °C reaction temperature).

The activation energy can be calculated by the Arrhenius plot with k_{p2} from the pseudo-second order model [14]. Since desorption kinetics was fitted with the pseudo-second order model at 25, 50, and 80 °C conditions (**Table 3-1**), the Arrhenius plot was induced from the k_{p2} of the pseudo-second order model. The activation energy calculated from the slope of the Arrhenius plot was 56.6 kJ/mol (**Fig. 3-2**), which is very higher than that of Cs desorption from zeolite using ion exchange (5.9 kJ/mol) [14]. Therefore, the desorption of Cs from biotite by oxalic acid required high activation energy, and temperature is an important factor in this desorption process.

Table 3-1. Parameters of desorption kinetics of Cs from biotite by oxalic acid treatment.

Biotite	Pseudo-first order			Pseudo-second order		
	R^2	q_e[a]	k_{p1}[b]	R^2	q_e[a]	k_{p2}[c]
25 °C	0.7334	6.94	0.034	0.9997	26.6	0.014
50 °C	0.1616	4.26	0.005	0.9965	34.4	0.003
85 °C	0.8182	27.58	0.022	0.9027	39.3	0.008

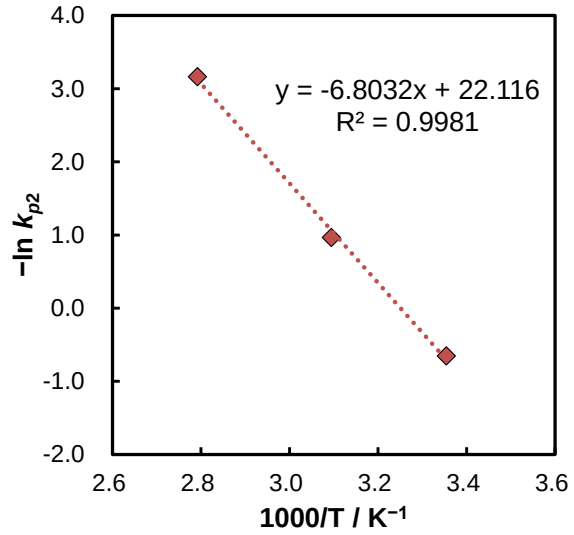

Fig. 3-2. Arrhenius plot of the desorption of Cs from Bio-T by oxalic acid.

3.3.2. Evaluation of structural change

The elemental compositions and structures of the residuals obtained after oxalic acid treatment were investigated using XRF and XRD. **Figure 3-3a** shows the elemental composition of residuals at each heating time. The Al content decreased moderately, whereas the Fe and Mg contents decreased drastically with increasing heating time. The contents of Al, Fe, and Mg decreased by 50%, 91%, and 95%, respectively, after 4 h of heating. The reduction rate of major elements in Bio-T plateaued after 4 h. Therefore, a treatment time of 4 h was used for further experiments. Al and Fe in the solids were eluted due to hydrolysis and complex formation with oxalic acid [10,15]. **Figure 3-3b** shows the XRD pattern of the original Bio-T (Original), Bio-T saturated with Cs (Cs-sat), and the residuals at each heating time (for 0.5 to 6.0 h). The basal spacing of the clay minerals was 1.0 nm after Cs adsorption. The original Bio-T used in this study had a broad peak around 8.0–8.3° (d = 1.1 nm), which shifted to 8.8° (d = 1.0 nm) after the adsorption of

Cs (Cs-sat). This peak decreased as the heating time increased, and no peak was detected after the heating time exceeded 2 h. These results indicate that the Al, Fe, and Mg in Bi-T were eluted into the solution by the oxalic acid treatment, and Bio-T was decomposed. In a previous study, the intensity at around 1.0 nm of illite, which is a 2:1 type clay mineral, was found to persist even after oxalic acid and HCl treatment [16]. Biotite and illite have a mica-like structure. The octahedral sheet of biotite consists mainly of Fe or Mg (trioctahedral), and the sheet of illite consists of Al (dioctahedral) [17], moreover, Fe- or Mg-rich clay minerals are less resistant to acid than Al-rich ones [18]. The contents of Fe and Mg in Bio-T used in this study are higher than that of illite in the previous study, and Bio-T was identified as having a trioctahedral sheet by XRD (Chapter 2). Therefore, the higher desorption efficiency observed in this study than in the previous one was attributed to the differences in the clay mineral structure.

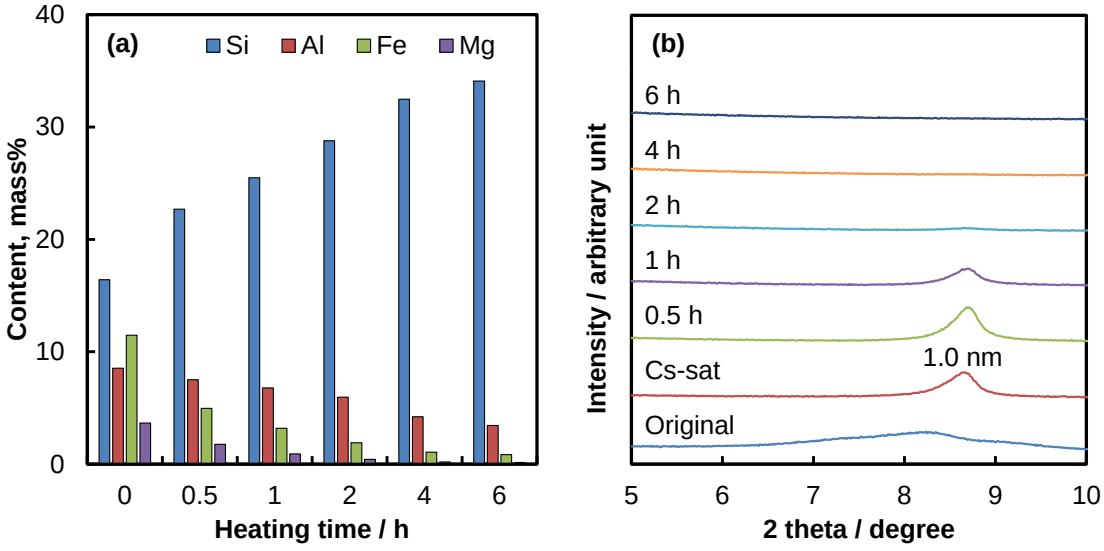

Fig. 3-3. (a) Chemical composition and **(b)** X-ray diffractograms of Bio-T after oxalic acid treatment.

3.3.3. Comparison with organic and inorganic acids

As shown in **Fig. 3-3a**, oxalic acids eluted elements such as Al, Fe, and Mg in Bio-T into the solution. The desorption efficiency of oxalic acid was compared with that of some organic and inorganic acids at the same concentration (0.5 mol/L) (**Table 3-2**). There was almost no change in the pH before and after treatment. Among the organic acids, oxalic acid showed the highest desorption efficiency. Although the solutions of most organic acids showed a pH 1.5–2.5, only oxalic acid had a pH below 1 due to its strong acidity. The pH of both 0.5 mol/L HCl and HNO_3 in this system was approximately 0.3, and the desorption efficiency for Cs was 95.3%. These results indicate that a high Cs desorption efficiency can be obtained under conditions where the pH is lower than 1. Acetic acid and citric acid solution, whose pH was adjusted to 0.8 with HNO_3, were able to desorb at a slightly higher efficiency of 52.8% and 72.2% than those without pH adjustment, respectively. The acid dissociation constants (pK_{a1}) of acetic, citric, and oxalic acids were 4.76, 2.90, and 1.04, respectively [19]. Acetic acid and citric acid have little dissociation at pH 0.8, and complex formation with metal ions cannot be expected. Fe dissolution with oxalic acid occurs via reduction and complex formation reaction, and the reduction of Fe(III) to Fe(II) with oxalic acid is ideal for complex formation at pH 1.5 [20]. Some parts of oxalic acid dissociate at pH 0.8 and can form a complex with metal ions. Veglio et al. reported complex formation between oxalic acid and Fe at pH 2–3 [20]. The experimental conditions used in this study may not be optimal, but oxalic acid has a more significant effect on Cs desorption from Bio-T than other organic acids because of the decomposition of Bio-T by reduction and complex formation.

In the alkaline and inorganic acids solution, the desorption efficiency by KOH was 48.8%, indicating that the basic conditions were not as effective as the acidic ones.

However, both HCl and HNO_3 had desorption efficiencies of greater than 95%. HCl and HNO_3 are known to desorb Cs from clay minerals due to the decomposition of the clay minerals [21,22]. However, the use of HCl is accompanied by the generation of hydrogen chloride gas, and HNO_3 has a high environmental impact owing to secondary contamination by nitrate ions. Since oxalic acid has a low environmental impact, its use is recommended for the desorption of Cs from Bio-T.

Table 3-2. Desorption efficiency of Cs from Bio-T by different extraction solutions. Bio-T: 0.05 g; the volume of each solution: 25 mL; concentration of extraction solution: 0.5 mol/L; heating time: 4 h; and temperature: 85 °C. Acetic acid (0.8) and citric acid (0.8) indicate acetic acid and citric acid adjusted to pH 0.8 with nitric acid, respectively.

Elution	Initial pH	After pH	Efficiency, %
DW	5.9	8.4	17.7
Acetic acid	2.5	2.7	37.3
Acetic acid (0.8)	0.8	0.8	52.8
Citric acid	1.6	1.7	66.4
Citric acid (0.8)	0.8	0.9	72.2
Malic acid	1.8	1.9	51.1
Malonic acid	1.5	1.6	56.5
Oxalic acid	0.8	0.8	94.8
Tartaric acid	1.6	1.7	68.9
KOH	13.4	13.3	48.8
HCl	0.3	0.4	95.3
HNO_3	0.3	0.3	95.3

3.3.4. Effect of concentration and solid/liquid (S/L) ratio

When 25 mL of 0.5 mol/L oxalic acid was added to 0.05 g of Bio-T, heating at 85 °C for 4 h was the optimum condition for the desorption of Cs. However, the amount of reagents used should be as small as possible. Therefore, the concentration of oxalic acid and solid/liquid (S/L) ratio was investigated in this study. The desorption efficiency of Cs

increased with increasing oxalic acid concentration (**Fig. 3-4a**). Although 0.5 mol/L provided the optimum conditions, over 90% of desorption efficiency was obtained at > 0.1 mol/L oxalic acid. **Figure 3-4b** shows the desorption efficiency at various S/L ratios at 0.5 mol/L oxalic acid. Although the desorption efficiency decreased slightly when the S/L ratio was small, 90% or more of Cs was desorbed even at the ratio of 1:50. A low S/L ratio is expected to increase the amount of contaminated soil that can be decomposed by oxalic acid. The concentration of oxalic acid decreased by 6.2% after the treatment. The redox reaction also contributes to the elution of Fe (**Eq. 3-2**) [8,23].

$$H^+ + Fe_2O_3 + 5HC_2O_4^- \rightarrow 2Fe(C_2O_4)_2^{2-} + 3H_2O + 2CO_2 \quad \textbf{(3-2)}$$

In this study, some amounts of oxalic acid were reduced due to the conversion into water and carbon dioxide by the redox reaction in **Eq. 3-2**. However, approximately 0.46 mol/L of oxalic acid remained, and it is possible to reuse it for the decomposition of biotite because even 0.1 mol/L of oxalic acid can desorb 90% of Cs from biotite (**Fig. 3-4a**).

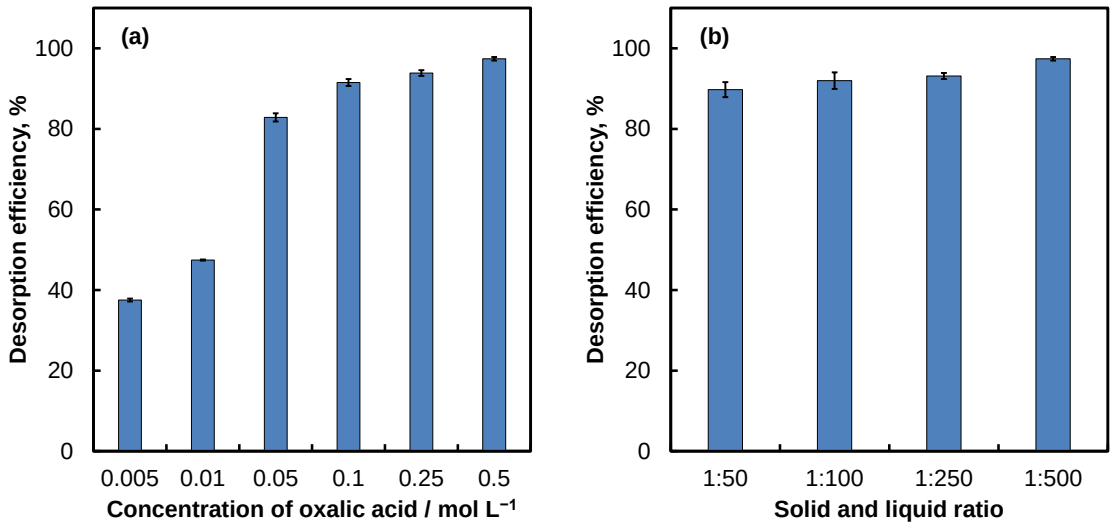

Fig. 3-4. (a) Desorption efficiency of Cs from biotite for the various concentrations of oxalic acid and **(b)** various solid and liquid ratios (0.5 mol/L oxalic acid). Heating time: 4 h; and temperature: 85 °C. Error bars indicate standard deviation (n = 3).

3.3.5. Effect of aging time for desorption efficiency

The main interaction between Cs and clay minerals (especially illite and vermiculite) was presumed to be an inner-sphere complex from extended X-ray absorption fine structure (EXAFS) analysis [24]. Moreover, the interaction between Cs and soil (weathered granite) is strong and Cs forms an inner-sphere complex with clay minerals derived from granite [25]. Since inner-sphere complexes are formed by strong interactions, desorption by ion exchange is difficult. Therefore, Cs in clay mineral having a longer aging time was more difficult to desorb by ion exchange. Since Li and Na have higher hydration energy than Cs, it is expected that these elements will desorb Cs by expanding the layers of the edge of the clay minerals. However, the desorption efficiency of radioactive Cs with Li from weathered biotite drastically decreased after 168 h of aging time [22]. Therefore, the effect of aging on desorption efficiency by oxalic acid treatment is important.

Figure 3-5 indicates that the desorption efficiency by oxalic acid treatment was 93.8%, 95.1%, and 97.9% for 1, 2, and 3 months of aging time, respectively. In contrast, Li can desorb Cs only 35.5%, 35.7%, and 33.7% after 1, 2, and 3 months of aging time, respectively. The ion exchange form of Cs in Bio-T was approximately 40% (Chapter 2), and Li can desorb this ion exchangeable form of Cs. This result indicates that oxalic acid can desorb not only the ion exchange form of Cs but also the more strongly bound form of Cs like the inner-sphere complex. High desorption efficiency with oxalic acid treatment was obtained even in biotite with 3 months of aging, indicating that desorption by oxalic acid treatment is hardly affected by aging. The desorption of Cs is accompanied by the decomposition of Bio-T (Section 3.3.3), and the effect of the chemical form of Cs in Bio-T is not significant in desorption efficiency. Therefore, this oxalic acid treatment has the

potential to desorb Cs from the soil after long aging (i.e., several months or years) because of the effects of the acid conditions and complex formation. Clarifying the effect of aging on the desorption of Cs by oxalic acid treatment, which had not been investigated in the previous study [16], will contribute to developing remediation technology for radioactive soil.

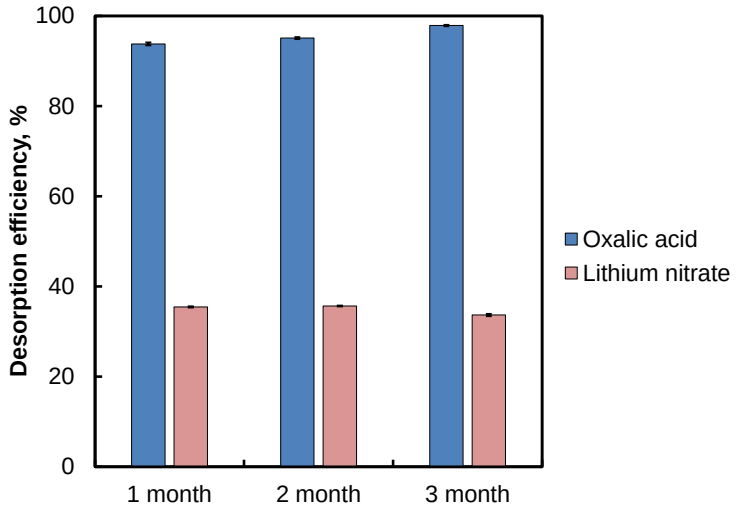

Fig. 3-5. Desorption efficiency of Cs from biotite as a function of aging time. Bio-T: 0.05 g; volume of each solution: 25 mL; concentration of extraction solution: 0.5 mol/L; heating time: 4 h; and temperature: 85 °C. Error bars indicate standard deviation (n = 3).

3.3.6. Oxalic acid leaching without heating

The temperature for the experiment was kept at 20 ± 5 °C during the 4 weeks. The pH was 5.9, 1.3, and 0.8 in the solutions of 1.0 mol/L $LiNO_3$, 0.1 mol/L oxalic acid, and 0.5 mol/L oxalic acid, respectively, and these values did not change throughout the experiment. **Figure 3-6** shows the desorption efficiency of Cs from biotite at each leaching time. $LiNO_3$ could desorb approximately 31.6% of Cs after 1 h of leaching time, and the desorption efficiency was constant throughout the experiment. In this study, Li desorbed the ion-exchangeable form of Cs from Bio-T and reached the equilibrium within

1 h of the leaching time.

The desorption efficiency by oxalic acid increased with leaching time, and the value of 85.3% (0.1 mol/L) and 94.9% (0.5 mol/L) were obtained after 2 weeks, and 89.8% (0.1 mol/L) and 96.1% (0.5 mol/L) were obtained after 4 weeks of the experiment. These efficiencies were higher than that of Li. The Cs has been considered to move into the interlayer of clay minerals and retain in an energy-stable site [22]. Since this study used Bio-T that has been saturated with Cs and aged for 3 months, Cs could have occupied the energy-stable sites that were inaccessible within the short aging time. Therefore, the high efficiency of oxalic acid can be attributed to the ability of oxalic acid to desorb Cs in both the outer-sphere complex and inner-sphere complex with Bio-T.

Al, Mg, Fe, and Si are the main components of clay minerals, and the concentration of each element in the extract solution was measured as a function of leaching time. When $LiNO_3$ was used as an extraction solution, Al, Mg, Fe, and Si were hardly observed in the solution (**Fig. 3-7c**). **Figure 3-8c** indicates X-ray diffractograms of Bio-T after each leaching time by $LiNO_3$. The basal spacing of clay mineral after Cs adsorption was 1.0 nm ($2\theta = 8.7°$) [26], indicating that Cs was still adsorbed in the interlayer of Bio-T. The intensity of this reflection (8.7°) did not change even after 4 weeks, the Bio-T structure was unaltered. This result also indicated that $LiNO_3$ desorbed only Cs in an ion-exchangeable form. In contrast, oxalic acid desorbed Al, Mg, Fe, and Si in Bio-T. The desorption rates of Al, Mg, and Fe were 68%, 83%, and 94% by 0.5 mol/L oxalic acid after 2 weeks of leaching, and this desorption rate did not significantly change until 4 weeks (**Fig. 3-7b**). Since the desorption efficiency of Cs by 0.5 mol/L oxalic acid also plateaued at a leaching time of 2 weeks (**Fig. 3-6**), these results indicate that the decomposition of Bio-T by oxalic acid (0.5 mol/L) can induce the desorption of Cs from

Bio-T at room temperature. When oxalic acid was 0.1 mol/L, the concentrations of Al, Mg, and Fe continued to increase even after 4 weeks (**Fig. 3-7a**). At 4 weeks of leaching time, the desorption rates of Al, Mg, and Fe were 60%, 78%, and 91%, respectively. The pH of the solution before and after leaching was 0.7–0.9, 1.2–1.3, and 5.7–6.1, in 0.5 mol/L oxalic acid, 0.1 mol/L oxalic acid, and 1.0 mol/L $LiNO_3$, respectively.

The complex between oxalic acid and metal was reported in several studies. Buckwheat has been reported to detoxify Al with oxalic acid released from its root, which forms an oxalate complex, with Al to oxalic acid ratio of 1:3 [27]. The reaction ratio between Fe and oxalic acid was 2:5 [23]. The concentration of Al and Fe in Bio-T used in this study was 3.2 mmol/g and 2.0 mmol/g, respectively. Therefore, even 0.1 mol/L of oxalic acid was sufficient to react with all Al and Fe to form their complexes with oxalic acid. The XRD results indicated that the intensity of Bio-T reflection decreased with leaching time (**Fig. 3-8**), although this Bio-T reflection (1.0 nm) has not completely disappeared with 0.1 mol/L of oxalic acid, even at a leaching time of 4 weeks (**Fig. 3-8a**). This result implied that the decomposition of biotite by 0.1 mol/L oxalic acid took a long time over 4 weeks. On the other hand, it almost completely disappeared with 0.5 mol/L oxalic acid after 2 weeks (**Fig. 3-8b**). The broad peak around 11.5° was estimated to be oriented from a hydrotalcite-like structure, which has XRD reflection at 11.7° and is similar to an octahedral sheet [28,29]. Assuming that Al and Fe eluted by oxalic acid leaching are metals that have existed in the tetrahedral sheet by isomorphous substitute with Si, it is considered that the tetrahedral sheet could not maintain its structure due to this elution. Since this reflection (11.5°) appears with the decrease in Bio-T reflection (8.7°), it is presumed to be from the remaining octahedral sheet. These results indicate that oxalic acid (0.5 mol/L) could desorb elements (Al, Mg, Fe, and Si) in biotite and

consequently decompose its structure. The Cs desorption from biotite due to the decomposition of its structure by oxalic acid can be performed even without heating.

Oxalic acid is a natural organic acid present in various plants and is highly effective in the field of environmental remediation [30,31]. Since the results of this study confirmed that Cs strongly bound in clay minerals can be desorbed with oxalic acid without heating, there is the possibility of introducing plants with oxalic acid content as a soil remediation technology option. Moreover, this oxalic acid leaching has the potential to be a low energy soil remediation as it does not require heating.

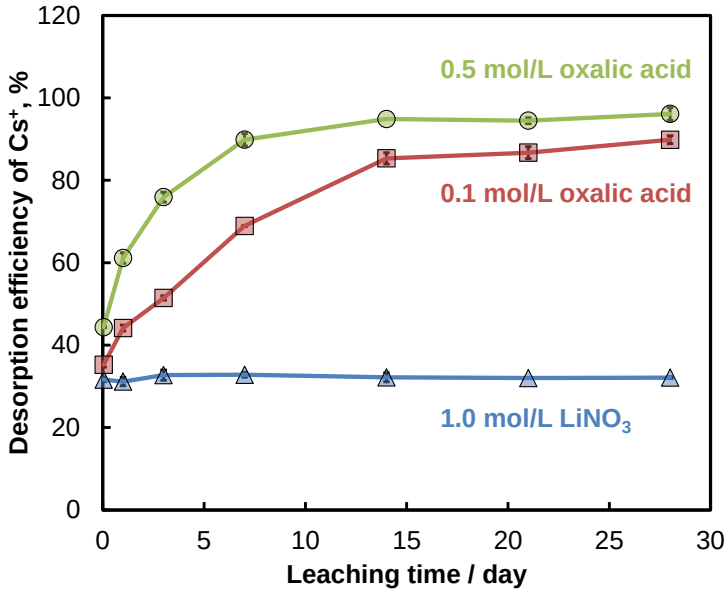

Fig. 3-6. Desorption efficiency of Cs from biotite at each leaching time without heating.

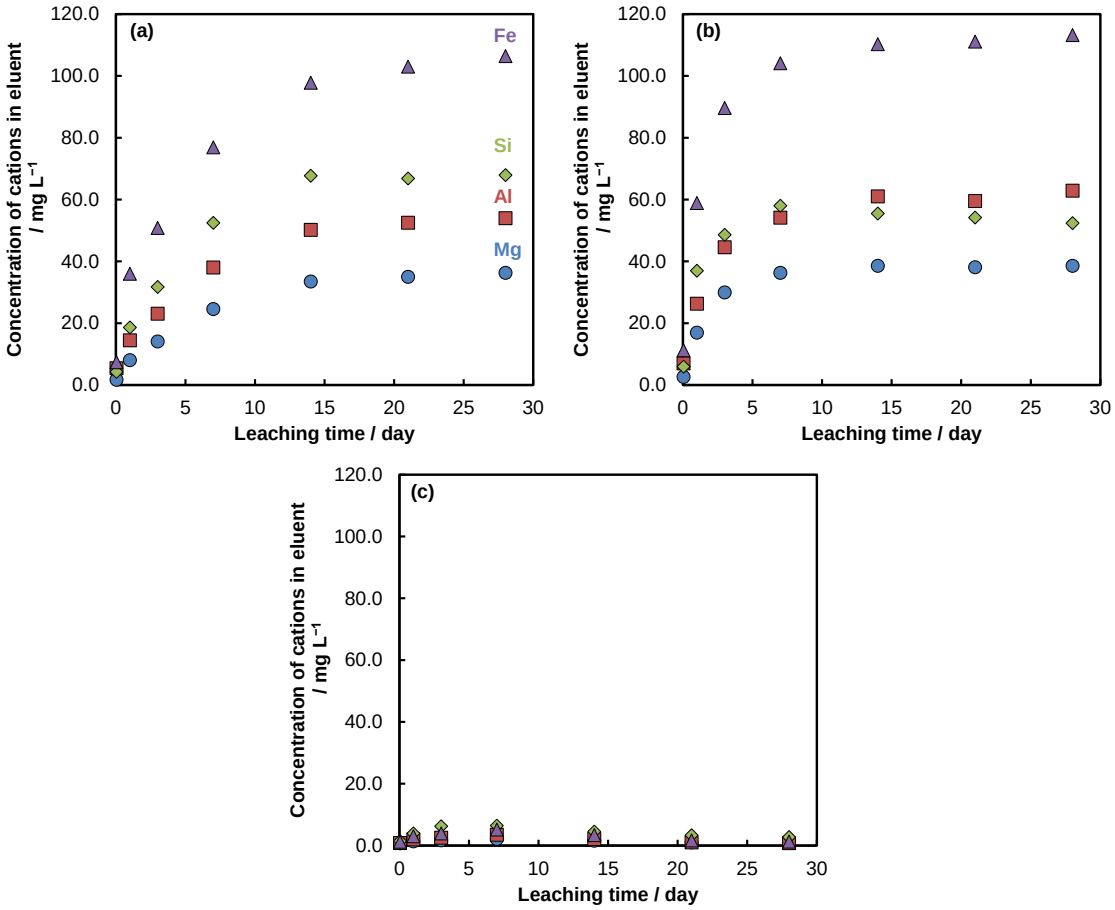

Fig. 3-7. Eluted elements from biotite under oxalic acid leaching; **(a)** 0.1 mol/L oxalic acid, **(b)** 0.5 mol/L oxalic acid; **(c)** 1.0 mol/L $LiNO_3$.

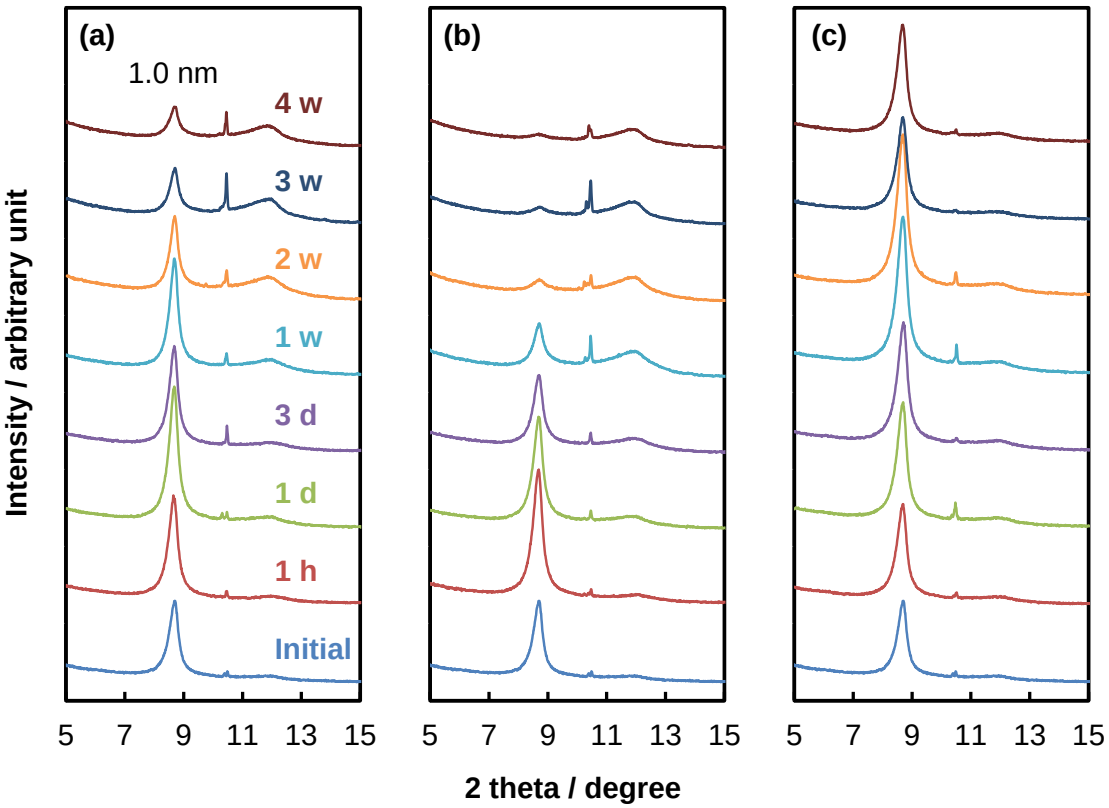

Fig. 3-8. X-ray diffractograms of biotite after each oxalic acid leaching without heating. **(a)** 0.1 mol/L oxalic acid, **(b)** 0.5 mol/L oxalic acid, **(c)** 1.0 mol/L $LiNO_3$.

3.3.7. Comparison with previous studies

The desorption efficiency by oxalic acid leaching in this study is compared with that from other previous studies (**Table 3-3**). Since the types of clay minerals were different in each study, it is difficult to make a detailed comparison. However, the oxalic acid treatment in this study showed high desorption efficiency under relatively low temperatures. Moreover, although it requires a longer leaching time, oxalic acid can desorb Cs from Bio-T under room temperature. Therefore, this method is considered to have a high potential as a desorption method of Cs from clay minerals.

Table 3-3. Comparison with previous studies on experimental conditions and desorption efficiency of Cs from clay mineral.

Target clay mineral	Temperature (cycles)	Time	Method or reagent	Efficiency, %	Ref.
Vermiculite	800 °C	3 min	Vacuum heat	40	[32]
Mg-type vermiculated biotite	100 °C (5)	30 min	0.01 mol/L $MgCl_2$	30	[33]
Mg-type vermiculated biotite	250 °C (5)	30 min	0.01 mol /L $MgCl_2$	100	[33]
Mg-type vermiculated biotite	250 °C (3)	30 min	1 mol/L $MgCl_2$	100	[34]
Mg-type vermiculated biotite	200 °C (5)	30 min	0.05 mol/L citric acid	95.4	[12]
Illite	70 °C	2 days	1.5 mol/L H_2SO_4	87	[16]
Illite	70 °C	2 days	1.5 mol/L oxalic acid	69	[16]
Biotite	85 °C	4 h	0.5 mol/L oxalic acid	94.8	This study
Biotite	r.t.	2 w	0.5 mol/L oxalic acid	94.9	This study

3.4. Summery

Oxalic acid treatment has a high potential for desorbing Cs from biotite and achieved the removal efficiency of 94.8% Cs from biotite. The optimal heating temperature was 85 °C, and the optimal treatment duration was 4 h. Desorption of Cs from Bio-T was facilitated by the dissolution of Al, Fe, and Mg from the Bio-T structure. Oxalic acid treatment was also effective in the desorption of Cs from Bio-T aged for 3 months. High desorption efficiency (94.9%) of Cs from Bio-T was obtained by 2 weeks of oxalic acid leaching without heating. Since this study focused on clay minerals on a laboratory scale, it is necessary to consider the effect of the coexistence of other soil particles and organic substances such as humic substances when upscaling in future experiments. Currently, there are only a few studies on Cs desorption from biotite around the boiling point of water. Moreover, although the desorption of Cs from Bio-T by oxalic acid leaching takes a long time (at least 2 weeks), the fact that no external energy is required for extraction is a great advantage. Therefore, oxalic acid leaching without heating can be used for the volume reduction of contaminated soil with radionuclides.

3.5. References

[1] Japan Ministry of the Environment, Development issues and goals for volume reduction treatment technology, 2015 (in Japanese). http://josen.env.go.jp/chukanchozou/facility/effort/investigative_commission/pdf/proceedings_191219_03-01.pdf.

[2] Japan Ministry of the Environment, Current status and future plans of volume reduction and recycling technology, 2019 (in Japanese). http://josen.env.go.jp/chukanchozou/facility/effort/investigative_commission/pdf/proceedings_191219_03-01.pdf.

[3] Japan Ministry of the Environment, Demonstration project for reuse of removed soil and technical demonstration, 2022 (in Japanese). http://josen.env.go.jp/chukanchozou/facility/effort/investigative_commission/pdf/proceedings_220330_02.pdf.

[4] T. Yasutaka, T. Kawamoto, T. Komai, Applicability of the acid extraction method to radioactive caesium contaminated soil, Radioisotopes. 62 (2013) 211–218 (in Japanese). doi:10.3769/radioisotopes.62.211.

[5] Japanese Society of Soil Science and Plant Nutrition, Soil standard analysis and measurement, Hakuyusha, Tokyo, (1986) (in Japanese).

[6] K. Murota, T. Saito, S. Tanaka, Desorption kinetics of cesium from Fukushima soils, J. Environ. Radioact. 153 (2016) 134–140. doi:10.1016/j.jenvrad.2015.12.013.

[7] A. Martínez-Luévanos, M.G. Rodríguez-Delgado, A. Uribe-Salas, F.R. Carrillo-Pedroza, J.G. Osuna-Alarcón, Leaching kinetics of iron from low grade kaolin by oxalic acid solutions, Appl. Clay Sci. 51 (2011) 473–477. doi:10.1016/j.clay.2011.01.011.

[8] A. Tuncuk, A. Akcil, Iron removal in production of purified quartz by hydrometallurgical process, Int. J. Miner. Process. 153 (2016) 44–50. doi:10.1016/j.minpro.2016.05.021.

[9] H. Mukai, A. Hirose, S. Motai, R. Kikuchi, K. Tanoi, T.M. Nakanishi, T. Yaita, T. Kogure, Cesium adsorption/desorption behavior of clay minerals considering actual contamination conditions in Fukushima, Sci. Rep. 6 (2016) 21543. doi:10.1038/srep21543.

[10] R. Giudici, H.W. Kouwenhoven, R. Prins, Comparison of nitric and oxalic acid in the dealumination of mordenite, Appl. Catal. A. 203 (2000) 101–110. doi:10.1016/S0926-860X(00)00470-1.

[11] J. Bergerman, J.S. Elliot, Method for direct colorimetric determination of oxalic

acid, Anal. Chem. 27 (1955) 1014–1015. doi:10.1021/ac60102a045.

[12] X. Yin, L. Zhang, M. Harigai, X. Wang, S. Ning, M. Nakase, Y. Koma, Y. Inaba, K. Takeshita, Hydrothermal-treatment desorption of cesium from clay minerals: The roles of organic acids and implications for soil decontamination, Water Res. 177 (2020) 115804. doi:10.1016/j.watres.2020.115804.

[13] D. Panias, M. Taxiarchou, I. Paspaliaris, A. Kontopoulos, Mechanisms of dissolution of iron oxides in aqueous oxalic acid solutions, Hydrometallurgy. 42 (1996) 257–265. doi:10.1016/0304-386X(95)00104-O.

[14] Y. Saito, S. Shimizu, S. Kumagai, T. Kameda, T. Yoshioka, Removal of cesium ions from A-type zeolites using sodium tetrakis(4-fluorophenyl)borate and sodium tetraphenylborate, J. Radioanal. Nucl. Chem. 327 (2021) 337–344. doi:10.1007/s10967-020-07514-w.

[15] M. Taxiarchou, D. Panias, I. Douni, I. Paspaliaris, A. Kontopoulos, Removal of iron from silica sand by leaching with oxalic acid, Hydrometallurgy. 46 (1997) 215–227. doi:10.1016/s0304-386x(97)00015-7.

[16] S.-M. Kim, I.-H. Yoon, I.-G. Kim, C.W. Park, Y. Sihn, J.-H. Kim, S.-J. Park, Cs desorption behavior during hydrothermal treatment of illite with oxalic acid, Environ. Sci. Pollut. Res. 27 (2020) 35580–35590. doi:10.1007/s11356-020-09675-3.

[17] The Clay Science Society of Japan, Handbook of Clays and Clay Minerals, third edit, Gihodo Shuppan Co., Ltd., Tokyo, (2009) (in Japanese).

[18] H. Shirozu, Introduction to Clay Mineralogy –Fundamentals for Clay Science–, Asakura Publishing Co., Ltd., Tokyo, (1988) (in Japanese).

[19] The Chemical Society of Japan, Handbook of Chemistry, sixth edit, Maruzen Publishing Co., Ltd., Tokyo, (2021) (in Japanese).

[20] F. Veglió, B. Passariello, M. Barbaro, P. Plescia, A.M. Marabini, Drum leaching tests in iron removal from quartz using oxalic and sulphuric acids, Int. J. Miner. Process. 54 (1998) 183–200. doi:10.1016/S0301-7516(98)00014-3.

[21] G.-N. Kim, S.-S. Kim, U.-R. Park, J.-K. Moon, Decontamination of soil contaminated with cesium using electrokinetic-electrodialytic method, Electrochim. Acta. 181 (2015) 233–237. doi:10.1016/j.electacta.2015.03.208.

[22] H. Mukai, K. Tamura, R. Kikuchi, Y. Takahashi, T. Yaita, T. Kogure, Cesium desorption behavior of weathered biotite in Fukushima considering the actual radioactive contamination level of soils, J. Environ. Radioact. 190–191 (2018) 81–88. doi:10.1016/j.jenvrad.2018.05.006.

[23] S.O. Lee, T. Tran, Y.Y. Park, S.J. Kim, M.J. Kim, Study on the kinetics of iron

oxide leaching by oxalic acid, Int. J. Miner. Process. 80 (2006) 144–152. doi:10.1016/j.minpro.2006.03.012.

[24] Q. Fan, N. Yamaguchi, M. Tanaka, H. Tsukada, Y. Takahashi, Relationship between the adsorption species of cesium and radiocesium interception potential in soils and minerals : an EXAFS study, J. Environ. Radioact. 138 (2014) 92–100. doi:10.1016/j.jenvrad.2014.08.009.

[25] H. Qin, Y. Yokoyama, Q. Fan, H. Iwatani, K. Tanaka, A. Sakaguchi, Y. Kanai, J. Zhu, Y. Onda, Y. Takahashi, Investigation of cesium adsorption on soil and sediment samples from Fukushima Prefecture by sequential extraction and EXAFS technique, Geochem. J. 46 (2012) 297–302. doi:10.2343/geochemj.2.0214.

[26] T. Kogure, K. Morimoto, K. Tamura, H. Sato, A. Yamagishi, XRD and HRTEM evidence for fixation of cesium ions in vermiculite clay, Chem. Lett. 41 (2012) 380–382. doi:10.1246/cl.2012.380.

[27] J.F. Ma, S.J. Zheng, H. Matsumoto, S. Hiradate, Detoxifying aluminium with buckwheat, Nature. 390 (1997) 569–570. doi:10.1038/37518.

[28] S. Miyata, Anion-Exchange Properties of Hydrotalcite-Like Compounds, Clays Clay Miner. 31 (1983) 305–311. doi:10.1346/CCMN.1983.0310409.

[29] E. Bernard, W.J. Zucha, B. Lothenbach, U. Mäder, Stability of hydrotalcite (Mg-Al layered double hydroxide) in presence of different anions, Cem. Concr. Res. 152 (2022) 106674. doi:10.1016/j.cemconres.2021.106674.

[30] M. Huang, C. Zhu, F. Zhu, G. Fang, D. Zhou, Mechanism of significant enhancement of VO2-Fenton-like reactions by oxalic acid for diethyl phthalate degradation, Sep. Purif. Technol. 279 (2021) 119671. doi:10.1016/j.seppur.2021.119671.

[31] L.G. da Costa, V.F. Brocco, J.B. Paes, G.T. Kirker, A.B. Bishell, Biological and chemical remediation of CCA treated eucalypt poles after 30 years in service, Chemosphere. 286 (2022) 131629. doi:10.1016/j.chemosphere.2021.131629.

[32] I. Shimoyama, N. Hirano, Y. Baba, T. Izumi, Y. Okamoto, T. Yaita, S. Suzuki, Low-pressure sublimation method for cesium decontamination of clay minerals, Clay Sci. 18 (2014) 71–77.

[33] X. Yin, X. Wang, H. Wu, T. Ohnuki, K. Takeshita, Enhanced desorption of cesium from collapsed interlayer regions in vermiculite by hydrothermal treatment with divalent cations, J. Hazard. Mater. 326 (2017) 47–53. doi:10.1016/j.jhazmat.2016.12.017.

[34] X. Yin, N. Horiuchi, S. Utsunomiya, A. Ochiai, H. Takahashi, Y. Inaba, X. Wang, T. Ohnuki, K. Takeshita, Effective and efficient desorption of Cs from hydrothermal-treated clay minerals for the decontamination of Fukushima radioactive soil, Chem. Eng. J. 333 (2018) 392–401. doi:10.1016/j.cej.2017.09.199.

Chapter 4

Development of collectable adsorbent based on vermiculite for cesium ion in an aquatic environment

4.1. Introduction

Alkali metal ions such as Cs and K have high solubility even in basic conditions, and it is difficult to collect them as precipitates of hydroxides. Therefore, adsorptive separation is effective for alkali metals and some adsorbents have been developed. For example, wood cellulosic adsorbent that is derived from natural products and has a large adsorption capacity (133.54 mg/g) was reported as an adsorbent for Cs [1]. However, the use of nitric acid, which has a large environmental impact, and the need for heating energy in the pretreatment are considered to be the environmental issue. The crown ether based adsorbent has been also developed [2]. Although this adsorbent has a high adsorption capacity and selectivity, the preparation process is so complicated. Natural products such as persimmon tannin have a low environmental impact and are expected to be used as adsorbents [3]. However, these natural adsorbents exhibit low adsorption capacity without any pretreatments.

As mentioned in Chapter 2, clay minerals have a high adsorption ability to collect Cs from solution and a low environmental impact because it is a natural product. Moreover, the adsorbed Cs is stable in clay minerals and is not easily desorbed [4], which is also a great advantage as the adsorbent. The adsorbent is ordinarily preferred to be reusable, however, it is not necessarily the case for radioactive species. At present, radioactive species are planned to be treated by vitrification and then stored in the geological disposal site. Thus, the adsorbent after adsorbing radioactive species is expected to also be treated in a similar procedure. The low desorption efficiency of Cs from clay minerals is significant to reduce the risk of re-diffusion into the environment. These properties of clay minerals are promising as an adsorbent.

On the other hand, since typically clay minerals have small particle sizes, the

collection of the clay minerals after the adsorption of Cs is not so easy. The strategy for the collection of adsorbents is required for the practical application of the adsorbent consisting of fine particles. Alginic acid, a natural organic substance in seaweed, is commonly used to encapsulate adsorbents in powder form [5–7]. For instance, montmorillonite encapsulated in an alginate gel bead has been investigated for the removal of Cs [8]. This adsorbent was modified with lithium to enhance the selectivity for Cs; however, lithium is not a cheap material for such modification procedures.

In this chapter, a novel collectable adsorbent for Cs removal from aquatic environments was developed by encapsulating vermiculite in alginate gel beads, based on a simple concept, not requiring external energy, and with a low environmental impact.

4.2. Materials and methods

4.2.1. Materials and chemicals

Vermiculite (Verm-I), which was used in Chapter 2, was used as an adsorbent.

Sodium alginate (Wako 1st grade, 300–400 cps), cesium chloride (CsCl, Wako Special Grade, 99.0%), sodium chloride (NaCl, Guaranteed Reagent, 99.5%), potassium chloride (KCl, Guaranteed Reagent, 99.5%) were purchased from FUJIFILM Wako Pure Chemical Corporation, Osaka, Japan. Hydrochloric acid (HCl, for trace analysis, 35.0–37.0%), nitric acid (HNO_3, for trace analysis, 60.0–61.0%), cesium hydroxide monohydrate ($CsOH \cdot H_2O$ > 85.5%), calcium chloride dihydrate ($CaCl_2 \cdot 2H_2O$, Guaranteed Reagent, > 99.0%), magnesium chloride hexahydrate ($MgCl_2 \cdot 6H_2O$, Guaranteed Reagent, > 99.0%), and trisodium citrate dihydrate ($C_6H_5Na_3O_7 \cdot 2H_2O$, Guaranteed Reagent, > 99.0%) were purchased from Kanto Chemical Co., Inc., Tokyo, Japan. Humic acid sodium salt was purchased from Sigma-Aldrich Co., MO, USA. These

chemicals were used without any pretreatment.

4.2.2. Characteristics of Verm-I

The Verm-I was crushed using an agate mortar to a particle size smaller than 53 μm. Since vermiculite clay sometimes forms a mixed layer with chlorite, Verm-I was identified by the following procedure. Typically, given that the basal spacing of vermiculite clay is known to decrease from 1.4 nm to 1.0 nm by the adsorption of K in the interlayer [9], the structural change of Verm-I was observed before and after the adsorption of K. Namely, Verm-I (0.1 g) was saturated with 25 mL of 1.0 mol/L KCl solution three times. The Verm-I was filtered (5C, 1 μm pore size, Toyo Roshi Kaisha Ltd., Tokyo, Japan) and washed with distilled water. After filtration, the Verm-I on the filter paper was dried at 105 °C for 16 h (Yamato Constant Temperature Oven DK-62, Yamato Scientific Co., Ltd., Tokyo, Japan). The prepared Verm-I was characterized using X-ray diffraction (XRD, SmartLab, Rigaku Corporation, Tokyo, Japan), using Cu Kα radiation (λ = 0.154 nm) at 40 kV and 30 mA with a speed of 1 °/min and an angular step of 0.01 °. The chemical composition of Verm was measured using an energy-dispersive X-ray fluorescence spectrometer (XRF, JSX-3100RII, JEOL Ltd., Tokyo, Japan), and the carbon content was measured using a CHNS elemental analyzer (vario EL cube, Elementar, Langenselbold, Germany). The adsorbents were characterized using Fourier Transform Infrared spectra (FT-IR, Spectrum 100, PerkinElmer, USA) in the ATR method. The morphology of the adsorbent was examined using a scanning electron microscope (SEM, JSM-6610LA, JEOL Ltd., Tokyo, Japan) at 20 kV accelerating voltage.

4.2.3. Pretreatment with sodium citrate

Typically, the interlayer material, such as the hydroxyl sheet that exists in the interlayer of chlorite, can be removed by sodium citrate treatment [10]. Here, this procedure was partially modified to improve the adsorption capacity of the Verm-I. Briefly, Verm-I was dispersed into 0.3 mol/L sodium citrate solution (pH 8.0) at a 1:200 solid/liquid ratio. The mixture was shaken at 150 rpm at various temperatures and for different contact times, and the Verm-I was filtered using filter papers (5C). The concentrations of Al, Fe, Mg, and Si in the filtrate were measured using inductively coupled plasma-atomic emission spectroscopy (ICP-AES, ICPS-8100, Shimadzu Corporation, Kyoto, Japan). The sample on the filter paper was dried at 105 °C for 16 h, and the treated Verm-I (Verm-I-Cit) was used to perform the adsorption experiment.

4.2.4. Adsorption experiment

Adsorption experiments were conducted using Verm-I and Verm-I-Cit. The Verm-I or Verm-I-Cit (0.05 g) was added to 25 mL of Cs solution, and the mixture was shaken at 150 rpm at 25 °C (BR-40LF, Taitec Corporation, Saitama, Japan). The mixture was filtered using filter paper (5C), and Cs concentration in the filtrate was measured using a flame atomic absorption spectrophotometer (AAS, ZA-3000, Hitachi High-Tech Corporation, Tokyo, Japan). The adsorption capacity (q, mg/g) was calculated using **Eq. 2-1** (Chapter 2).

The effects of sodium citrate treatment temperature and time were evaluated based on the obtained adsorption capacity for Cs. The XRD of the adsorbent after Cs adsorption was measured and assessed for basal spacing. The solution pH was measured using a pH meter (D-51, Horiba Ltd., Kyoto, Japan). The adsorption experiment was operated under

various conditions of Cs concentrations, pH, and contact times. The effect of pH was evaluated using a CsOH solution prepared at various pH values, and adjusted with HCl to avoid interfering with Na.

The effect of coexisting ions on the adsorption capacity of the prepared Verm-I-Cit for Cs was evaluated by mixed solutions (Cs and cations) prepared using chloride. Since Mg and Ca are divalent ions, they were prepared at half the concentration of monovalent cations. The solution containing coexisting ions at the same concentration as Cs and 10 times higher concentration were prepared. The effect of organic substances on the adsorption capacity was evaluated by humic acid sodium salt, the concentration of carbon was 1, 10, and 100 mg/L, respectively. The detailed adsorption condition was the same procedure above and the contact time was 24 h.

4.2.5. Evaluation by using model

The adsorption kinetics was evaluated using the pseudo-first order, pseudo-second order, Elovich, and Intraparticle diffusion (IPD) kinetics models, and the adsorption isotherms were evaluated using the Langmuir and Freundlich isotherm models. The details of the model equations are indicated in Chapter 2. The Elovich kinetics model (**Eq. 4-1**) and IPD kinetics model (**Eq. 4-2**) were expressed below equations.

$$q_t = \beta^{-1} \ln(\alpha \cdot \beta \cdot t) \quad \textbf{(4-1)}$$

$$q_t = k_{IPD} \cdot t^{0.5} + C \quad \textbf{(4-2)}$$

where q_t is adsorption capacity at time t (mg/g), β denotes the Elovich kinetic parameter correlated with the adsorbent surface coverage (mg/g) and α is the initial rate of adsorption (mg/g/min). The k_{IPD} indicates the IPD rate constant (mg/g/min$^{0.5}$), and C represents the thickness of the outer film, which is the intercept of the IPD curve.

4.2.6. Ion-exchange isotherm

The ion-exchange isotherm is useful for evaluating the selectivity of the adsorbent [11–13] and was used for the developed adsorbent (Verm-I-Cit). Sodium prepared using chloride salt was used as the competing ion. The prepared solution contained Cs and Na in various proportions. The total normality of Cs and Na was 5 mmol/L. The adsorption experiment was carried out using the procedure described in Section 4.2.4. The concentrations of Cs and Na in the filtrate were measured using AAS and were used to calculate the ratio of Cs in the solution and soil. The Vanselow selectivity coefficient (K^{V}_{NaCs}) was calculated using **Eq. 4-3** [13].

$$K^{V}_{NaCs} = \frac{CsX\,(Na^{+})}{NaX\,(Cs^{+})} \quad \textbf{(4-3)}$$

where *CsX* and *NaX* are mole fractions in the exchange phase of clay mineral, and (Na^{+}) and (Cs^{+}) are present activities calculated using Visual MINTEQ (version 3.1). When there is non-preference in the exchange between cations, the value of K^{V}_{NaCs} is unity.

4.2.7. Preparation of AG-Verm-I-Cit beads

Clay minerals have a large adsorption capacity; however, as they are powders, they are difficult to collect after the adsorption of pollutants. Therefore, encapsulation by alginate gel (AG) beads was attempted. The AG-Verm-I and AG-Verm-I-Cit were prepared according to the following procedure: Verm-I or Verm-I-Cit was added to distilled water, and powdered sodium alginate (1wt%) while stirring with a magnetic stirrer. If distilled water is added to the sodium alginate powder first, or clay minerals are added to the prepared sodium alginate solution, it does not disperse well. The prepared AG-Verm-I or AG-Verm-I-Cit solution was dripped into 0.1 mol/L $CaCl_2$ solutions using a peristaltic pump (MP-1000, Tokyo Rikakikai Co., Ltd, Tokyo, Japan) through a silicon

tube (ID: 3 mm) with a Luer fitting (VRM306, Nordson Medical Corporation, Westlake, OH, USA) at the tip. The dripping speed was approximately 2 mL/min (almost 30 drops/min). A $CaCl_2$ solution containing AG beads was continuously stirred with a magnetic stirrer for 3 h for the bead maturation [36] (**Fig. 4-1**). Then, the prepared AG-Verm-I and AG-Verm-I-Cit beads were used for adsorption experiments. The procedure is the same as in Section 2.4, and twenty-five beads were added to 25 mL of 500 mg (Cs^+)/L solution (pH 6.0). As AG beads include water molecules, it is difficult to compare the adsorption capacities of AG beads with powder form adsorbents. Therefore, the prepared AG beads were lyophilized to obtain the dry weight (FDU-1200, Tokyo Rikakikai Co., Ltd, Tokyo, Japan), which was used to calculate the adsorption capacities of AG-Verm-I and AG-Verm-I-Cit.

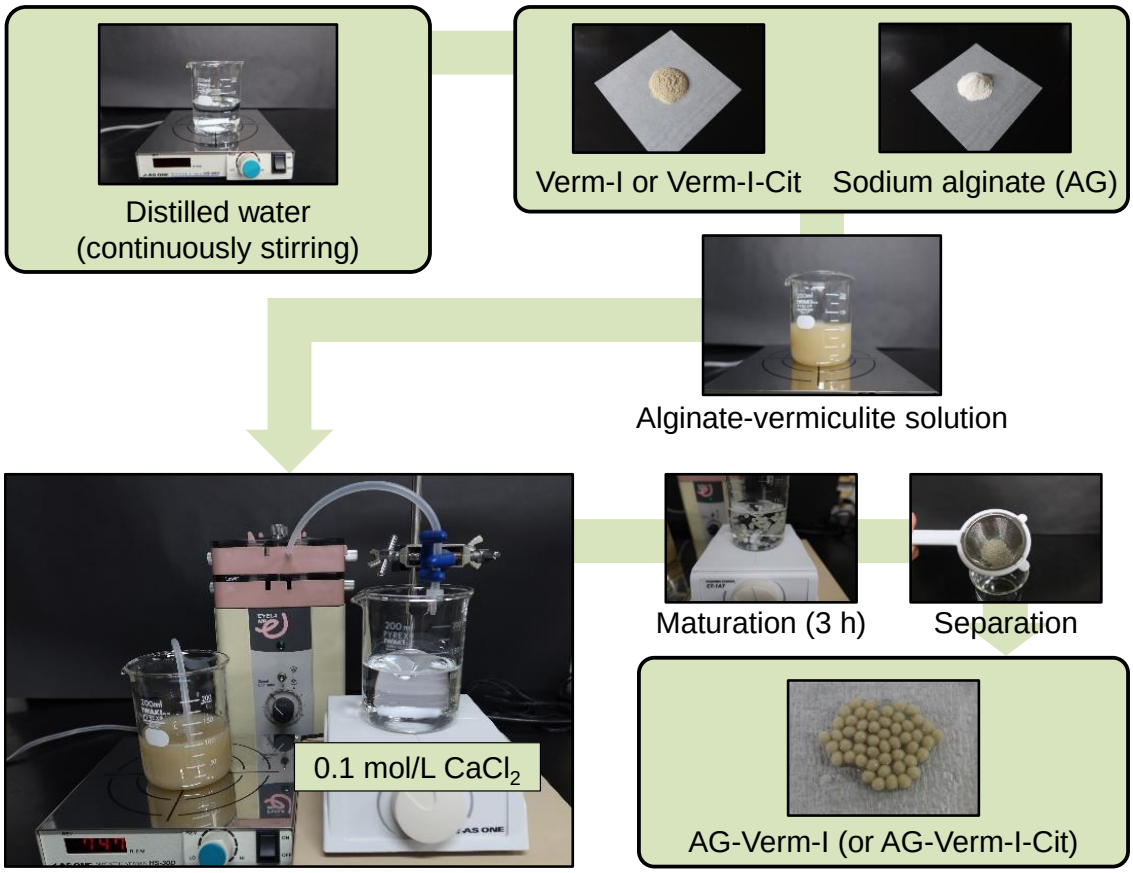

Fig. 4-1. Flow chart of the preparation of AG-Verm-I and AG-Verm-I-Cit

4.3. Results and discussion

4.3.1. Characterization of clay mineral

The morphology of Verm-I is shown in **Fig. 4-2**; Verm-I has a layered structure like common clay minerals. The chemical composition and X-ray diffractograms of Verm used in this study are shown in **Table 4-1** and **Fig. 4-3**. The carbon content of Verm was below the quantitative lower limit of the CHNS elemental analyzer (< 0.2%). The Verm used in this study had a 1.4 nm of basal spacing (**Fig. 4-3a**), a typical property of vermiculite clay. Although the basal spacing of Verm-I-Cit generally becomes 1.0–1.1 nm after K saturation [9], Verm-I was kept at a basal spacing of 1.4 nm (**Fig. 4-3b**). Chlorite,

also a phyllosilicate clay mineral, has a sheet-like interlayer material in the interlayer, and the basal spacing does not narrow after K saturation. Because vermiculite clay and chlorite are often produced as mixtures, the Verm-I used in this study probably has a partial chlorite structure.

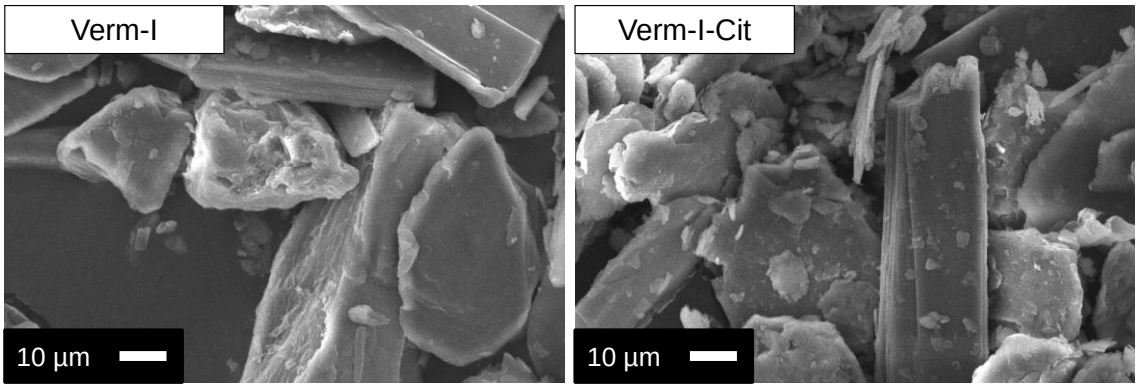

Fig. 4-2. SEM image of adsorbent.

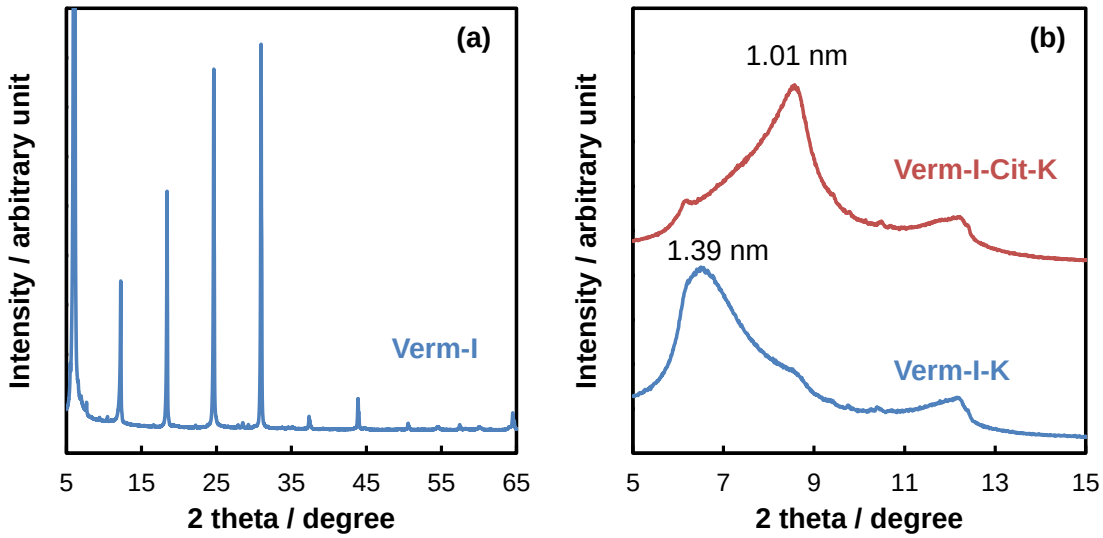

Fig. 4-3. (a) X-ray diffractograms of Verm-I, **(b)** Verm-I and Verm-I-Cit after K saturation.

Table 4-1. Chemical composition of vermiculite (Verm-I) and sodium citrate-pretreated vermiculite (Verm-I-Cit).

Chemical composition, wt%	Verm-I	Verm-I-Cit
SiO_2	43.7	43.1
Al_2O_3	14.7	14.3
Fe_2O_3	6.3	5.9
MgO	34.2	32.0
Na_2O	ND	3.8

4.3.2. Condition of the sodium citrate treatment

The conditions for sodium citrate treatment were investigated to improve the adsorption capacity of Verm-I. **Figure 4-4a** shows the adsorption capacity for Cs at each treatment temperature, and "Original" indicates the adsorption capacity of Verm-I without any treatment. In a previous study, sodium citrate treatment was conducted at 100 °C for 6 h to remove the interlayer material of the chlorite [10]. In this study, the adsorption capacity of Verm-I was improved even at 25 °C for 6 h, and this capacity was constant up to 80 °C. The adsorption capacity did not change at various treatment periods at 25 °C (**Fig. 4-4b**). **Figure 4-4c** shows the X-ray diffractograms of Verm-I (Original) and Verm-I-Cit, which adsorbed Cs in each sodium citrate treatment period at 25 °C. Although the basal spacing of Verm-I (Original) became 1.24 nm after Cs adsorption, the basal spacing of Verm-I-Cit was 1.15 nm after any treatment time. The basal spacing of clay minerals was known to be around 1.0 nm due to Cs adsorption [14]. These results suggest that more Cs can penetrate the interlayer as the interlayer material of Verm-I was removed by sodium citrate treatment. As a result, the Cs adsorption capacity is improved. **Figure 4-4d** shows the eluted elements from the Verm-I by sodium citrate treatment. The most eluted element by sodium citrate treatment was Mg; almost the same amount of Mg was eluted even in the treatment with 0.3 mol/L NaCl (**Fig. 4-4d**). This result suggests that the

eluted Mg is an ion-exchangeable form and is not an element that constitutes the interlayer material. The next most eluted element was Si. The amount eluted with NaCl treatment was estimated to derive from soluble silicate as an impurity in Verm-I. The third most eluted element was Al, which was not eluted with NaCl. The interlayer material, eluted with sodium citrate, could be identified as a 1:1 type clay mineral or 2:1 type clay mineral-like structure based on the Si/Al molar ratio in the eluent [15], The Si/Al molar ratio in the eluent was calculated by subtracting the amount of Si eluted with NaCl (**Fig. 4-5)**. The Si/Al molar ratio was 1.8–1.9 in this study; the interlayer material could be regarded as the 2:1 type clay mineral-like structure [15].

The obtained conditions for the sodium citrate treatment were 25 °C and 2 h of treatment, which is enough to enhance the adsorption capacity of Verm-I. The interlayer material was removed in a shorter time than in previously reported studies [10] because the Verm-I used in this study was relatively weathered and only had a partial chlorite structure. The morphology of Verm-I was unaltered before and after sodium citrate treatment (**Fig. 4-2**), and the structure of Verm-I was constant.

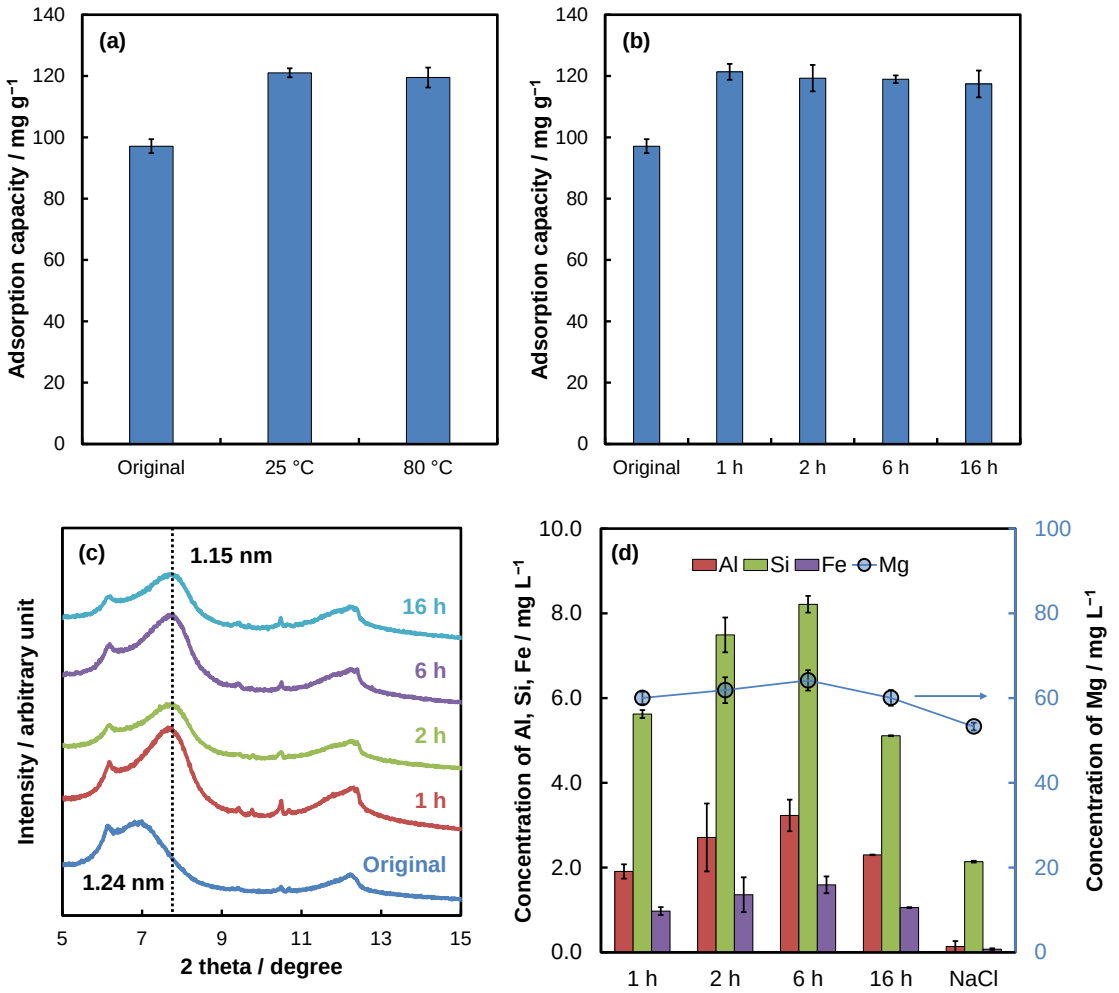

Fig. 4-4. Effect of sodium citrate treatment condition for the adsorption capacity of vermiculite (Verm-I): **(a)** effect of temperature; **(b)** treatment time; **(c)** basal spacing of Verm-I-Cit after adsorption of Cs; **(d)** desorbed elements from Verm-I (0.1 g) by sodium citrate treatment (20 mL) and by NaCl. All experiments were performed 24 h contact time. Error bars indicate the standard deviation (n = 3).

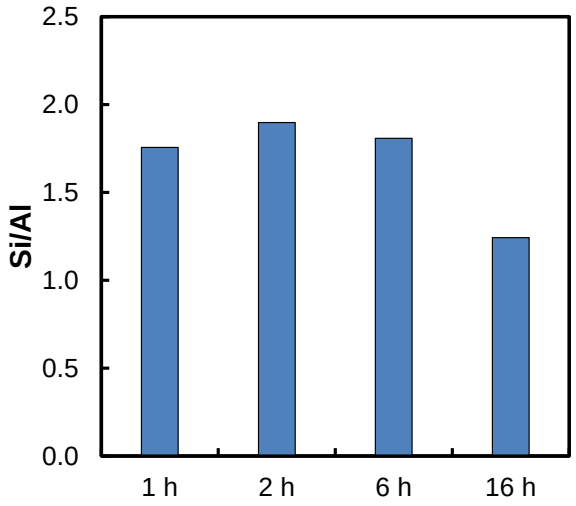

Fig. 4-5. Si/Al molar ratio of eluent from Verm-I with sodium citric treatment.

4.3.3. Effect of the removal of interlayer material on Cs adsorption

The effects of the removal of the interlayer material on Cs adsorption were evaluated. The Si/Al molar ratio should be 2:1 in 2:1 type clay mineral without any isomorphous substitution. The adsorbed Cs has existed in the hollow of six-membered rings on a tetrahedral sheet of clay mineral. Since the Si forming the six-membered ring is shared with an adjacent six-membered ring, the ratio of Si and Cs should be 2:1 in the clay mineral after Cs adsorption. When Cs were fixed in the interlayer of clay minerals, Cs were held between two tetrahedral sheets, and the ratio of Si and Cs became 4:1. Here, the eluted interlayer material with sodium citrate treatment was a 2:1 type clay mineral-like structure, the Al and Si molar ratio in the eluent should be similar to the ratio in the 2:1 type clay mineral structure. Since the ratio of Si and Al of 2:1 type clay mineral is 2:1, the molar ratio of eluted Al:Cs should be 2:1. Since the concentration of Al was 0.020 mmol/g after the 2 h sodium citrate treatment, the available adsorption sites for Cs were calculated to be 0.010 mmol/g due to the removal of the interlayer material directly. The increased adsorption capacity for Cs of Verm-I due to the 2 h sodium citrate solution

treatment was 22 mg/g (0.17 mmol/g) by subtracting the capacity of untreated Verm-I from the capacity of sodium citrate-treated Verm-I. This calculation indicates that the adsorbed Cs were around 17 times higher than the estimated capacity.

The adsorption for Cs on the Verm-I occurred not only where the interlayer material was removed, but also on sites that became accessible due to the removal of the interlayer material. If the interlayer material is on the edge of the clay mineral and Mg ions are located far from the edge, the interlayer material interferes with Cs adsorption, and Mg ions cannot be exchanged with Cs. Since most of the Al was not eluted by NaCl treatment (**Fig. 4-4d**), NaCl did not affect the removal of the interlayer material. Thus, the increase Mg concentration observed after NaCl treatment was likely due to the elution of exchangeable Mg ions from the Verm-I with interlayer material. The accessible adsorption site due to the removal of interlayer material with the sodium citrate treatment was estimated by subtracting the amount of Mg eluted following NaCl treatment from the amount of Mg eluted with sodium citrate treatment. The eluted amount of Mg after the 2 h sodium citrate treatment was 0.51 mmol/g, and after NaCl treatment was 0.44 mmol/g, the accessible adsorption site was estimated to be 0.07 mmol/g. The adsorbed amount of Cs increased by 0.17 mmol/g due to 2 h sodium citrate treatment. Since the adsorption capacity of 0.010 mmol/g was due to the removal of the interlayer material indicated above, the increased adsorption capacity, except for the direct effect of removing the interlayer material, was calculated to be 0.16 mmol/g. The ion exchange ratio considering these charges should ideally be 1:2, and an exchange ratio of Mg and Cs was 1:2.2 in this study. Mg in the interlayer is exchanged with Na derived from sodium citrate treatment, and Cs is adsorbed in the interlayer by exchanging with Na in the interlayer.

From these calculations, it can be concluded that the adsorption sites generated by

the sodium citrate treatment include two types. The first one is the sites directly occupied by the interlayer material, and the second one is sites containing Mg ions that were inaccessible due to the presence of the interlayer material (**Fig. 4-6**).

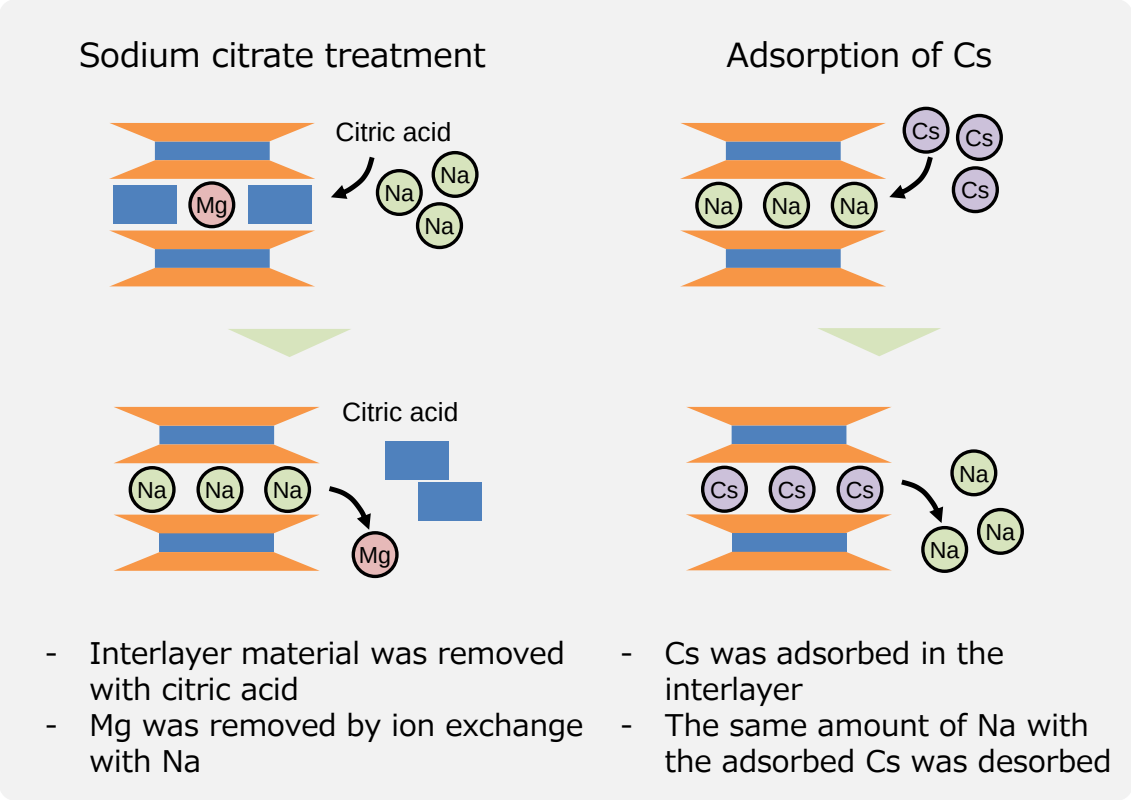

Fig. 4-6. Generated adsorption sites on vermiculite with sodium citrate treatment.

Although the treatment with citric acid reportedly enhances the adsorption capacity of adsorbents made from leaf due to the modification of carboxylic groups [16], the carbon content of Verm-I-Cit in this study was below the quantitative lower limit (< 0.2%) before and after the sodium citrate treatment. Moreover, the amount of carboxyl group on the Verm-I-Cit was evaluated by the calcium acetate method [17], and the carboxyl group was not detected on the Verm-I-Cit. Moreover, since the FT-IR spectra of Verm-I and

Verm-I-Cit was no significant difference (**Fig. 4-7**), the special functional groups are not modified on the surface of the Verm-I by sodium citrate treatment. These results indicated that the enhancement of the adsorption capacity of Verm-I after sodium citrate treatment was due to the removal of the interlayer material and not to the modification of specific functional groups like carboxylic groups by citric acid.

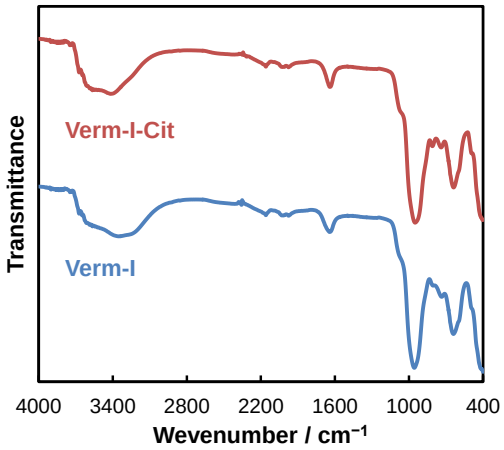

Fig. 4-7. FT-IR spectra of Verm-I and Verm-I-Cit.

4.3.4. Adsorption kinetics of Verm-I and Verm-I-Cit

The adsorption capacities of Verm-I and Verm-I-Cit at each contact time are shown in **Fig. 4-8a**. The Elovich model described well the adsorption kinetics of Verm-I, and the pseudo-second order model described the adsorption kinetics of Verm-I-Cit (**Table 4-2**). Since Verm-I is a natural product and has interlayer materials, it fitted the Elovich model with a heterogeneous surface. The IPD kinetics model indicated the three stage adsorption in Verm-I and Verm-I-Cit (**Fig. 4-8b**). The first stage is rapid adsorption due to the interaction between Cs and the surface of clay minerals. The second stage is slow adsorption due to the penetration and diffusion of Cs into the mineral structure. Similar behavior has been reported in a previous study [18]. The third stage is slow distribution

and reaching equilibrium. The adsorption isotherm was evaluated at a condition of contact time of 24 h (**Fig. 4-9**). The Langmuir adsorption isotherm well described the Cs adsorption in both Verm-I and Verm-I-Cit (**Table 4-3**); monolayer adsorption was considered. The adsorption of Cs by clay minerals with a large basal spacing follows the Langmuir adsorption isotherm. The Cs and interlayer sites have strong interactions, and the ratio of adsorption in the interlayer was the highest in the total adsorption capacity (Chapter 2). Since an equal amount of Na as the adsorbed Cs is eluted from Verm-I-Cit, the adsorption of Cs is due to ions exchangeable with Na.

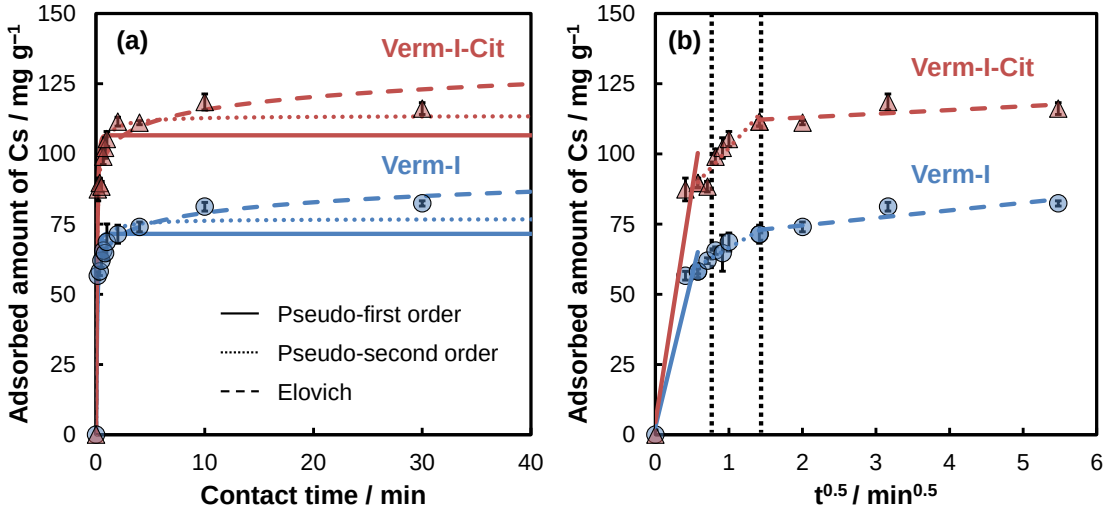

Fig. 4-8. (a) Adsorbed amount of Cs in each contact time by Verm-I and Verm-I-Cit and **(b)** Linearized plot for IPD kinetics model. The initial concentration of Cs was 500 mg/L (pH 6.0); the temperature was 25 °C; the adsorbent dose was 2 g/L. Error bars indicate the standard deviation (n = 3).

Table 4-2. Adsorption kinetics parameters of Verm-I and Verm-I-Cit for Cs adsorption.

Model	Parameter	Verm-I	Verm-I-Cit
Pseudo-first order	q_e[a]	71.5	106.6
	k_{p1}[b]	7.07	7.93
	R^2	0.910	0.928
	χ^2	4.98	5.77
Pseudo-second order	q_e[a]	76.9	113.6
	k_{p2}[c]	0.142	0.116
	R^2	0.969	0.976
	χ^2	1.40	1.61
Elovich	α[d]	1.12×10^6	2.64×10^6
	β[e]	0.184	0.127
	R^2	0.975	0.894
	χ^2	0.37	2.16
Intraparticle diffusion (IPD)	$k_{IPD\text{-}1}$[f]	107.73	166.13
	$C_{IPD\text{-}1}$[g]	2.862	4.423
	R^2	0.931	0.931
	$k_{IPD\text{-}2}$[f]	15.13	28.754
	$C_{IPD\text{-}2}$[g]	51.380	73.314
	R^2	0.875	0.862
	$k_{IPD\text{-}3}$[f]	2.673	1.332
	$C_{IPD\text{-}3}$[g]	69.189	110.300
	R^2	0.798	0.441

[a] q_e in mg g^{-1}

[b] k_{p1} in min^{-1}

[c] k_{p2} in g mg^{-1} min^{-1}

[d] α in mg g^{-1} min^{-1}

[e] β in g mg^{-1}

[f] k_{IPD} in mg g^{-1} $min^{-0.5}$

[g] C_{IPD} in mg g^{-1}

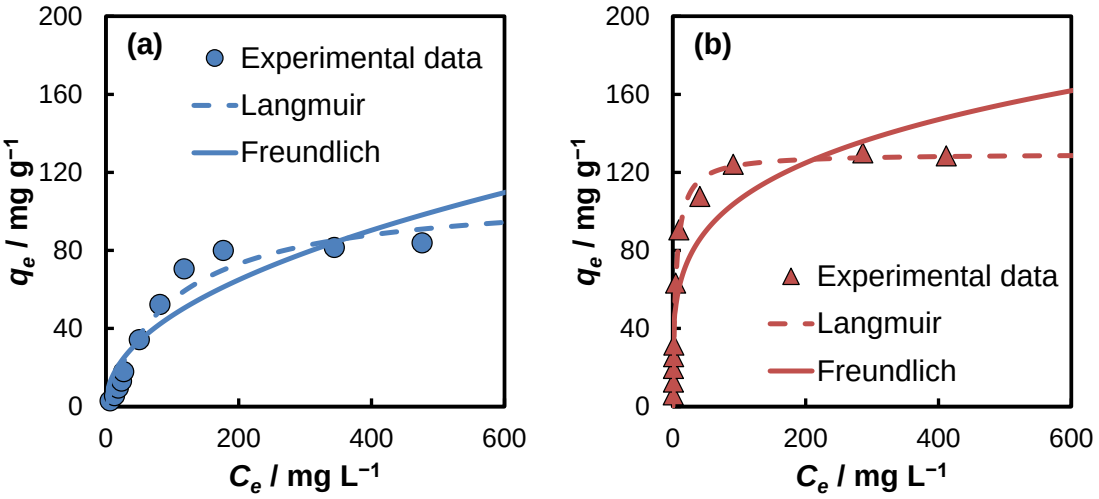

Fig. 4-9. Adsorption isotherm for Cs: **(a)** Verm-I; **(b)** Verm-I-Cit. The Cs solution was pH 6.0; the contact time was 24 h; the temperature was 25 °C; the adsorbent dose was 2 g/L.

Table 4-3. Parameters of adsorption isotherm models for Cs adsorption onto adsorbents.

Clay	Langmuir				Freundlich			
mineral	R^2	K_L[a]	Q_{max}[b]	χ^2	R^2	K_F[c]	$1/n$	χ^2
Verm	0.963	0.010	110.4	17.6	0.865	5.2	0.477	46.7
Verm-Cit	0.992	0.208	129.7	8.5	0.868	35.7	0.236	78.1

[a] K_L in L g^{-1}

[b] Q_{max} in mg g^{-1}

[c] K_F in (mg g^{-1})(L mg^{-1})$^{1/n}$

Figure 4-10 shows the adsorption capacity under various pH conditions. Cs speciation was evaluated using Visual MINTEQ (version 3.1), Cs existed as Cs^+ between pH 2–12 in this adsorption experiment condition. The adsorption capacity of Verm-I was approximately 80–100 mg/g under neutral and basic conditions but decreased sharply at pH 2. This tendency was the same for the Verm-I-Cit. Clay minerals have both variable and permanent charges. The variable charge depends on the pH condition; typically, its

charge becomes negatively strong under basic conditions, and H^+ neutralizes it under acidic conditions. Therefore, the variable charge could not contribute to the Cs adsorption under low pH conditions, and the adsorption capacity decreased at pH 2. The difference between the adsorption capacities at pH 2 and 6 was approximately 40 mg/g in both Verm-I and Verm-I-Cit, corresponding to the variable charge amount. Verm-I-Cit had a large adsorption capacity (75.1 mg/g) even at pH 2. The negative charge generated by removing the interlayer material was immediately neutralized by Na derived from sodium citrate. Since Cs were adsorbed by ion exchange with Na in the interlayer, the adsorption capacity increased by the amount that the interlayer material was removed from the interlayer.

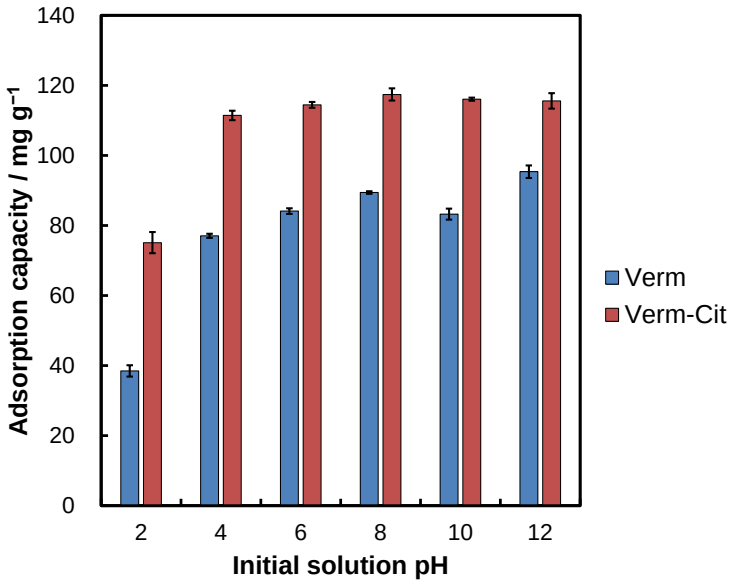

Fig. 4-10. Adsorption capacity for Cs of Verm-I and Verm-I-Cit in various pH conditions. The concentration of Cs was 500 mg/L; the contact time was 24 h; the temperature was 25 °C; the adsorbent dose was 2 g/L. Error bars indicate the standard deviation (n = 3).

4.3.5. Selectivity

The ion-exchange isotherm of Verm-Cit was used to evaluate selectivity for Cs and Na. If the isotherm is convex-upward, the adsorbent has a higher selectivity for Cs than Na. As shown in **Fig. 4-11a**, Verm-Cit has a higher selectivity for Cs than Na. **Figure 4-11b** shows the variation of the Vanselow selectivity coefficient (K^{V}_{NaCs}) of Verm-Cit. The value of ln K^{V}_{NaCs} was 3.2 ± 0.6 and suggesting high selectivity for Cs than for Na.

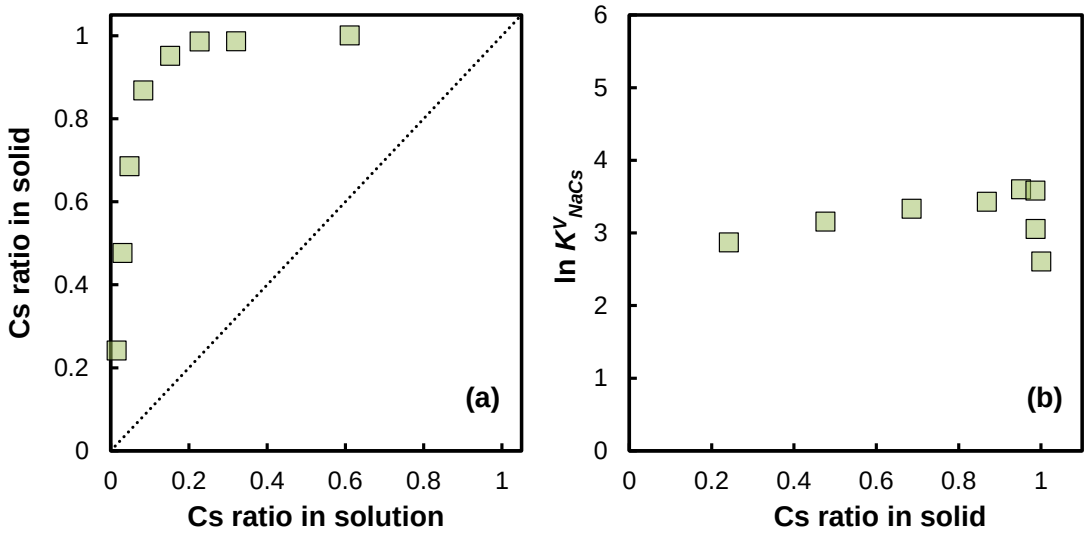

Fig. 4-11. (a) Ion-exchange isotherm of Verm-Cit and **(b)** the variation of the Vanselow selectivity coefficient as ln K^{v}_{NaCs}. The total concentration of Cs and Na was 5 mmol/L; contact time was 24 h; the temperature was 25 °C; the adsorbent dose was 2 g/L.

When Cs and coexisting ions were included in equivalent amounts, the adsorption capacity was decreased slightly by these monovalent cations about 2 to 10%. The presence of divalent cations was more affected than monovalent cations, but it was less than 30%. In the presence of 10-fold coexisting ions relative to Cs, the adsorption capacity

was decreased, by 20–30% for monovalent cations and 50–60% for divalent cations (**Fig. 4-12a**). Typically, the higher the valence of the ion, the stronger the interaction with the adsorbent, so it was considered that the divalent ions interfered more strongly with the adsorption capacity of Verm-I-Cit.

In the case of humic acid coexistence, the Cs adsorption capacity of Verm-I-Cit did not change in each concentration as shown in **Fig. 4-12b**. It seems that the Cs adsorption by vermiculite is not affected apparently by organic impurities like humic substances. However, Wei et al. reported that Cs could be adsorbed on humic substances covering the surface of the clay mineral [19]. Therefore, the effect of humic substances on adsorption capacity in **Fig. 4-12b** might include the amount of Cs adsorbed at humic substance on the surface of Verm-Cit.

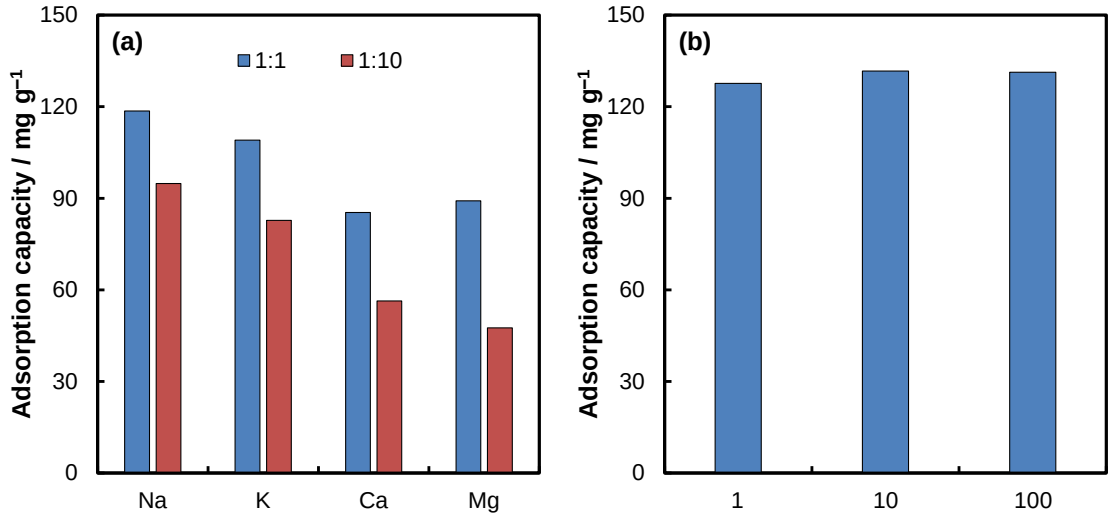

Fig. 4-12. Adsorption capacity of Verm-Cit under **(a)** various coexisting ions and **(b)** coexisting humic substance (1, 10, and 100 mg/L as carbon).

4.3.6. Adsorption kinetics of AG-Verm-I and AG-Verm-I-Cit

The adsorption of Cs by the powder form Verm-I was discussed before, and the performance of the adsorbent encapsulated in AG beads will be described in this section. **Figure 4-13a** shows the adsorbed amount of Cs by AG-Verm-I and AG-Verm-I-Cit at various contact times; the parameters of adsorption kinetics are indicated in **Table 4-4**. Both AG-Verm-I and AG-Verm-I-Cit were described by the pseudo-second order model. The IPD kinetics model indicated the three stage adsorption in AG-Verm-I and AG-Verm-I-Cit similar to powder Verm-I and Verm-I-Cit (**Fig. 4-13b**). The adsorption capacity of AG without Verm-I was 1.02 mg/g in this study. This small capacity was also reported in the previous study [20]. Therefore, the adsorption capacity of AG-Verm-I and AG-Verm-I-Cit was significantly affected by the encapsulated vermiculite, yielding a similar adsorption behavior (Section 3.4). The encapsulated Verm-I significantly contributes to adsorption while maintaining its structure. Compared with powdered Verm-I and Verm-I-Cit, showed in **Fig. 4-8**, the time to reach equilibrium was longer, and the equilibrium time was over 360 min. After one month of contact, the adsorption capacity was 84.8 and 98.5 mg/g in AG-Verm-I and AG-Verm-I-Cit, respectively, which were almost unchanged after two months of contact. Typically, the adsorption rate of bead-like adsorbent tends to decrease because it needs a step in which the adsorbate diffuses inside of the adsorbent [21]. In this study, since Cs should pass through the alginate gel network before Cs contact with the encapsulated Verm-I-Cit, the equilibrium adsorption time increased and the slope of the IPD kinetics model became gentler. These results indicate that the contact efficiency between Verm-I or Verm-I-Cit and Cs was reduced by encapsulation in AG beads. However, AG-Verm-I-Cit could adsorb 60.5 mg/g even in 30 min, and a relatively higher adsorption capacity was achieved.

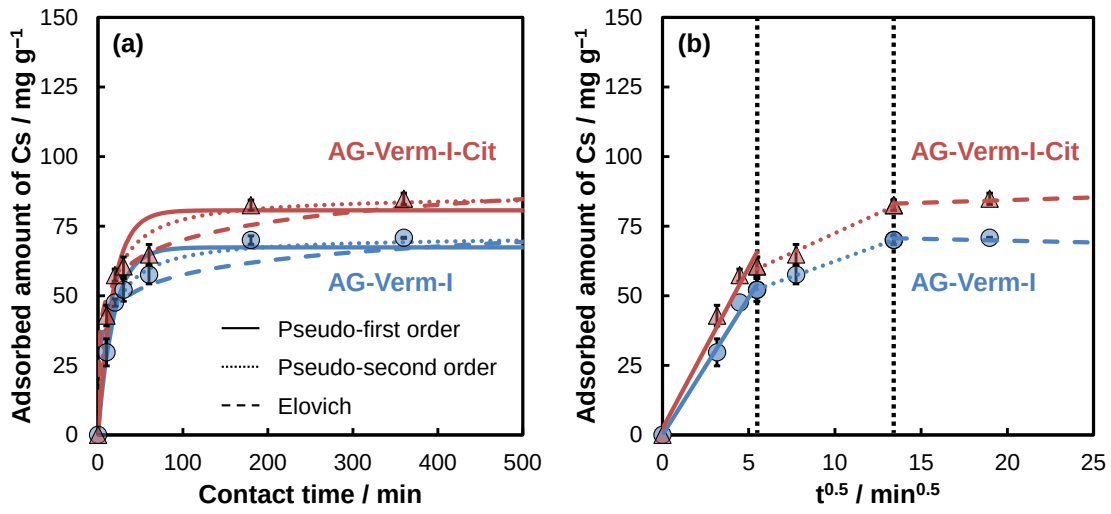

Fig. 4-13. (a) Adsorbed amount of Cs by alginate gel vermiculite (AG-Verm) beads and alginate gel sodium citrate-pretreated vermiculite (AG-Verm-Cit) beads in each contact time, and **(b)** the linearized plot for IPD kinetics model. The concentration of Cs was 500 mg/L (pH 6.0); the temperature was 25 °C; the adsorbent dose was 25 beads in 25 mL. Error bars indicate the standard deviation (n = 3).

Table 4-4. Adsorption kinetics parameters of AG-Verm-I and AG-Verm-I-Cit for Cs adsorption.

Model	Parameter	AG-Verm-I	AG-Verm-I-Cit
Pseudo-first order	q_e[a]	67.4	80.7
	k_{p1}[b]	0.054	0.058
	R^2	0.979	0.943
	χ^2	1.15	3.65
Pseudo-second order	q_e[a]	71.5	86.2
	k_{p2}[c]	0.001	0.001
	R^2	0.989	0.986
	χ^2	0.441	0.956
Elovich	α[d]	189.2	200.7
	β[e]	0.136	0.110
	R^2	0.752	0.911
	χ^2	4.84	1.69
Intraparticle diffusion (IPD)	k_{IPD-1}[f]	9.869	11.559
	C_{IPD-1}[g]	-0.011	2.318
	R^2	0.989	0.974
	k_{IPD-2}[f]	2.240	2.841
	C_{IPD-2}[g]	40.012	44.064
	R^2	0.999	0.991
	k_{IPD-3}[f]	-0.131	0.192
	C_{IPD-3}[g]	72.427	80.518
	R^2	0.817	0.937

[a] q_e in mg g^{-1}

[b] k_{p1} in min^{-1}

[c] k_{p2} in g mg^{-1} min^{-1}

[d] α in mg g^{-1} min^{-1}

[e] β in g mg^{-1}

[f] k_{IPD} in mg g^{-1} $min^{-0.5}$

[g] C_{IPD} in mg g^{-1}

The FT-IR spectra of AG-Verm-I-Cit have a pattern in which the peaks of AG and Verm-I-Cit are superimposed (**Fig. 4-14a**). Alginate has the main absorption band at around 1620 and 1425 cm^{-1} attributed to the asymmetric and symmetric stretching of the carboxyl group [22]. These absorption bands can be also found in the FT-IR of AG-Verm-I-Cit, and thus Cs has a possibility to be adsorbed by the interaction with the carboxyl group, but the adsorbed amount was low. As mentioned before, the adsorption capacity of alginate beads for Cs was only 1.02 mg/g in this study. The X-ray diffractograms of AG-Verm-I-Cit have a reflection at a similar degree (approximately 7.7°) to that of the Verm-I-Cit, although that was not a clear reflection compared to the powder form Verm-I-Cit after Cs adsorption (**Fig. 4-14b**). However, a strong reflection of 1.4 nm was observed before Cs adsorption (AG-Verm-I-Cit), and this reflection disappeared after Cs adsorption (AG-Verm-I-Cit-Cs). This result indicates that the basal spacing of AG-Verm-I-Cit also narrows accompanying Cs adsorption, similarly to the Verm-I-Cit.

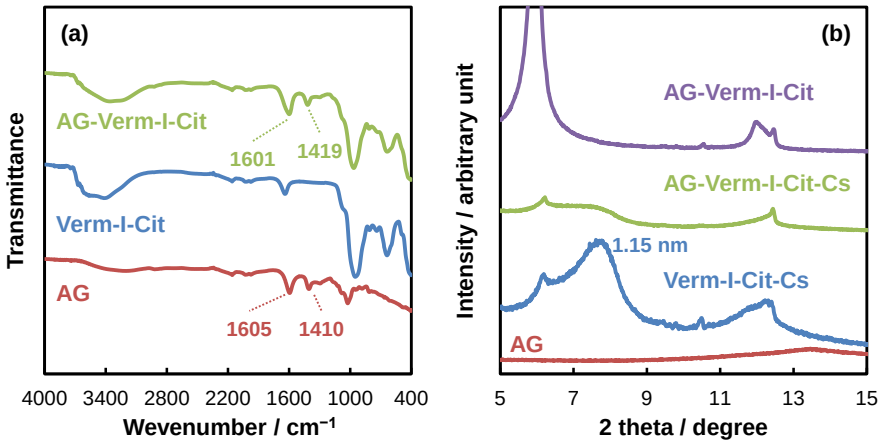

Fig. 4-14. (a) FT-IR spectra of AG, Verm-I-Cit, and AG-Verm-I-Cit, and **(b)** X-ray diffractograms of AG, Verm-I-Cit-Cs, AG-Verm-I-Cit-Cs, and AG-Verm-I-Cit. Verm-I-Cit-Cs and AG-Verm-I-Cit-Cs indicate the adsorbent after Cs adsorption.

Since the diameter of the developed alginate gel vermiculite (AG-Verm-I or AG-Verm-I-Cit) is approximately 3 mm, 100% of the recovery rate can be achieved by using mesh under 3 mm. A tea strainer with 0.5 mm mesh was used to collect adsorbent in our experiment, and the recovery rate was 100%. Since the wastewater can easily pass through 0.5 mm mesh without clogging, the separation of adsorbents and treated water is effortless and fast. Moreover, as shown in **Fig. 4-15**, the volume of AG-Verm-I-Cit can be reduced by air-drying without heating. The diameter decreased to 1.3 mm from 3 mm, with a weight loss of 88%. When this adsorbent was considered a sphere, its volume was reduced to approximately one-sixteenth. Based on this observation, the volume of the adsorbent that has adsorbed the pollutant can be significantly reduced by air-drying. This property will contribute to the stable management of adsorbents with radionuclides such as vitrification and geological disposal.

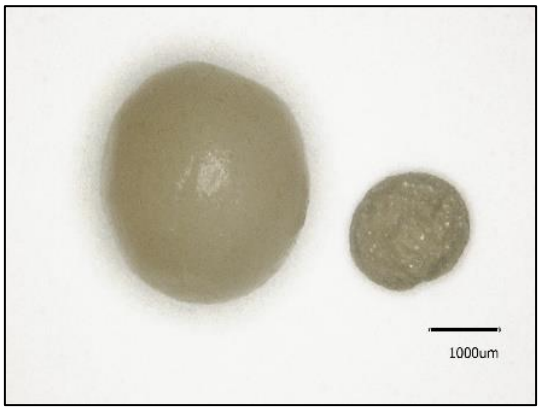

Fig. 4-15. Photograph of alginate gel sodium citrate-pretreated vermiculite (AG-Verm-I-Cit) beads before (left) and after (right) drying overnight at room temperature (approximately 22 °C).

4.3.7. Comparison with previous studies

The developed adsorbent was compared with previous studies (**Table 4-5**), and AG-Verm-I-Cit has a similar or higher adsorption capacity than previous studies. As mentioned in Section 3.5, it requires a longer time to reach equilibrium adsorption. Still, the adsorption capacity at 30 min was 60.5 mg/g; a large amount of Cs could be adsorbed within a short contact time. Although some reported adsorbents have larger adsorption capacity than our adsorbent, these adsorbents require various pretreatments during preparation [1,2] and are heated at 550 °C to reduce the volume of the adsorbent [1]. Moreover, since many of the reported adsorbents are in powder form, after Cs adsorption, adsorbents were separated by filtration [1,2,18,23,24]. However, the filtration of powder form adsorbents is a challenge in terms of practical application. As one of the solutions to this challenge, it is conceivable to encapsulate the adsorbent into beads. It has been reported that chitosan and polyacrylonitrile are used in addition to alginate, and magnetite is added to enable magnetic separation [25–27]. However, these bead-like adsorbents also have disadvantages, such as the requirement for heating, the complex manufacturing procedure, and the use of reagents with a load on wastewater treatment. In this regard, our adsorbent allows us to easily separate Cs from contaminated water due to the encapsulation in AG bead, which offers several advantages, including easy preparation and low environmental impact.

By changing the substances contained in the AG beads, broader applications for the adsorption of various pollutants are possible. These bead-encapsulated adsorbents are promising materials because they are derived from nature and can significantly contribute to the development of water treatment technology.

Table 4-4 Compares of adsorption abilities for Cs in this and previous studies.

	Capacity / mg g^{-1}	Adsorption time	Ref.
Powder form adsorbent			
Wood cellulosic	133.54	5 h	[1]
Crown ether based mesoporous adsorbent	107.16	30 min	[2]
Vermiculite modified with ethylamine	78.17	2 h	[18]
Montmorillonite-Prussian blue hybrid	57.47	2 h	[23]
Sewage sludge molten slag	52.36	2 h	[24]
Prussian blue modified magnetite	16.2	1 h	[28]
Sphere form adsorbent			
Copper hexacyanoferrate-PAN	25.5	4.6 h	[25]
Maghemite PVA	32.15	5 h	[26]
Magnetic bentonite-chitosan	57.1	6 h	[27]
AG-Verm-Cit beads (not equilibrium)	60.5	at 30 min	This study
AG-Verm-Cit beads (at equilibrium)	98.5	1 month	This study

4.4. Summery

A collectable adsorbent with a low environmental impact was developed using Verm and AG beads to remove Cs from an aquatic environment. Sodium citrate can remove the interlayer material and improve the adsorption capacity of the adsorbent. The adsorption capacity increased to 119 mg/g (Verm-I-Cit) from 97.1 mg/g (Verm-I). The sodium citrate treatment increased the adsorption capacity of Verm-I. The collectability was added to powder form adsorbent by encapsulating Verm-I and Verm-I-Cit in AG beads. Although this encapsulation led to a longer equilibrium time, AG-Verm-I-Cit still had a large adsorption capacity (60.5 mg/g) even within a short contact time (30 min). Moreover, the volume of AG-Verm-I-Cit can easily be reduced by air-drying, and the generation of sludge in the treatment of contaminated water containing Cs can be reduced.

4.5. References

[1] M.N. Hasan, M.A. Shenashen, M.M. Hasan, H. Znad, M.R. Awual, Assessing of cesium removal from wastewater using functionalized wood cellulosic adsorbent, Chemosphere. 270 (2021) 128668. doi:10.1016/j.chemosphere.2020.128668.

[2] M.R. Awual, Ring size dependent crown ether based mesoporous adsorbent for high cesium adsorption from wastewater, Chem. Eng. J. 303 (2016) 539–546. doi:10.1016/j.cej.2016.06.040.

[3] B. Pangeni, H. Paudyal, K. Inoue, K. Ohto, H. Kawakita, S. Alam, Preparation of natural cation exchanger from persimmon waste and its application for the removal of cesium from water, Chem. Eng. J. 242 (2014) 109–116. doi:10.1016/j.cej.2013.12.042.

[4] H. Mukai, T. Hatta, H. Kitazawa, H. Yamada, T. Yaita, T. Kogure, Speciation of radioactive soil particles in the Fukushima contaminated area by IP autoradiography and microanalyses, Environ. Sci. Technol. 48 (2014) 13053–13059. doi:10.1021/es502849e.

[5] G. Annadurai, R.-S. Juang, D.-J. Lee, Factorial design analysis for adsorption of dye on activated carbon beads incorporated with calcium alginate, Adv. Environ. Res. 6 (2002) 191–198. doi:10.1016/S1093-0191(01)00050-8.

[6] A.N. Bezbaruah, S. Krajangpan, B.J. Chisholm, E. Khan, J.J. Elorza Bermudez, Entrapment of iron nanoparticles in calcium alginate beads for groundwater remediation applications, J. Hazard. Mater. 166 (2009) 1339–1343. doi:10.1016/j.jhazmat.2008.12.054.

[7] S.C.W. Sakti, R.A. Wijaya, N. Indrasari, M.Z. Fahmi, A.A. Widati, Abdulloh, Nuryono, C.-H. Chen, Magnetic hollow buoyant alginate beads achieving rapid remediation of oil contamination on water, J. Environ. Chem. Eng. 9 (2021) 104935. doi:10.1016/j.jece.2020.104935.

[8] M. Xia, X. Zheng, M. Du, Y. Wang, A. Ding, J. Dou, The adsorption of Cs^+ from wastewater using lithium-modified montmorillonite caged in calcium alginate beads, Chemosphere. 203 (2018) 271–280. doi:10.1016/j.chemosphere.2018.03.129.

[9] H. Shirozu, Introduction to Clay Mineralogy –Fundamentals for Clay Science–, Asakura Publishing Co., Ltd., Tokyo, (1988) (in Japanese).

[10] T. Tamura, Identification of clay minerals from acid soils, J. Soil Sci. 9 (1958) 141–147. doi:10.1111/j.1365-2389.1958.tb01906.x.

[11] H.E. Jensen, K.L. Babcock, Cation-exchange equilibria on a Yolo loam, Hilgardia. 41 (1973) 475–487. doi:10.3733/hilg.v41n16p475.

[12] J.J. Call, M.E. Essington, S. Rakshit, The cation exchange behavior of tylosin in loess-derived soil, Chemosphere. 233 (2019) 615–624. doi:10.1016/j.chemosphere.2019.06.028.

[13] M. Ishiguro, Basic theories of solute transport and adsorption in soils, III. Multilayer adsorption, cooperative adsorption and selectivity coefficient, J. Japanese Soc. Soil Phys. 20 (2020) 11–20 (in Japanese). doi:10.34467/jssoilphysics.145.0_11.

[14] T. Kogure, K. Morimoto, K. Tamura, H. Sato, A. Yamagishi, XRD and HRTEM evidence for fixation of cesium ions in vermiculite clay, Chem. Lett. 41 (2012) 380–382. doi:10.1246/cl.2012.380.

[15] K. Wada, An invitation to soil clay mineralogy, Nendo Kagaku. 26 (1986) 1-11 (in Japanese). doi:10.11362/jcssjnendokagaku1961.26.1.

[16] E. Siswoyo, N. Endo, Y. Mihara, S. Tanaka, Agar-encapsulated adsorbent based on leaf of platanus sp. to adsorb cadmium ion in water, Water Sci. Technol. 70 (2014) 89–94. doi:10.2166/wst.2014.190.

[17] Japanese Humic Substances Society, Handbook of Humic Substances Analysis, second edi, Rural Culture Association, Tokyo, (2019) (in Japanese).

[18] H. Long, P. Wu, L. Yang, Z. Huang, N. Zhu, Z. Hu, Efficient removal of cesium from aqueous solution with vermiculite of enhanced adsorption property through surface modification by ethylamine, J. Colloid Interface Sci. 428 (2014) 295–301. doi:10.1016/j.jcis.2014.05.001.

[19] X. Wei, Y. Sun, D. Pan, Z. Niu, Z. Xu, Y. Jiang, W. Wu, Z. Li, L. Zhang, Q. Fan, Adsorption properties of Na-palygorskite for Cs sequestration: Effect of pH, ionic strength, humic acid and temperature, Appl. Clay Sci. 183 (2019) 105363. doi:10.1016/j.clay.2019.105363.

[20] Y. Mihara, M.T. Sikder, H. Yamagishi, T. Sasaki, M. Kurasaki, S. Itoh, S. Tanaka, Adsorption kinetic model of alginate gel beads synthesized micro particle-Prussian blue to remove cesium ions from water, J. Water Process Eng. 10 (2016) 9–19. doi:10.1016/j.jwpe.2016.01.001.

[21] H. Zeng, S. Sun, K. Xu, W. Zhao, R. Hao, J. Zhang, D. Li, Iron-loaded magnetic alginate-chitosan double-gel interpenetrated porous beads for phosphate removal from water: Preparation, adsorption behavior and pH stability, React. Funct. Polym. 177 (2022) 105328. doi:10.1016/j.reactfunctpolym.2022.105328.

[22] S.M.H. Dabiri, A. Lagazzo, F. Barberis, M. Farokhi, E. Finochio, L. Pastorino, Characterization of alginate-brushite in-situ hydrogel composites, Mater. Sci. Eng. C. 67 (2016) 502–510. doi:10.1016/j.msec.2016.04.104.

[23] H.A. Alamudy, K. Cho, Selective adsorption of cesium from an aqueous solution by a montmorillonite-prussian blue hybrid, Chem. Eng. J. 349 (2018) 595–602. doi:10.1016/j.cej.2018.05.137.

[24] S. Khandaker, Y. Toyohara, S. Kamida, T. Kuba, Effective removal of cesium from wastewater solutions using an innovative low-cost adsorbent developed from sewage sludge molten slag, J. Environ. Manage. 222 (2018) 304–315. doi:10.1016/j.jenvman.2018.05.059.

[25] A. Nilchi, R. Saberi, M. Moradi, H. Azizpour, R. Zarghami, Adsorption of cesium on copper hexacyanoferrate–PAN composite ion exchanger from aqueous solution, Chem. Eng. J. 172 (2011) 572–580. doi:10.1016/j.cej.2011.06.011.

[26] Z. Majidnia, A. Idris, Evaluation of cesium removal from radioactive waste water using maghemite PVA–alginate beads, Chem. Eng. J. 262 (2015) 372–382. doi:10.1016/j.cej.2014.09.118.

[27] K. Wang, H. Ma, S. Pu, C. Yan, M. Wang, J. Yu, X. Wang, W. Chu, A. Zinchenko, Hybrid porous magnetic bentonite-chitosan beads for selective removal of radioactive cesium in water, J. Hazard. Mater. 362 (2019) 160–169. doi:10.1016/j.jhazmat.2018.08.067.

[28] T. Sasaki, S. Tanaka, Magnetic separation of cesium ion using Prussian blue modified magnetite, Chem. Lett. 41 (2012) 32–34. doi:10.1246/cl.2012.32.

Chapter 5

Evaluation of cesium stability in model contaminated soil by electrokinetic process

5.1. Introduction

The interaction between Cs and clay minerals was evaluated in Chapters 2 and 3 through batch experiments in solution. However, to estimate the long-term movement of Cs in the actual soil in detail, it is necessary to know the dynamic behavior of Cs in the soil, that is, whose water content in the soil is 10–30%, as well as the static one obtained from the batch experiment. Ordinary, a column method is used as a conventional dynamic equilibrium experiment to obtain information on the dynamic behaviors of pollutants. However, it is difficult to apply the column method to clayey soil because water cannot flow through the clayey soil, which has a very low permeability. In addition, in the batch adsorption test, the solid-liquid ratio differs greatly from the actual soil environment not to guarantee the validity of the evaluation method. Therefore, the development of technology that enables an evaluation of the dynamic behavior of substances in low permeability soil is required.

The electrokinetic (EK) process is one of the soil remediation technologies, which has been applied to remove various pollutants from soil [1]. The electroosmotic flow (EOF), which occurred by the EK process, can pass through the soil sample independent of its water permeability [2,3]. The removal behavior of various pollutants, such as heavy metals [4–6], anions [7–9], organic compounds [10–12], and complexes [13–15] have been investigated by the EK process. The EOF was discovered by Reuss in the 19th century along with electrophoresis and has been widely used as a driving force in capillary electrophoresis in analytical chemistry and dehydration from the ground in civil engineering. Recently, contact lenses that do not dry easily and drug delivery in injections have been studied using EOF phenomena [16–18], and the research field of the EOF is expanding.

In this study, the adsorption and desorption of Cs ions on two kinds of clay minerals under static and dynamic conditions were attempted by the EOF.

5.2. Materials and methods

5.2.1. Materials and chemicals

Two types of 2:1 clay mineral having different electric charges and basal spacings in the structure were used in this study. These are White clay (Practical grade, Wako Pure Chemical Industries, Ltd., Japan) and vermiculite (Verm-E, Exfoliated for horticultural use, Kenis Ltd., Japan). White clay was used in the experiments without any pretreatment. Verm-E was the same vermiculite as Chapter 2, and the same pretreatments such as crush and sieve and was performed before the experiment.

CsCl, KCl, $MgCl_2$, NaOH, CH_3COONa, CH_3COONH_4, CH_3COOH, and oxalic acid were purchased from Fujifilm Wako Pure Chemical Corporation, Japan. Hydroxylammonium chloride was purchased from Junsei Chemical Co., Ltd., Japan. HNO_3 and HCl were purchased from Kanto Chemical Co., Inc., Japan. All reagents were used without any pretreatment. The ion exchange water made by Autostill WA73 (Yamato Scientific Co., Ltd., Japan) was used for the preparation and dilution of the sample solutions.

5.2.2. Characteristics of clay minerals

The characteristics of clay minerals were investigated. The basal spacing of clay minerals was measured by X-ray diffraction (XRD). X-ray diffractograms were recorded with Cu Kα radiation (λ = 0.154 nm) at 30 kV and 15 mA in the range of 5-70° by Miniflex X-ray diffractometer (XRD, Rigaku Corporation, Japan). Fourier Transform Infra-Red

(FT-IR) spectra of clay minerals were measured (FT-IR 4100, JASCO, Japan) by using the KBr disk technique. The chemical compositions were measured by an Energy-Dispersive X-Ray Fluorescence Spectrometer (XRF, JSX-3100RII, JEOL, Japan). The zeta potential was measured by Zeta-potential & Particle Size Analyzer (ELSZ-1000, Otsuka Electronics Co., Ltd., Japan). The sample concentration was about 2 g/L, and the pH was adjusted with 0.1 mol/L HCl and NaOH.

5.2.3. Preparation of model contaminated soil

Four kinds of the model soils (100 g) whose Verm-E content were 0, 5, 10, and 100wt% (i.e., 100, 95, 90, and 0wt% of white clay) were mixed with 200 mL of deionized water for the complete dispersal. After adding 10 mL of the CsCl solution (1,000 mg (Cs^+) /L), the mixture was horizontally shaken for 24 h at 170 rpm (Multi Shaker MMS-3010, EYELA, Japan). Then, the mixture was dried at 80 °C in an oven (Yamato Constant Temperature Oven DK-62, Yamato Scientific Co., Ltd., Japan) overnight. The Cs content in each model contaminated soil was 0.1 mg/g. Before the model soil was placed in the EK equipment, the water content was adjusted to 30% with deionized water.

5.2.4. Equipment and experiment for electrokinetic process

The equipment for the EK process in this study is shown in **Fig. 5-1**. The cylindrical EK cell was made from acrylic resin. It consists of a migration chamber (10 cm in width and 3 cm in diameter) and two electrode chambers (5 cm in width and 3 cm in diameter) at both ends of the migration chamber. The silicon O-rings (Kokugo Co., Ltd., Japan) and filter papers (5C, Toyo Roshi Kaisha Ltd., Japan) were inserted between the migration chamber and the electrode chamber to avoid the leakage of soil into the electrode

chambers. Titanium gauze electrodes coated with platinum (Tanaka Kikinzoku Kogyo K.K., Japan) were set in both electrode chambers. The prepared model contaminated soil was filled into the migration chamber, the electrolyte was added to the electrode chamber, and after that, the electrodes in the chambers were connected with the electric power, and then constant voltage was applied. In all experiments, a constant voltage was applied by a DC power supply (MP-7612D, Marisol Co., Ltd., Japan). The potential gradient was 1 V/cm, and it was applied for 72 h. A measuring cylinder was connected to the cathode chamber to receive the water transported by the EOF as an overflow from the cathode chamber. Since the electrolyte at the anode decreased with the generation of EOF, a liquid level gauge with a quartz sensor (Fujiwara Scientific Co., Ltd., Japan) was connected to adjust the constant anolyte at all operation times.

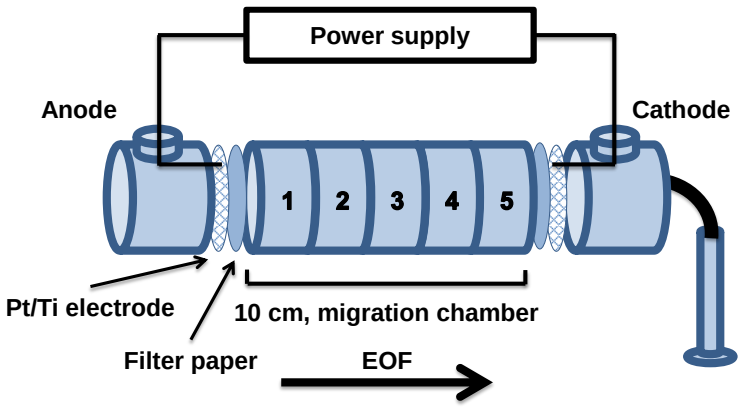

Fig. 5-1. Schematic diagram of the electrokinetic process.

5.2.5. Analytical procedure

After the EK process, the soil in the migration chamber was divided into five sections. About 2.5 g of the soil was taken from each section as it included the water to avoid changing the chemical form of Cs in the model soil by drying. These wet soil

samples were used for the sequential extraction analysis of Cs. The remaining soil samples were dried at 80 °C for 24 h and were used to measure the water contents. The soil amount in the wet soil samples was calculated by subtracting the amount of water in the wet sample from the weight of the wet soil sample. This calculated soil amount of the wet soil sample was used for the calculation of the Cs concentration in the soil after the EK process. Sequential extraction analysis was used for the investigation of the chemical forms of Cs in the soil samples. Each fraction was defined according to the previous paper by Tessier et al.[19]: fraction 1 (F1) is exchangeable, fraction 2 (F2) is bound to carbonates, fraction 3 (F3) is bound to Fe–Mn oxides, fraction 4 (F4) is bound to organic matters, and fraction 5 (F5) is residuals. In this section, 0.5 mol/L oxalic acid was substituted for the ordinary extraction procedure of F5 (treatment with HF and $HClO_4$) as described in Chapter 3. In the sequential extraction analysis, about 2.5 g of wet soil sample were taken into 50 mL centrifuge tubes, and 20 mL of 1.0 mol/L magnesium chloride was added and shaken for 6 h at 1,000 rpm. After centrifugation for 15 min at 4,000 rpm, the supernatant was obtained (F1). The residual of F1 was added to 20 mL of 1.0 mol/L sodium acetate (pH 5.0, adjusted with acetic acid) and shaken for 6 h at 1,000 rpm. After shaking, the sample was filtered with 5C filter paper, and the filtrate was adjusted to 50 mL (F2). The residual of F2 was transferred to a 200 mL conical beaker and added 20 mL of 0.04 mol/L hydroxylammonium chloride was in 25% (v/v) acetic acid. The mixture was heated at 95 °C for 3 h. After standing to cool, it was filtered with 5C filter paper, and the filtrate was adjusted to 50 mL (F3). The residual of F3 was transferred to a 200 mL conical beaker and 5 mL of 0.02 mol/L nitric acid and 10 mL of 30% hydrogen peroxide (pH 2.0, adjusted with nitric acid) were added. The mixture was heated at 85 ± 5 °C for 2 h. New 10 mL of 30% hydrogen peroxide (pH 2.0, adjusted with nitric acid) was added and heated again at

85 ± 5 °C for 3 h. After cooling, 10 mL of 3.2 mol/L ammonium acetate in 20% (v/v) nitric acid was added and agitated for 30 min. The mixture was filtered with 5C filter paper, and the filtrate was adjusted to 50 mL (F4). The sample (0.5 g) from the residue of F4 was transferred to a 200 mL conical beaker and 25 mL of 0.5 mol/L oxalic acid was added. The mixture was heated at 85 ± 5 °C for 4 h. After cooling, it was filtered with 5C filter paper, and the filtrate was adjusted to 50 mL (F5). The concentration of Cs was measured by using atomic adsorption spectrophotometer (AAS, A-2000, Hitachi Ltd., Japan) at 852.1 nm. Soil pH was measured by pH meter (M-13, Horiba, Ltd., Japan) after 1:5 water extraction method for the dried soil sample in each section.

Since the anode solution, cathode solution, and EOF after the EK process might contain a small amount of clay minerals from the migration chamber, the concentration of Cs in these solutions was measured by AAS after filtration through a 0.45 μm membrane filter paper. The migration efficiency was calculated by **Eq (5-1).**

$$\text{Migration efficiency (\%)} = \frac{A_{Soln.}}{A_I} \times 100 \quad \textbf{(5-1)}$$

Here $A_{Soln.}$ indicates the amount of Cs in the cathode and EOF solutions after the EK process, and A_I is the initial amount of Cs in the model soil before the EK process.

5.3. Results and discussion

5.3.1. Characterization of clay mineral

The XRD results for each clay mineral are shown in **Fig. 5-2**. In the X-ray diffractograms of white clay, the peaks of pyrophyllite were observed at 9.54°, 19.2° and 29.0° and the peaks of quartz were also observed at 20.8°, 26.6° and 50.1° in the 2θ scale, respectively. White clay was identified as the mixture of pyrophyllite (Joint Committee on Powder Diffraction Standards, JCPDS 46-1308) and quartz (JCPDS 46-1045) by the

Hanawalt method. Furthermore, the X-ray diffractograms at 55-65° and FT-IR spectra of white clay are shown in **Fig. 5-3**. In the classification of an octahedral sheet, one of the characteristics of the dioctahedral sheet is the reflection at 0.149 nm (2θ = 62°) in X-ray diffraction and the other one is the two absorption bands around 500 cm^{-1} in FT-IR spectra. The Si-O-Al and Si-O bending vibrations have an absorption band of around 524 and 466 cm^{-1} [20,21]. The dioctahedral sheet is consisted of Al and has Si-O-Al and Si-O bands. On the other hand, the trioctahedral sheet has Mg or Fe which is replaced by Al, and the absorption band of Si-O-Al (around 524 cm^{-1}) has not appeared. These differences are used for the identification of the octahedral sheet [22]. In white clay, two reflections at 0.152 nm (2θ = 60°) and 0.149 nm (2θ = 62°) were observed in X-ray diffractograms (**Fig. 5-3a**), it was difficult to identify the octahedral sheet by only XRD analysis. The absorption band at 537 and 481 cm^{-1} appeared (**Fig. 5-3b**). Pyrophyllite has a dioctahedral sheet [23], and FT-IR spectra support its characteristics. The reflection at 0.152 nm (2θ = 60°) is considered to be due to quartz because quartz has a reflection around 2θ = 60°. The peaks of the Verm-E were 8.72°, 26.6°, and 45.3° on the 2θ scale. While these peaks did not match any data for vermiculite clay (JCPDS 60-340 or 60-341), they showed a similar tendency to biotite (JCPDS 57-812). The basal spacing of vermiculite clay is originally 1.4 nm, and it becomes 1.0 nm by high temperature treatment [22]. The Verm-E seems to have a biotite-like structure by the treatment at high temperatures for horticultural use. As described in Chapter 2, Verm-E has a trioctahedral sheet. The primary reflection of XRD shows the basal spacing of each clay mineral. The calculated basal spacing was 0.93 nm for white clay, and 1.01 nm for Verm-K. The chemical compositions of each clay mineral are summarized in **Table 5-1**.

Table 5-1. Characteristics of each clay mineral in this study.

Category	White clay	Verm-E
pH (H_2O)	4.3	8.9
Mineral (%)		
SiO_2	79.9	47.5
Al_2O_3	17.8	20.6
Fe_2O_3	0.11	7.4
MgO	ND	15.9
K_2O	0.46	5.6
TiO_2	0.36	1.6
CaO	0.26	1.4
Na_2O	ND	ND
Total	98.9	100.0

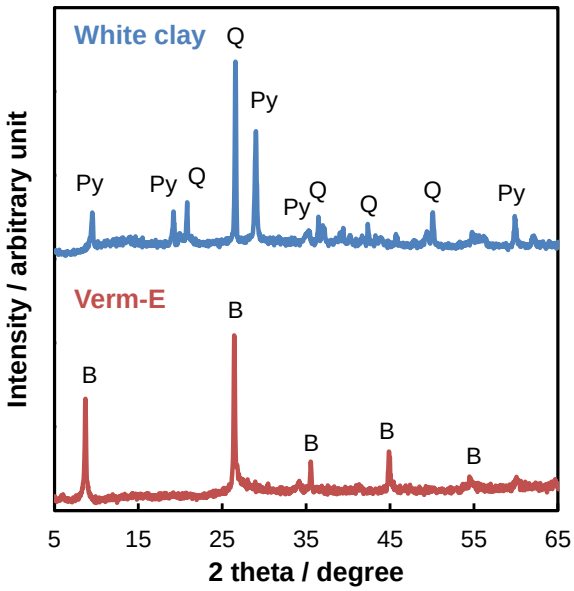

Fig. 5-2. X-ray diffractograms of white clay and Verm-E. Py: Pyrophyllite, Q: Quartz, B: Biotite.

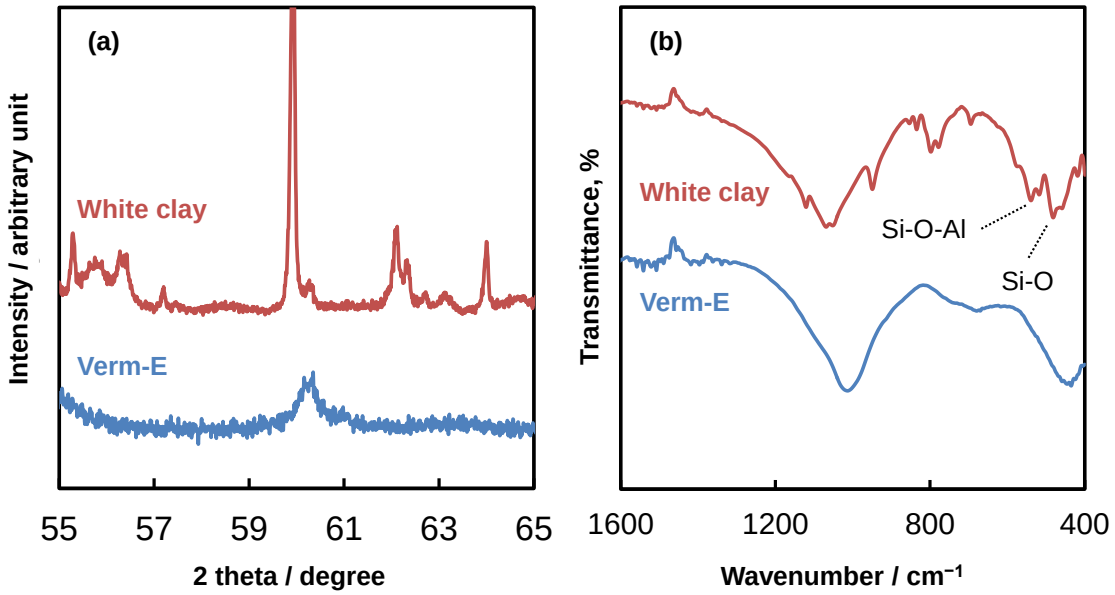

Fig. 5-3. (a) X-ray diffractogram at 55-65° and **(b)** FT-IR spectra at 1600–400 cm^{-1} of white clay and Verm-E for the identification of the octahedral structure.

5.3.2. Adsorption capacity and zeta potential

The adsorption capacity and zeta potential of white clay and Verm-E in each pH condition are shown in **Fig. 5-4**. The adsorption capacity of white clay was one-tenth of that of Verm-E. **Fig. 5-5** shows the basal spacing of each clay mineral which was measured by XRD. The basal spacing of white clay was 0.93 nm, and then the width of the interlayer was insufficient to capture Cs into their interlayer. On the other hand, the basal spacing of vermiculite was 1.01 nm, and Cs can enter the interlayer of Verm-E. The difference in the adsorption capacity between the two clay minerals was explained by the width of the interlayer that works as the adsorption sites for Cs.

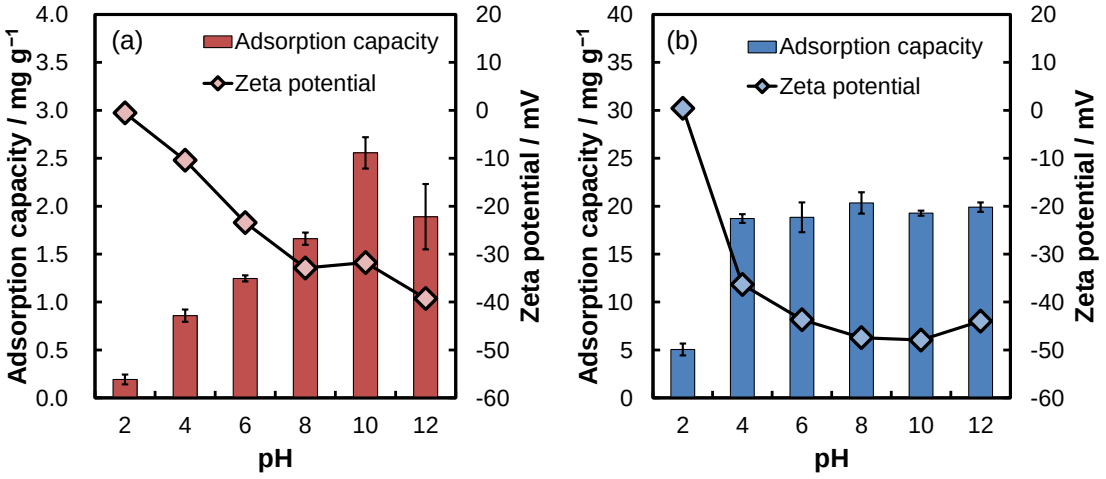

Fig. 5-4. Adsorption capacity for Cs ions and the zeta potential of **(a)** white clay and **(b)** Verm-E at various pH conditions.

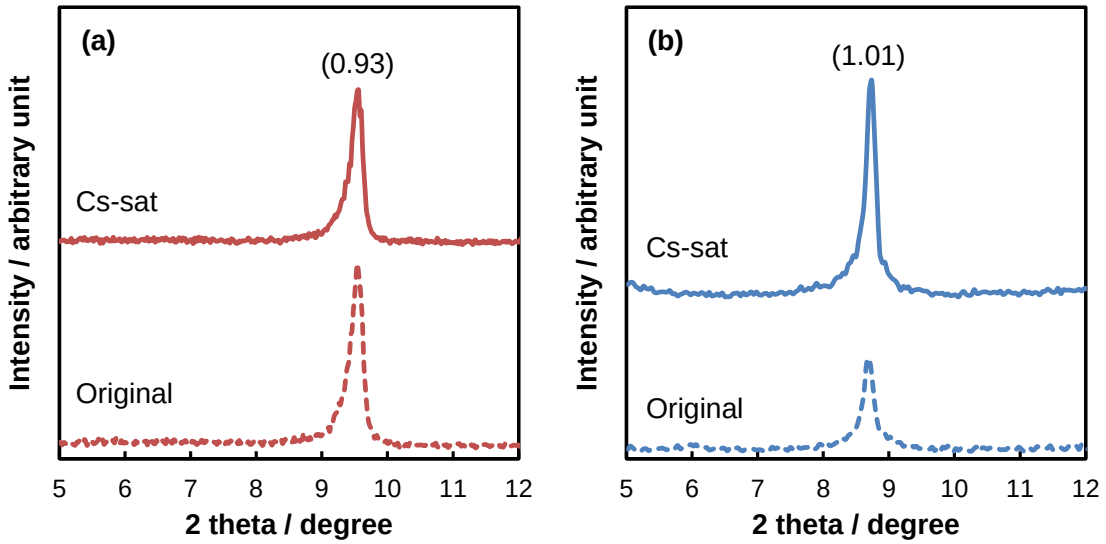

Fig. 5-5. X-ray diffractograms of **(a)** white clay and **(b)** Verm-E before (original) and after the saturated adsorption of Cs (Cs-sat). The number in parentheses indicates d-value.

There are mainly two types of negative charges on the surface of clay minerals, one is variable charges and the other is permanent charges. The variable charges are depending on pH because the dissociation of OH groups on the surface and edge of clay minerals depends on pH. The permanent charges are caused by the isomorphous substitution in the structure of clay minerals. This isomorphous substitution is known that Si^{4+} in the tetrahedral sheet is replaced with Al^{3+} or Fe^{3+}, and Al^{3+} in the octahedral sheet is replaced with Fe^{2+} or Mg^{2+}, as a result, an excessive negative charge is generated in the structure of clay mineral. These charges are not affected by pH [22]. **Table 5-1** shows the results of XRF, mainly SiO_2 and Al_2O_3 were detected from white clay, and the content of Fe_2O_3 and MgO were very low and not detected. While the content of Fe_2O_3 and MgO in Verm-E was higher than that of white clay. It means that there were very few places where the isomorphous substitution was generated in the structure of white clay, on the other hand, the isomorphous substitution was generated in the whole structure of Verm-E.

The adsorption capacity of white clay increased as the pH increased except pH 12, and the zeta potential of white clay became more negative as the pH increased. The negative charges of white clay at the higher pH might work as the driving force for the adsorption of Cs by the electrostatic interaction. Therefore, the negatively charged surface of white clay could act as a weak adsorption site but the interlayers did not, and the adsorption capacity of white clay was significantly smaller than that of Verm-E. In the case of pH 12, Na from NaOH for the adjustment of pH interfered in the adsorption of Cs to white clay, and then the adsorption capacity at pH 12 was decreased. In the case of Verm-E, the adsorption capacity was unchanged in various pHs, and the zeta potential was almost constant between -30 and -50 mV from pH 4 to 12. These results showed that the permanent charges of vermiculite could work as the driving force for the adsorption

of Cs^+ and the interlayers also worked as a cavity for the intercalation of Cs. The basal spacing of Verm-E was also unchanged after the saturated adsorption of Cs (**Fig. 5-5)**. Since the basal spacing becomes 1.0 nm after the adsorption of Cs, it cannot be determined whether Cs was adsorbed in the interlayer or not by XRD. Although the value of zeta potential was close to each other at pH 8, the adsorption capacity of vermiculite was higher than that of white clay at pH 8. These results indicated the other adsorption site worked for Cs except for the electrostatic interaction. Therefore, it was considered that Cs was adsorbed in the interlayer of Verm-E. These results showed that the adsorption capacity of the clay minerals depended strongly on the basal spacing.

5.3.3. Distribution of cesium after the EK process

In this section, the migration behavior of Cs in the model contaminated soil was evaluated by the EK process.

The distribution of Cs species in each model soil after the EK process for 72 h was shown in **Fig. 5-6**. During the operation time of 72 h, about 20–40 mL of water passed through the model soil as the EOF. The migration efficiencies of Cs in the Verm-E content 0, 5, 10, and 100wt% were 21.7, 7.5, 1.4, and 0.0%, respectively. The migration efficiency of Cs by the EK process decreased as the Verm-E content increased. Since Cs exists as a monovalent cation, it was migrated to the cathode side by electromigration. The concentration of Cs in section 5 slightly decreased in 0–10% Verm-E soil. It showed that Cs was migrated to the cathode side by the electromigration and EOF. However, Cs in 100% Verm-E soil were not migrated practically. According to the results of the sequential extraction analysis, Cs mainly existed as F2 in 0% Verm-E soil, while F5 was the main chemical form of Cs in 100% Verm-E soil. These results showed that Cs in white clay

existed as a form that is easy to migrate, and Cs in Verm-E existed as a form that is difficult to migrate.

The results of the sequential extraction analysis showed that Cs in white clay mainly existed as F1 and F2, and some Cs existed as F3 and F4. These results showed that there were some different types of interactions between Cs and white clay. That is, there was the ion-exchangeable form extracted easily with Mg^{2+} and other forms extracted only under the oxidation or reduction reaction at high temperature. Since the species of Cs as F1 and F2 were decreased in section 1 by the EK process, these forms of Cs were removed from the soil by the EK process. On the other hand, most parts of Cs in Verm-E existed as F5 and then Cs was not extracted without the degradation of the structure of Verm-E. Cs in F5 was considered to be the form fixed strongly in the cavity built with two tetrahedral sheets of vermiculite. The EK process was not effective to move Cs existing as F5 in soil. The inert chemical forms such as F3, F4, and F5 increased as the Verm-E content increased. Since even in 10% Verm-E content soil, most of the Cs existed as F3, F4, and F5, it was not easy to migrate by the EK process. It means that Cs bound on Verm-E moves scarcely by a water flow.

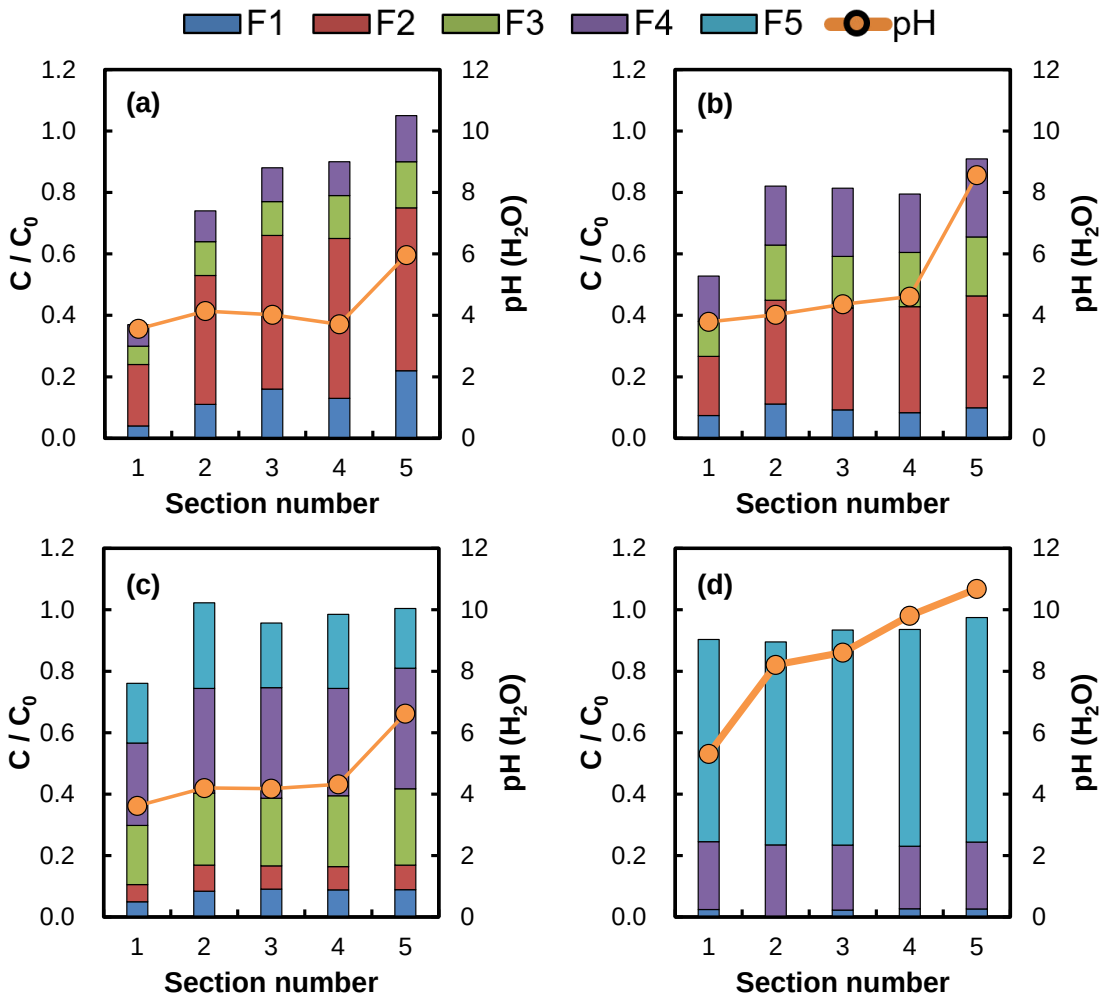

Fig. 5-6. Distribution of Cs species and pH in **(a)** 0, **(b)** 5, **(c)** 10, and **(d)** 100wt% Verm-E after the EK process. The initial concentration of Cs ions was 0.10 mg/g, the potential gradient was 1 V/cm, the operating time was 72 h, the migration solution was deionized water, and the fractionation of Cs ions was analyzed by modified sequential extraction analysis.

The concentration of Cs in the cathode chamber and the overflow of the EOF are shown in **Fig. 5-7a**. The results showed that the concentration of Cs there decreased as the Verm-E content increased. As shown in **Fig. 5-7b**, the volume of EOF increased as the operation time of the EK process increased. Although the volume of EOF from 100% and 0% Verm-E soil (i.e. 100% white clay) was over 30 mL after 72 h operation time, Cs in 100% vermiculite soil was not migrated as shown in **Fig. 5-7a**. The similarity in the volume of EOF in 0% and 100% Verm-E soil meant that almost the same amount of water passed through 0% and 100% Verm-E soil, however, Cs in 100% Verm-E soil was not migrated. These results revealed that Cs existed as the inert form in Verm-E, and it was consistent with the results of the sequential extraction analysis (**Fig. 5-6**). Therefore, the interaction between Cs and Verm-E was significantly stronger than that with white clay, and it was not easy to extract Cs from Verm-E and migrate them by the EK process. The advantage of the EK process is to enable the production of a water flow even in clayey soil with low permeability to water. The very low migration efficiency for Cs in Verm-E by the EK process means that it is difficult to move Cs adsorbed on vermiculite by a water flow and then the Cs will stay there for a long time.

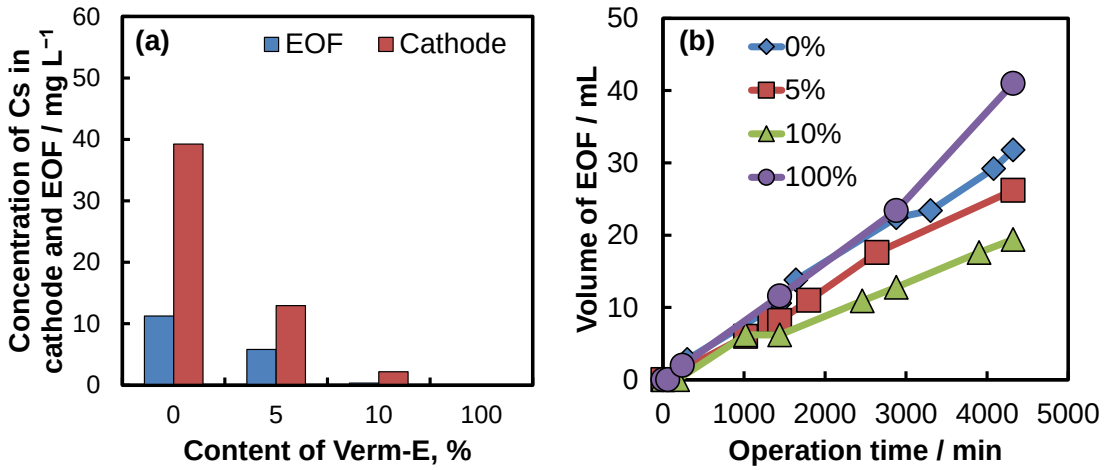

Fig. 5-7. (a) Concentration of Cs ions in the cathode solution and EOF from each model soil. **(b)** Accumulated EOF in each model soil. The percentage in legend was the content of vermiculite, the potential gradient was 1 V/cm, and the migration solution was deionized water.

Clay minerals which adsorbed Cs were estimated to expose to water for a long time, but the estimation of the stabilization of Cs in clay minerals was difficult. To evaluate the stability of Cs in clay minerals against water, a liquid flow examination was needed. However, since clay mineral is a small particle and has low permeability, it takes a long time to pass through water into clay mineral. At this point, the EK process can carry water even in low permeable soil. Since there is no report that the EK process was used for the evaluation of the stabilization of pollutants, a new possibility of the EK process was found.

5.4. Summery

The interaction between Cs and two kinds of 2:1 clay mineral was evaluated by the adsorption experiment, XRD, and zeta potential analysis, and the effect of these interactions on the migration efficiency of Cs by the EK process was investigated. The adsorption capacity of white clay for Cs was about 10 times lower than that of Verm-E, and it was significantly affected by these basal spacing. In the adsorption, Cs cannot enter the interlayer of white clay, while Verm-E can capture Cs in the interlayer. As the result, the interlayer of white clay cannot work as an adsorption site for Cs and the adsorption capacity of white clay was lower than that of Verm-E. The zeta potential of white clay and Verm-E was negative from pH 4 to 12 and those values were close to each other. These results revealed that one of the interactions between clay minerals and Cs was due to the electrostatic interaction and the other is the intercalation into the interlayer of clay minerals, and both of them determined the adsorption capacity of Cs on these clay minerals.

The results of the distribution of Cs species in various Verm-E content soils after the EK process indicated that the migration efficiency of Cs decreased as the Verm-E content increased. Additionally, 80% of Cs in Verm-E existed as F5. Since Cs was fixed inertly in the interlayer of Verm-E, the distribution of Cs species in 100% Verm-E soil did not change before and after the EK process. Therefore, the migration efficiency of Cs was significantly affected by the Verm-E content in the soil. The results obtained in this chapter will contribute to considering the interaction between Cs and clay minerals in the flowing water in the soil and to predict the movement of Cs in the future.

5.5. References

[1] Y.B. Acar, A.N. Alshawabkeh, Principles of electrokinetic remediation, Environ. Sci. Technol. 27 (1993) 2638–2647. doi:10.1021/es00049a002.

[2] R.F. Probstein, R.E. Hicks, Removal of contaminants from soils by electric fields, Science. 260 (1993) 498–503. doi:10.1126/science.260.5107.498.

[3] A.P. Shapiro, R.F. Probstein, Removal of contaminants from saturated clay by electroosmosis, Environ. Sci. Technol. 27 (1993) 283–291. doi:10.1021/es00039a007.

[4] G.C.C. Yang, S.-L. Lin, Removal of lead from a silt loam soil by electrokinetic remediation, J. Hazard. Mater. 58 (1998) 285–299. doi:10.1016/S0304-3894(97)00139-8.

[5] D.B. Gent, R.M. Bricka, A.N. Alshawabkeh, S.L. Larson, G. Fabian, S. Granade, Bench- and field-scale evaluation of chromium and cadmium extraction by electrokinetics, J. Hazard. Mater. 110 (2004) 53–62. doi:10.1016/j.jhazmat.2004.02.036.

[6] T. Suzuki, M. Niinae, T. Koga, T. Akita, M. Ohta, T. Choso, EDDS-enhanced electrokinetic remediation of heavy metal-contaminated clay soils under neutral pH conditions, Colloids Surfaces A Physicochem. Eng. Asp. 440 (2014) 145–150. doi:10.1016/j.colsurfa.2012.09.050.

[7] K. Manokararajah, R. Sri Ranjan, Electrokinetic retention, migration and remediation of nitrates in silty loam soil under hydraulic gradients, Eng. Geol. 77 (2005) 263–272. doi:10.1016/j.enggeo.2004.07.017.

[8] D.-H. Kim, J.-M. Jung, S.-U. Jo, W.-S. Kim, K. Baek, Photovoltaic powered electrokinetic restoration of saline soil, Sep. Sci. Technol. 47 (2012) 2235–2240. doi:10.1080/01496395.2012.697510.

[9] S. Zhu, D. Zhu, X. Wang, Removal of fluorine from red mud (bauxite residue) by electrokinetics, Electrochim. Acta. 242 (2017) 300–306. doi:10.1016/j.electacta.2017.05.040.

[10] A.N. Alshawabkeh, H. Sarahney, Effect of current density on enhanced transformation of naphthalene, Environ. Sci. Technol. 39 (2005) 5837–5843. doi:10.1021/es049645f.

[11] M.T. Alcántara, J. Gómez, M. Pazos, M.A. Sanromán, Electrokinetic remediation of PAH mixtures from kaolin, J. Hazard. Mater. 179 (2010) 1156–1160. doi:10.1016/j.jhazmat.2010.03.010.

[12] A.A. Prakash, N.S. Prabhu, A. Rajasekar, P. Parthipan, M.S. AlSalhi, S. Devanesan, M. Govarthanan, Bio-electrokinetic remediation of crude oil

contaminated soil enhanced by bacterial biosurfactant, J. Hazard. Mater. (2020) 124061. doi:10.1016/j.jhazmat.2020.124061.

[13] K. Maturi, K.R. Reddy, Simultaneous removal of organic compounds and heavy metals from soils by electrokinetic remediation with a modified cyclodextrin, Chemosphere. 63 (2006) 1022–1031. doi:10.1016/j.chemosphere.2005.08.037.

[14] S. Annamalai, M. Santhanam, M. Sundaram, M.P. Curras, Electrokinetic remediation of inorganic and organic pollutants in textile effluent contaminated agricultural soil, Chemosphere. 117 (2014) 673–678. doi:10.1016/j.chemosphere.2014.10.023.

[15] S. Mohamadi, M. Saeedi, A. Mollahosseini, Enhanced electrokinetic remediation of mixed contaminants from a high buffering soil by focusing on mobility risk, J. Environ. Chem. Eng. 7 (2019) 103470. doi:10.1016/j.jece.2019.103470.

[16] S. Kusama, K. Sato, Y. Matsui, N. Kimura, H. Abe, S. Yoshida, M. Nishizawa, Transdermal electroosmotic flow generated by a porous microneedle array patch, Nat. Commun. 12 (2021) 658. doi:10.1038/s41467-021-20948-4.

[17] B. Zhang, D. Zheng, S. Yiming, K. Oyama, M. Ito, M. Ikari, T. Kigawa, T. Mikawa, T. Miyake, High-efficient and dosage-controllable intracellular cargo delivery through electrochemical metal–organic hybrid nanogates, Small Sci. 1 (2021) 2100069. doi:10.1002/smsc.202100069.

[18] H. Abe, K. Sato, N. Kimura, S. Kusama, D. Inoue, K. Yamasaki, M. Nishizawa, Porous microneedle patch for electroosmosis-promoted transdermal delivery of drugs and vaccines, Adv. NanoBiomed Res. 2 (2022) 2100066. doi:10.1002/anbr.202100066.

[19] A. Tessier, P.G.C. Campbell, M. Bisson, Sequential extraction procedure for the speciation of particulate trace metals, Anal. Chem. 51 (1979) 844–851. doi:10.1021/ac50043a017.

[20] S. Susumu, Clay mineral research method, Souzousha, Hyogo, (1985) (in Japanese).

[21] H. Shirozu, Introduction to Clay Mineralogy –Fundamentals for Clay Science–, Asakura Publishing Co., Ltd., Tokyo, (1988) (in Japanese).

Chapter 6

Electrokinetic remediation for cesium contaminated soil with oxalic acid leaching

6.1. Introduction

The contaminated soil with radioactive species, which has a long half-life such as ^{137}Cs, will continue to affect the ecosystem for a long time. Therefore, the technologies to remove such pollutants in soil are required strongly. Soil remediation technologies can be broadly classified into three types, degradation, containment, and separation [1]. The degradation can be applied to only organic pollutants but is unsuitable for inorganic pollutants. Although the containment can prevent pollutants from spreading into the environment, pollutants remain in the contaminated area. Therefore, the development of separation technology is required for contaminated soil with radioactive species. In this respect, the electrokinetic (EK) process has the advantages of applying to low permeability soil and in-site remediation [2,3] and is a promising technology for the removal of Cs from soil [4].

The EK process has been investigated as the separation method of Cs from contaminated soil. Oguri et al. reported that when 40 voltages were applied to the Andosol (one type of soil) contaminated with Cs for 24 h, almost half of the Cs in the soil could be removed [5]. After 240 h of the operation time, 80% of Cs could be removed from kaolin and natural soil [6]. The arrangement of electrodes for the EK process and the combination of an organic acid with the EK process to remove Cs were also reported [7,8]. In South Korea, the EK process was demonstrated for the actual soil contaminated with radionuclides [9–12]. The total removal efficiency of ^{60}Co and ^{137}Cs from the artificially contaminated soil (2,000 Bq/kg) were 95.8% after the operation time of 55 days [13]. The EK process was reported to be effective even for aging soils after about 30 years since the contamination with radionuclides occurred [14]. Since these studies focus on the actual soil, the results are beneficial for considering the EK process as a remediation

technology for Cs in the soil. However, the effect of the interaction of Cs with clay minerals in the EK process has not been mentioned. For the remediation of Cs from the clayey soil, considering the strong adsorption and fixation of Cs on biotite or vermiculite is essential. In this respect, due to the different properties of the soils used in these experiments, similar results may not be obtained with other types of soil. Therefore, it is necessary to clarify the possibility and limitations of the EK process in the application of clay minerals having a strong interaction with Cs such as biotite. The information on the chemical forms of Cs in clayey soil is needed to improve the removal efficiency of the EK process.

In this chapter, the EK process combined with the oxalic acid leaching in Chapter 3 was attempted to remove Cs in biotite soil, which is reported to adsorb Cs in the soil of Fukushima Prefecture, Japan.

6.2. Materials and methods

6.2.1. Materials and chemicals

Biotite (Bio-T, Fukushima Prefecture, Japan) used in Chapters 2 and 3, and white clay used in Chapter 5 were used in this chapter. The detailed characteristics were indicated in these chapters. Potassium dihydrogen phosphate, potassium hydroxide, perchloric acid, and hydrofluoric acid were purchased by Kanto Chemical Co., Inc., Japan.

6.2.2. Preparation of model soil

Bio-T was crushed in an agate mortar and sieved below 250 μm. Batch adsorption experiments have shown that the adsorption rate for Cs does not change significantly for smaller particles than this range [15]. The adsorption of Cs was performed according to

Chapter 2 (Section 2.2.3), and the adsorption capacity was calculated by **Eq. 2-1**. The model contaminated soil containing 1% Bio-T was prepared by mixing Bio-T saturated with Cs and white clay in a plastic bottle by shaking well. The water content was adjusted to be approximately 30% by KH_2PO_4/KOH (pH 6.0) or oxalic acid before the EK process.

6.2.3. Leaching procedure

Oxalic acid can desorb Cs from biotite under room temperature according to the result of Chapter 3. The water content of the prepared mixed model soil was adjusted with 0.5 mol/L oxalic acid, and then it was mixed well with a stainless spoon and stored in a plastic bag with a zipper at room temperature.

6.2.4. Condition of EK process

The same equipment as that used in Chapter 5 was used for the EK process was used with Chapter 5 (**Fig. 5-1**). Titanium gauze electrodes coated with platinum (Tanaka Kikinzoku Kogyo K.K., Japan) were located in both electrode chambers. A constant voltage (1 V/cm) was applied by a direct current (DC) power supply (Program Multioutput Power Supply, PPS303, AS ONE Corporation, Japan), and the current value was measured sequentially by an ammeter built into the power supply. A measuring cylinder was connected to the cathode chamber to receive the water transported by EOF as an overflow from the cathode chamber.

The removal efficiency (R_e) was calculated by **Eq. 6-1**:

$$R_e = \frac{A_{Soln}}{A_{Ini}} \times 100 \quad \textbf{(6-1)}$$

where A_{Soln} indicates the amount of Cs in the cathode and EOF which is transported out of the model contaminated soil after the EK process (mg), A_{Ini} indicates that initial amount

of Cs in the model contaminated soil before the EK process (mg).

After the EK process, the soil was taken out from the anode side by each 2 cm and was dried at 105 °C for 16 h. The dried samples were crushed by an agate mortar and then used for analysis.

6.2.5. Analytical procedure of Cs in soil

The total amount of Cs in Bio-T was evaluated by the hydrofluoric acid decomposition. This procedure was partially modified and performed [16]. Approximately 0.1 g of dried sample was taken in a Teflon beaker, 5 mL of concentrated nitric acid and perchloric acid were added, and then it was heated on a sand bath to dryness. Next, $HClO_4$ (5 mL) and HF (10 mL) were added, and the mixture was further heated to produce $HClO_4$ white fumes for about 15 min, and then the heating was stopped. Further HF (10 mL) was added and then the sample was heated in the sand bath and evaporated to dryness. Ultrapure water (5 mL), concentrated HCl (5 mL), and HNO_3 (1 mL) were added to the sample to dissolve the precipitation, and the volume was adjusted. The concentration of Cs in the solution was measured by AAS.

The amount of Cs in the prepared model soil was evaluated in two kinds of chemical forms. One is the ion exchangeable form, which is relatively easily removed by the EK process, as described in Chapter 5. The dried soil sample after the EK process was added to 1.0 mol/L ammonium acetate (solid/liquid ratio was 1:10), and the mixture was shaken for 6 h [17]. The sample was centrifuged at 10,000 rpm for 10 min, and then the supernatant was filtered by a 0.45 μm membrane filter. The concentration of Cs was measured by AAS.

Another is the residual form, which is not easily desorbed by ion exchange. The

amount of residual form in the prepared model soil was calculated by subtracting the amount of ion exchangeable form from the total amount of Cs in Bio-T determined by hydrofluoric acid decomposition.

The concentration of carbon in the soil was evaluated by the below procedure. The ultrapure water was added to the dried soil sample (solid/liquid ratio was 1:5), and the mixture was shaken at 1,000 rpm for 1 h. After centrifugation at 10,000 rpm for 15 min, the supernatant was filtered by a 0.45 μm Omnipore hydrophilic membrane filter. The concentration of carbon in the filtrate was measured by a total organic carbon analyzer (TOC-VCPH, Shimadzu Corporation, Japan).

6.3. Results and discussion

6.3.1. Initial distribution of Cs in prepared soil

The detailed chemical composition and structure of Bio-T and white clay were described in Chapters 3 and 5. The total amount of the adsorbed Cs by Bio-T was 36.5 mg/g. When KH_2PO_4/KOH or oxalic acid was added to adjust the water content of model mixed soil (1% biotite), the ion exchangeable form rate was 43 and 64%, respectively. Moreover, this ion exchange form rate became 88% after 2 weeks of oxalic acid leaching (**Fig. 6-1**). The water content of the model contaminated soil before and after oxalic acid leaching for 2 weeks was 33.0 and 31.9%, and it was not significantly different. The room temperature was observed to be kept at 20 ± 5 °C during the 2 weeks leaching process.

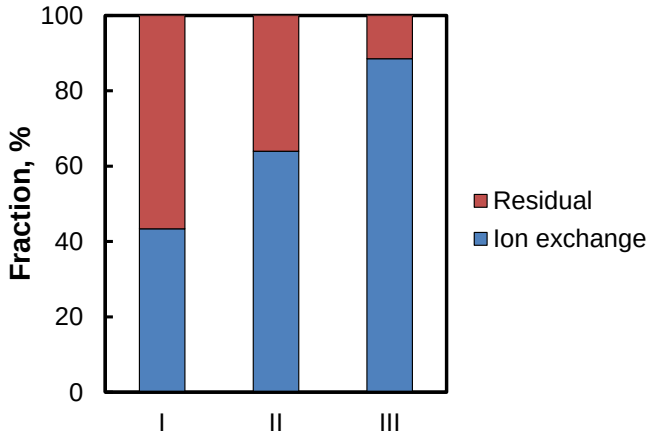

Fig. 6-1. Fractionation of Cs in initial model soil. I: 0.1 mol/L KH_2PO_4/KOH, II: 0.5 mol/L oxalic acid, and III: 0.5 mol/L oxalic acid with 2 weeks leaching.

6.3.2. Removal efficiency by EK process

The distribution of ion exchangeable form of Cs after the EK process was shown in **Fig. 6-2**. When 0.1 mol/L KH_2PO_4/KOH was used to adjust the water content, R_e was 17% after the EK process for 24 h operation (**Fig. 6-2a**). In section 1, the concentration of Cs as ion exchangeable form was 0.04 mg/g, it decreased by 75% compared with the initial ion exchangeable concentration. On the other hand, the ion exchangeable form of Cs was 0.19 mg/g in section 5, which was 1.2 times higher than that of the initial concentration. The concentration of Cs was high in section 5 because Cs from the anode side section was moved by electromigration and electroosmotic flow (EOF). These results indicate that Cs as ion exchangeable form in soil could be removed by the EK process. Since the operation of the EK process was a shorter time (only 24 h) than in typical studies of the EK process (1 week or more), ion exchangeable form of Cs remained in the soil section. When a longer operation time was performed, the ion exchangeable Cs will migrate to the cathode side and the removal efficiency will be improved. On the other hand, the concentration of the residual form of Cs was not changed after the EK process,

these results indicate that the removal of Cs existed as the residual form in the soil is difficult.

When oxalic acid was used to adjust the water content, the higher concentration of Cs was detected as ion exchangeable form than that of KH_2PO_4/KOH. As described in Chapter 3, Bio-T was decomposed by oxalic acid and Cs was released from Bio-T. Thus, the residual form of Cs was transferred into the ion exchangeable form even in the initial concentration (**Fig. 6-1**). After 24 h of the operation time, R_e was only 3% which was quite a low value than that of KH_2PO_4/KOH. Typically, the electromigration velocity decrease as the ionic strength of the solution increase due to the influence of the ionic atmosphere around the particle [18]. Although R_e was low, it is important that the ion exchangeable fraction increased, and the yield of ion exchangeable form against the total initial amount of Cs was 80% after the EK process. These results indicate the potential for the removal of Cs from the soil by the EK process.

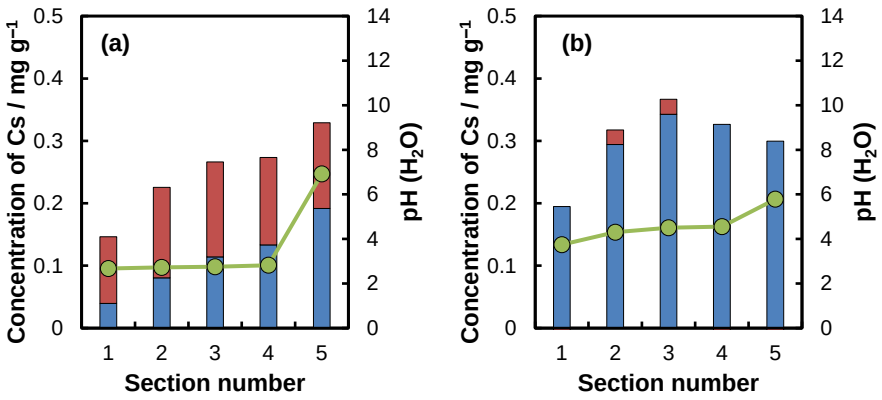

Fig. 6-2. Distribution of Cs in model contaminated soil which was adjusted water content with **(a)** 0.1 mol/L KH_2PO_4/KOH (pH 6.0) and **(b)** 0.5 mol/L oxalic acid after the EK process for 24 h. The black and blue dashed lines indicate the total initial concentration of Cs and the initial concentration of Cs in ion exchangeable form. The blue and red bars indicate the concentration of Cs in ion exchangeable form and residual form. The green line indicates the soil pH after the EK process.

According to Chapter 3, since the optimal leaching time was 2 weeks at room temperature, the EK process was performed by using model soil after 2 weeks of oxalic acid leaching. As the result, R_e was only 2% after 24 h operation, however, the yield of ion exchangeable form against the total initial amount of Cs was 88% after the EK process (**Fig. 6-3**). The ion exchangeable ratio slightly increased compared to without the leaching, very little Cs existed as the residual form.

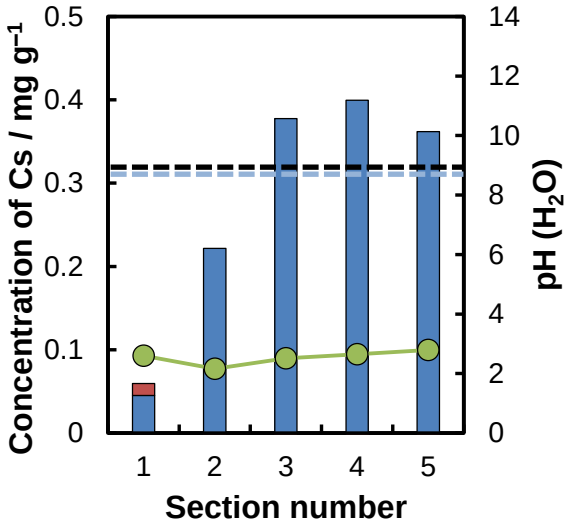

Fig. 6-3. Distribution of Cs in model contaminated soil after the EK process for 24 h combined with oxalic acid leaching. The black and blue dashed lines indicate the total initial concentration of Cs and the initial concentration of Cs in ion exchangeable form. The blue and red bars indicate the concentration of Cs in ion exchangeable form and residual form. The green line indicates the soil pH after the EK process.

6.3.3. Amount of EOF

The flow rate of EOF is also important for the removal efficiency in the EK process. When 0.1 mol/L KH_2PO_4/KOH was used to adjust the water content, the obtained amount of EOF was 10.0 mL after 24 h of the EK process (0.42 mL/h). On the other hand, when 0.5 mol/L oxalic acid was used to adjust the water content, it was 7.0 mL (0.29 mL/h).

The amount of EOF has been affected not only by operation time but also by soil cross-sectional area. When the flow rate of EOF was compared with a similar soil cross-sectional area, approximately 3.9–4.3 mL/h of flow rate was reported and it was higher than that in this study [19,20]. The low flow rate of this study is due to the low soil pH. According to **Eq. 1-3**, the anode electrolyte becomes low pH owing to electrolysis, and the generated proton makes an acid region in the soil near the anode. Since the amount of EOF is affected by the zeta potential of soil particles (**Eq. 1-2**), the flow rate decreases when the charge of soil particles was neutralized by the surrounding environment. In these previous studies, the system to circulate the electrolyte solutions of the cathode and anode and neutralize them to keep the pH constant at 7 was developed and the generation of the acid region could be prevented by the system. The point of zero charges of white clay in this study was around pH 2, and although the EOF does not stop completely, it was not a suitable condition to produce a large amount of EOF. Moreover, the soil pH decreased due to the addition of oxalic acid as a leaching solution. If the soil pH could be kept constant around neutrality, it is possible to expect a further amount of EOF generation and at the same time improve the removal efficiency of Cs.

6.3.4. Effect of operation time

Figure 6-4 shows the results of the distribution of Cs, pH, and TOC when the EK process was performed for 72 h after 2 weeks of oxalic acid leaching. The removal efficiency was 33%, which was higher than that of 24 h operation. As with 24 h operation, the residual form of Cs in the model soil transformed into the ion exchangeable form due to oxalic acid leaching. Since this model soil does not contain carbon, the value of the TOC indicates that of the added oxalic acid. Usually, oxalic acid has a negative charge

due to deprotonation depending on pH. The acid dissociation constant (pK_{a1}) of oxalic acid is 1.04 [21], it should have a negative charge and migrate to the anode side. However, the concentration of oxalic acid increased near the cathode side and the concentration was higher at the cathode (420 mg/L) than at the anode (140 mg/L). The electromigration mobility decreases with the particle size, for example, the mobility of humic substances was affected more by EOF than by electromigration, therefore, moved to the cathode [19]. Although the molecular weight of oxalic acid is not as large as that of humic substances, it was considered to be affected by EOF. Moreover, since oxalic acid makes a complex with Fe or Al released from biotite, the electromigration mobility will decrease more.

Although NaOH (0.1 mol/L) was used as the electrolyte to prevent the generation of the acid regions in the soil, the soil pH was still low (pH 3–4) and this system was insufficient. The flow rate of EOF was 0.41 mL/h with no drastic improvement, therefore, a circulation system of electrolytes is required to keep the constant pH and generate a large amount of EOF. On the other hand, since the removal efficiency of Cs was improved simply by increasing the operation time, more improvement in removal efficiency can be expected by the longer operation time.

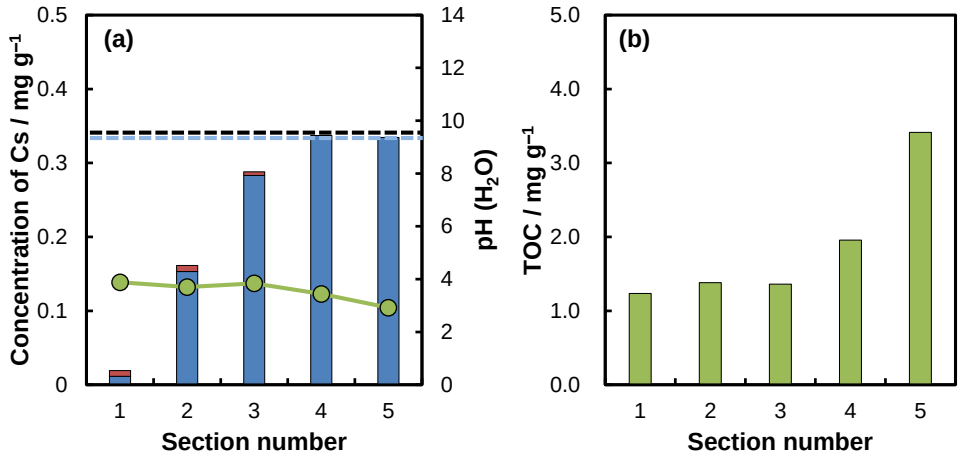

Fig. 6-4. Distribution of **(a)** Cs and pH (green line), and **(b)** TOC in model contaminated soil after the EK process for 72 h. The contaminated soil was leached with 0.5 mol/L oxalic acid for 2 weeks before the EK process. The black and blue dashed lines indicate the total initial concentration of Cs and the initial concentration of Cs in ion exchangeable form. The blue and red bars indicate the concentration of Cs in ion exchangeable form and residual form.

The removed Cs from the model soil by the EK process existed in the electrolyte of the cathode and EOF solution. The EOF was basic (pH 11.6) due to the hydroxide ion produced by electrolysis and the original electrolyte (0.1 mol/L NaOH). Since typical metal ions will precipitate under these basic conditions, the concentration of the matrix will be not so high. On the other hand, some cations in the original electrolytes will remain in EOF. Therefore, the types of electrolytes should be considered to collect Cs in EOF solution using adsorbents. Fortunately, such a low matrix and high pH condition will be favorable for the developed adsorbents [22–24]. In simple extraction methods such as washing with an inorganic acid, it is difficult to make low matrix conditions. Therefore, the separation of Cs from contaminated soil by the EK process has an advantage not only applicable to low permeability soil and in-site remediation but also preparation of favorable conditions for wastewater treatment.

6.3.5. Energy consumption

The change in current value during 72 h of operation is indicated in **Fig. 6-5**. Since the electrode distance between the anode and cathode was 10 cm in length, the constant voltage was 10 V to make a potential gradient of 1 V/cm. The energy consumption depended on the experimental conditions such as target pollutants, treatment area, and clearance level. The energy consumption was calculated to be 153 kWh/m^3 from the average current value obtained under the conditions when 33% of Cs was removed. Although this value may fluctuate due to optimization of the experimental conditions, this value was within the range of some previous studies (approximately 65–200 kWh/m^3) [3,25,26].

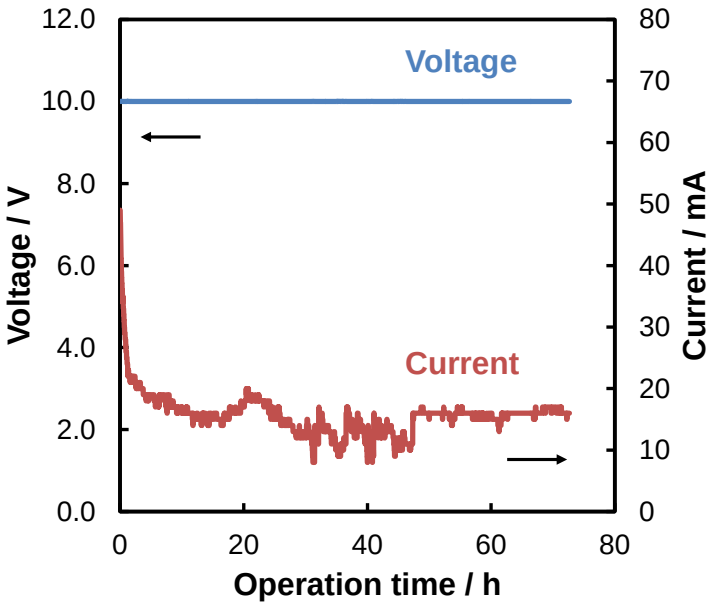

Fig. 6-5. Distribution of voltage and current in the EK process for 72 h operation time. The contaminated soil was leached with 0.5 mol/L oxalic acid for 2 weeks. The electrolyte was 0.1 mol/L NaOH.

6.4. Summery

In this chapter, the EK process for the removal of residual form Cs from model soil was attempted in combination with oxalic acid leaching. As mentioned in Chapter 3, oxalic acid leaching can desorb Cs not only in ion exchangeable form but also in residual form, and similar results were obtained in this chapter. Although the ion exchangeable form of Cs can be removed by electromigration and EOF under the EK process, the residual form was difficult to move. The residual form Cs was not transformed into ion exchangeable form due to the addition of potassium ion, however, oxalic acid can transform it. The increase of ion exchangeable form rate has a positive effect on the remediation by the EK process, approximately 33% of Cs can be removed after 72 h of operation. The removed Cs existed in EOF with low matrix and high pH, this condition is favorable for the developed adsorbent for Cs from an aquatic environment. These results indicated the possibility of removing the residual form of Cs by the EK process, which has been considered to be difficult and can contribute to the development of soil remediation in the future.

6.5. References

[1] Graduate School of Environmental Science Hokkaido University, Science and Technology of Environmental Remediation, Hokkaido University Press, Sapporo, (2007) (in Japanese).

[2] Y.B. Acar, A.N. Alshawabkeh, Principles of electrokinetic remediation, Environ. Sci. Technol. 27 (1993) 2638–2647. doi:10.1021/es00049a002.

[3] R. Lageman, Electroreclamation. Applications in the Netherlands, Environ. Sci. Technol. 27 (1993) 2648–2650. doi:10.1021/es00049a003.

[4] M. Igawa, K. Ishiyama, B. Nanzai, Removal of cesium ions from soil by electrokinetic remediation, Bull. Soc. Sea Water Sci. Japan. 72 (2018) 88-95 (in Japanese). doi:10.11457/swsj.72.2_88.

[5] Y. Oguri, K. Miyake, H. Fukuda, J. Kaneko, J. Hasagawa, M. Ogawa, M. Shiho, Application of PIXE analysis to the study of electrokinetic removal of cesium from soil, Int. J. PIXE. 14 (2004) 49–56. doi:10.1142/S0129083504000094.

[6] S.S. Al-Shahrani, E.P.L. Roberts, Electrokinetic removal of caesium from kaolin, J. Hazard. Mater. B122 (2005) 91–101. doi:10.1016/j.jhazmat.2005.03.018.

[7] T. Miura, M. Kabir, M. Suzuki, N. Shunsuke, S. Mori, Effect of organic acids on cesium removal from contaminated soil by the electrokinetic remediation, J. Inst. Electrost. Japan. 40 (2016) 14–19.

[8] M. Kabir, Y. Hatakeyama, S. Nakajima, Manufacturing method of cathode electrode for FEM-EK process to adsorb cesium (Cs) ion, Nat. Environ. Pollut. Technol. 17 (2018) 237–241.

[9] G.-N. Kim, W.-K. Choi, C.-H. Jung, J.-K. Moon, Development of a washing system for soil contaminated with radionuclides around TRIGA reactors, J. Ind. Eng. Chem. 13 (2007) 406–413.

[10] G.-N. Kim, B.-I. Yang, W.-K. Choi, K.-W. Lee, Development of vertical electrokinetic-flushing decontamination technology to remove ^{60}Co and ^{137}Cs from a Korean nuclear facility site, Sep. Purif. Technol. 68 (2009) 222–226. doi:10.1016/j.seppur.2009.05.015.

[11] G.-N. Kim, S. Kim, H.-M. Park, W.-S. Kim, U.-R. Park, J.-K. Moon, Cs-137 and Cs-134 removal from radioactive ash using washing–electrokinetic equipment, Ann. Nucl. Energy. 57 (2013) 311–317. doi:10.1016/j.anucene.2013.02.016.

[12] G.-N. Kim, S.-S. Kim, U.-R. Park, J.-K. Moon, Decontamination of soil contaminated with cesium using electrokinetic-electrodialytic method, Electrochim. Acta. 181 (2015) 233–237. doi:10.1016/j.electacta.2015.03.208.

[13] G.-N. Kim, S.-S. Lee, D.-B. Shon, K.-W. Lee, U.-S. Chung, Development of

pilot-scale electrokinetic remediation technology to remove ^{60}Co and ^{137}Cs from soil, J. Ind. Eng. Chem. 16 (2010) 986–991. doi:10.1016/j.jiec.2010.05.014.

[14] G.-N. Kim, H.-M. Park, W.-S. Kim, J.-K. Moon, B.-S. Lee, J.-G. Lee, D.-B. Shon, Effect of soil aging period on Cs-137 removal from soil by complex electrokinetic equipment, 11th International Symposium on Electrokinetic Remediation (2012) 5–6.

[15] N. Suzuki, K. Ochi, T. Chikuma, Cesium adsorption behavior of vermiculite and it's application to the column method, J. Ion Exch. 25 (2014) 122–125. doi:10.5182/jaie.25.122.

[16] Japanese Society of Soil Science and Plant Nutrition, Soil standard analysis and measurement, Hakuyusha Co Ltd., Tokyo, (1986) (in Japanese).

[17] A. Tessier, P.G.C. Campbell, M. Bisson, Sequential extraction procedure for the speciation of particulate trace metals, Anal. Chem. 51 (1979) 844–851. doi:10.1021/ac50043a017.

[18] K. Shimao, Basic principles of electrophoresis., SEIBUTSU BUTSURI KAGAKU. 41 (1997) 1-11 (in Japanese). doi:10.2198/sbk.41.1.

[19] A. Sawada, S. Tanaka, M. Fukushima, K. Tatsumi, Electrokinetic remediation of clayey soils containing copper(II)-oxinate using humic acid as a surfactant, J. Hazard. Mater. 96 (2003) 145–154. doi:10.1016/S0304-3894(02)00168-1.

[20] A. Sawada, K. Mori, S. Tanaka, M. Fukushima, K. Tatsumi, Removal of Cr(VI) from contaminated soil by electrokinetic remediation, Waste Manag. 24 (2004) 483–490. doi:10.1016/S0956-053X(03)00133-8.

[21] The Chemical Society of Japan, Handbook of Chemistry, sixth edit, Maruzen Publishing Co., Ltd., Tokyo, (2021) (in Japanese).

[22] B. Pangeni, H. Paudyal, K. Inoue, K. Ohto, H. Kawakita, S. Alam, Preparation of natural cation exchanger from persimmon waste and its application for the removal of cesium from water, Chem. Eng. J. 242 (2014) 109–116. doi:10.1016/j.cej.2013.12.042.

[23] Y. Mihara, M.T. Sikder, H. Yamagishi, T. Sasaki, M. Kurasaki, S. Itoh, S. Tanaka, Adsorption kinetic model of alginate gel beads synthesized micro particle-Prussian blue to remove cesium ions from water, J. Water Process Eng. 10 (2016) 9–19. doi:10.1016/j.jwpe.2016.01.001.

[24] K. Wang, H. Ma, S. Pu, C. Yan, M. Wang, J. Yu, X. Wang, W. Chu, A. Zinchenko, Hybrid porous magnetic bentonite-chitosan beads for selective removal of radioactive cesium in water, J. Hazard. Mater. 362 (2019) 160–169. doi:10.1016/j.jhazmat.2018.08.067.

[25] D.-H. Kim, J.-C. Yoo, B.-R. Hwang, J.-S. Yang, K. Baek, Environmental assessment on electrokinetic remediation of multimetal-contaminated site: a case study, Environ. Sci. Pollut. Res. 21 (2014) 6751–6758. doi:10.1007/s11356-014-2597-1.

[26] E.-K. Jeon, S.-R. Ryu, K. Baek, Application of solar-cells in the electrokinetic remediation of As-contaminated soil, Electrochim. Acta. 181 (2015) 160–166. doi:10.1016/j.electacta.2015.03.065.

Chapter 7

General conclusions

7.1. Knowledge obtained in this study

In order to estimate the possibility of the electrokinetic (EK) process in the application to the removal of Cs from the contaminated soil, the interaction between Cs and clay minerals and the desorption behavior of Cs from soil were investigated in this study by batch adsorption experiments, chemical compositions analysis, and structural evaluation of clay minerals. Based on the obtained results, an EK process combined with oxalic acid leaching treatment was developed and applied to remove Cs from contaminated soil.

The adsorption behavior of Cs to 2:1 type clay minerals such as biotite and vermiculite was evaluated by batch adsorption experiments and structural evaluation. Vermiculite with wide basal spacing can adsorb a large amount of Cs in the interlayer, conversely, biotite with narrow basal spacing has a low adsorption capacity. Even though the adsorption capacity of biotite is low, it does not mean that the adsorption sites with strong interactions such as interlayer and frayed edge sites (FES) do not act for the adsorption of Cs. Some parts of Cs were shown to be adsorbed on biotite in a form that could not be desorbed by ion exchange. The desorption behavior of Cs from biotite, which is considered to be the main clay mineral that adsorbs Cs in Fukushima Prefecture, Japan, was investigated by the treatment with inorganic and organic acids. Oxalic acid was able to desorb Cs with a high efficiency of approximately 95% from biotite, and not only ion exchangeable form of Cs but also residual form in the adsorption sites with strong interactions could be desorbed. Moreover, this desorption also was able to be performed at room temperature with a long leaching time.

These clay minerals with high adsorption capacity could be used as an adsorbent for Cs in an aquatic environment. The effect of sodium citrate treatment was investigated

to enhance the adsorption capacity of vermiculite, which has a partial chlorite structure. Sodium citrate can desorb the interlayer material of the chlorite structure, and then the desorbed space can act as a new adsorption site for Cs. Although the vermiculite pretreated with sodium citrate had the disadvantage of being powder form and being difficult to collect after adsorption of Cs, a collectable adsorbent can be prepared by encapsulating the vermiculite in alginate gel beads.

The dynamic behavior and stability of Cs in the low permeability soil were investigated by using the electroosmotic flow (EOF) generated in the EK process. Although Cs was moved in white clay with weak interaction, hardly Cs migrated in soil containing only 5% vermiculite. The result will contribute to the prediction of the movement of Cs in soil by flowing water. On the other hand, this result indicates the difficulty in removing Cs from clay minerals with strong interaction. Based on these results, the EK process to remove Cs from the soil with strong interaction was investigated in the combination with oxalic acid leaching. Oxalic acid leaching can transfer Cs to the ion exchangeable form from the residual form under low water content similar to real soil conditions. The EK process can remove 33% of Cs from model soil after oxalic acid leaching under the potential gradient of 1 V/cm and 72 h of the operation time. These results indicated the possibility of removing the residual form of Cs by the EK process, which has been considered to be difficult so far.

7.2. Recommendation and limitations

After the accident at Fukushima Daiichi Nuclear Power Plant in 2011, a large area of Fukushima and neighboring prefectures was contaminated with radioactive species, especially Cs. In these places, stripping the contaminated surface soil has been carried

out. The stripped contaminated soil has been enclosed in a flexible container bag (1–1.5 t) and stored in the intermediate storage facilities. Since the volume of the contaminated soil collected in the intermediate storage facilities is enormous, a reduction of the volume is required. Although the EK process has an advantage of in-situ remediation, where the EK process is applied to the contaminated land directly, the EK process can also be applied to the soil collected in a container. Therefore, the EK system combined with oxalic acid leaching developed in this study is assumed to be effective for the soils in the intermediate storage facilities. Since the residue after oxalic acid leaching consists mainly of Si, these residues may be recycled as a material for civil engineering, if the radioactivity would become lower than 8,000 Bq/kg after the EK process. In the EK process, the desorbed Cs in the soil pore water can be migrated into the solution of the cathode chamber. Therefore, solid/liquid separation such as filtration and centrifugation is not necessary unlike the soil washing method. The removed Cs into the cathode solution can be collected by various developed adsorbents. An image of the application of the EK process to Cs contaminated soil is shown in **Fig. 7-1**.

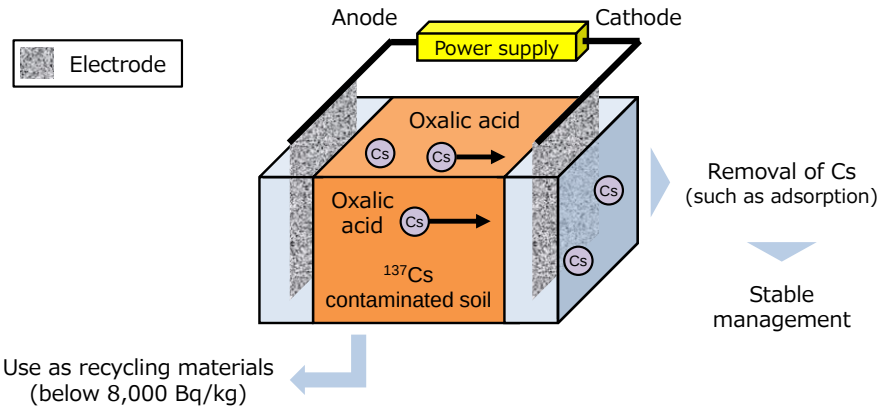

Fig. 7-1. Schematic diagrams of the electrokinetic remediation with oxalic acid leaching of Cs contaminated soil.

This EK process with oxalic acid leaching still has some limitations when the system will be applied to the actual contaminated soil. For example, the influence of organic substances in the soil, such as cellulose and humic substances, on the removal efficiency of Cs by this system is not clear. The effect of the types of clay minerals, the proportion of these clay minerals in the soil, and the electrolytes used in the EK process on the removal efficiency of Cs from the soil should be investigated. The cost of the reagents used in the treatment, especially oxalic acid, and energy for the EK process should be estimated in more detail, although there is a possibility that oxalic acid produced by some plants can be used in this system.

In conclusion, the demonstration of the possibility to remove Cs from the clayey soil by the EK system combined with oxalic acid leaching will contribute to the expansion of the applications of the EK process and the development of effective remediation for contaminated soil with radioactive species.

Appendix: Research achievement

1) **Yasuhiro Akemoto**, Masahiko Kan, Shunitz Tanaka, Static Adsorption of cesium ions on kaolin/vermiculite and dynamic adsorption/desorption using the electrokinetic process, Journal of Chemical Engineering of Japan, 52, (7), 2019, 662–669. https://doi.org/10.1252/jcej.18we312.

2) **Yasuhiro Akemoto**, Satya Candra Wibawa Sakti, Masahiko Kan, Shunitz Tanaka, Interpretation of the interaction between cesium ion and some clay minerals based on their structural features, Environmental Science and Pollution Research, 28, (11), 2021, 14121–14130. https://doi.org/10.1007/s11356-020-11476-7.

3) **Yasuhiro Akemoto**, Toko Iwamura, Seira Takahashi, Masahiko Kan, Shunitz Tanaka, Desorption of Cs^+ from contaminated biotite with a low molecular mass organic acid, Journal of Environmental Chemical Engineering, 9, (5), 2021, 106101. https://doi.org/10.1016/j.jece.2021.106101.

4) **Yasuhiro Akemoto**, Seira Takahashi, Toko Iwamura, Masahiko Kan, Shunitz Tanaka, Extraction of Cs bound with biotite by addition of oxalic acid without heating, Journal of Soils and Sediments, 22, 2022, 1787–1791. https://doi.org/10.1007/s11368-022-03196-x

5) **Yasuhiro Akemoto**, Seira Takahashi, Yuhi Inaba, Masahiko Kan, Satya Candra Wibawa Sakti, Shunitz Tanaka, Collectable adsorbent based on the adsorption characteristics of sodium citrate-pretreated vermiculite for cesium ion in an aquatic environment, Journal of Water Process Engineering, 50, 2022, 103280. https://doi.org/10.1016/j.jwpe.2022.103280

Acknowledgment

This thesis summarized that research was mainly conducted at the Graduate School of Environmental Science, Hokkaido University, and some additional results were obtained at Industrial Research Institute, and Research Institute of Energy, Environment and Geology, Industrial Technology and Environment Research Department, Hokkaido Research Organization (HRO).

I want to express my deep gratitude to Emeritus Professor Shunitz Tanaka (Hokkaido University). He provided me with a wide range of research environments, a global personal network, and many opportunities for domestic and international conferences. I would not have been able to continue this research without his support.

My sincere thanks to Professor Shin-ichiro Noro, Professor Tatsufumi Okino, Professor Yuichi Kamiya, Associate Professor Masaaki Kurasaki, and Associate Professor Kazuhiro Toyoda (Faculty of Environmental Earth Science, Hokkaido University) for their useful comments and suggestions on this research. My sincere thanks are extended to Associate Professor Taiki Umezawa for his help on the FT-IR measurement.

I am also deeply thankful to Professor Munehide Ishiguro (Research Faculty of Agriculture, Hokkaido University) for reviewing this thesis and giving me a valuable opportunity to write a review and book at the Japanese Society of Soil Science and Plant Nutrition. And also, thanks to the late Associate Professor Masami Fukushima (Faculty of Engineering, Hokkaido University) for his help on zeta potential analysis and giving me a lot of advice and comments.

The evaluation of clay minerals was carried out using a particle size distribution, XRF, XRD, and SEM/EDS apparatus at the Joint-use Facilities: Laboratory of Nano-Micro Material Analysis and Laboratory of XPS analysis, Hokkaido University.

I am deeply grateful to Dr. Toshiyuki Akazawa (Fellow of HRO), Mr. Hiroyuki Mitsuhashi, Mr. Toshihiro Kitaguchi, Mr. Satoru Ono, Mr. Hideo Hoshina, Dr. Hiroyuki Inano, Mr. Tatsuyuki Kamada, Mr. Takema Sasaki, Mr. Keiichi Tomita, Mr. Motoomi Wakasugi, and many researchers in HRO for providing research environment and a lot of support.

I am also grateful to Associate Professor Masahiko Kan (Hokkaido University of Education Sapporo). He received me from humanities and suggested to go to graduate school. Even after I graduated from Hokkaido University of Education Sapporo, he continuously gave me a lot of comments as a collaborative researcher. My life as a researcher would not be started without his recommendation.

There were many foreign postdoctoral researcher, short-term stay, and research students from many countries such as Indonesia, Taiwan, Guyana, and China in the Laboratory of Environmental Remediation. I could obtain a valuable experience through discussions with different research fields and cultures.

Finally, I received a lot of encouragements from many seniors and juniors, and some of them helped me as co-author in my research papers; Dr. Takahiro Sasaki, Dr. Yoshihiro Mihara, Dr. Rudy Syah Putra, Dr. Yustiawati, Mr. Yasuhisa Ohkawa, Mr. Yuiga Hamade, Dr. Satya Candra Wibawa Sakti, Ms. Aoi Nasu, Mr. Min Guo, Mr. Shintaro Saijo, Mr. Yuhi Inaba, Ms. Nozomi Endo, Mr. Chihiro Kitagawa, Mr. Yasuyuki Narita, Mr. Ryosuke Miyamura, Mr. Tomoaki Moriya, Ms. Toko Iwamura, Ms. Seira Takahashi, and all the members of the Laboratory of Environmental Remediation (Shunitz Tanaka's Laboratory).

March 2023

Yasuhiro Akemoto